FLEXIBLE FLOATING THIN FILM PHOTOVOLTAIC (PV) ARRAY CONCEPT FOR MARINE AND LACUSTRINE ENVIRONMENTS

by

Kim Trapani

Thesis submitted in partial fulfilment

of the requirements for the degree of

Doctor of Philosophy (PhD) in Natural Resources Engineering

The School of Graduate Studies

Laurentian University

Sudbury, Ontario, Canada

THESIS DEFENCE COMMITTEE/COMITÉ DE SOUTENANCE DE THÈSE

Laurentian Université/Université Laurentienne
School of Graduate Studies/École des études supérieures

Title of Thesis Titre de la thèse	FLEXIBLE FLOATING THIN FILM PHOTOVOLTAIC (PV) ARRAY CONCEPT FOR MARINE AND LACUSTRINE ENVIRONMENTS
Name of Candidate Nom du candidat	Trapani, Kim
Degree Diplôme	Doctor of Philosophy

Department/Program Département/Programme	Natural Resources Engineering	Date of Defence Date de la soutenance	April 25, 2014

APPROVED/APPROUVÉ

Thesis Examiners/Examinateurs de thèse:

Dr. Dean Lee Millar
(Supervisor/Directeur de thèse)

Dr. Charles Ramcharan
(Committee member/Membre du comité)

Dr. Marc Arsenault
(Committee member/Membre du comité)

Dr. Krishna Challagulla
(Committee member/Membre du comité)

Dr. Lars Johanning
(External Examiner/Examinateur externe)

Dr. Louis Mercier
(Internal Examiner/Examinateur interne)

Approved for the School of Graduate Studies
Approuvé pour l'École des études supérieures
Dr. David Lesbarrères
M. David Lesbarrères
Director, School of Graduate Studies
Directeur, École des études supérieures

ACCESSIBILITY CLAUSE AND PERMISSION TO USE

Abstract

The focus of the research is on the development of the concept of floating flexible thin film arrays for renewable electricity generation, in marine and lacustrine application areas. This research was motivated by reliability issues from wave energy converters which are prone to large loads due to the environment which they are exposed in; a flexible system would not need to withstand these loads but simply yield to them. The solid state power take off is an advantage of photovoltaic (PV) technology which removes failure risks associated with mechanical machinery, and also potential environmental hazards such as hydraulic oil spillage. The novelty of this technology requires some development before it could even be considered feasible for large scale installation. Techno-economics are a big issue in electricity developments and need to be scoped in order to ensure that they would be cost-competitive in the market and with other technologies.

Other more technical issues relate to the change in expected electrical yield due to the modulation of the PV array according to the waves and the electrical performance of the PVs when in wet conditions. Results from numerical modelling of the modulating arrays show that there is not expected variation in electrical yield at central latitudes (slightly positive), although at higher latitudes there could be considerable depreciation. With regards to the electrical performance a notable improvement was measured due to the cooling effect, slight decrease in performance was also estimated due to water absorption (of ~ 1.4%) within the panels. Overall results from both economic and technical analysis show the feasibility of the concept and that it is a possibility for future commercialisation.

Keywords

floating PV; techno-economics floating PV; modelling flexible thin film; water absorption laminated PV; electrical reliability water saturated PV; mechanical reliability water saturated PV; floating PV prototype;

Acknowledgements

My first and foremost thanks go to my supervisor Prof. Dean Millar, who offered me the opportunity to undertake this research and had the patience to guide me through the process. I will always appreciate the friendship, advice and scientific knowledge I have gained from him.

This life rewarding journey would not have been possible without MIRARCO who have funded my research and sponsored me throughout my years in Canada, and for this I will be always grateful. The three years of my PhD would not have been the same without my colleagues at MIRARCO, and I would like to thank them for their friendship, assistance and the beloved discussions we had.

I would like to acknowledge all the help and support the ERCM team have been throughout my PhD. Thanks also to Dave Parish and Helen Smith, from the University of Exeter, Steve Martens, from Power Film, Miguel Redon Santafe, from the University of Valencia and Adam Walli, from Laurentian University, who helped me with the design and electronics of the prototype and provided some very useful data. Special mention goes to Michelle Levesque, Monica Carvalho, Kendra Driscoll, Chris Groccia, Salina Yong, Nader Golchinfar and Karam Panesar who not only been great friends but have also helped me with the experimentation, getting tools and carrying parts of the project around.

I would like to deeply thank all of my friends in Canada and abroad, without which this experience would not have been as great and which company meant a lot to me. Finally, I would like to thank my family in Malta who I know love me a lot and who always support me and keep me motivated. I am blessed to have you in my life.

Thank you all,

Kim Trapani

Mining Innovation and Applied Research Corporation – MIRARCO
Sudbury, 10th December 2013

Table of Contents

List of Tables

List of Figures

Nomenclature

u	tidal velocity (m/s)
V_w	water drag coefficient
$C_{d\ water}$	water density (kg/m^3)
ρ_w	added mass coefficient
C_m	tidal inertia coefficient
V_w	volume of water displaced (m^3)
$\dot{X}$	velocity of thin film PV array (m/s)
$\ddot{X}$	acceleration of thin film PV array (m^2/s)
ρ_a	density of air (kg/m^3)
$C_{d\ air}$	air drag coefficient
A_d	surface area of drag (m^2)
U	wind velocity (m/s)
C_L	lift coefficient
A_L	lift surface area (m^2)
C_a	aerodynamic moment coefficient
F_H	wave excitation force (N)
F_w	aerodynamic force (N)
B	buoyancy (N)
W	weight (N)
L	air lift (N)
D_{air}	air drag (N)
I_{air}	aerodynamic inertia (N)
D_{tide}	tidal drag (N)
N_{tide}	tide down force (N)
I_{tide}	tidal inertia (N)
I_{wave}	wave inertia (N)
S	surface tension (N)
T	mooring tension (N)
A	wave amplitude (m)
c	water colour coefficient
H	wave height (m)
I	current (A)

$I_{SC\,STC}$	short circuit current at STC (A)
I_{BH}	direct solar radiation intensity on a horizontal plane (W/m^2)
$I_{B\beta}$	direct solar radiation intensity on an inclined plane (W/m^2)
I_{DH}	diffused solar radiation intensity on a horizontal plane (W/m^2)
$I_{D\beta}$	diffused solar radiation intensity on an inclined plane (W/m^2)
$I_{R\beta}$	reflected solar radiation intensity on an inclined plane (W/m^2)
I_{SC}	short circuit current (A)
$I_{t\beta}$	total solar radiation intensity on an inclined plane (W/m^2)
L_o	line passing through (0,0,0), parallel to S_p and perpendicular to $\vec{S}$
$\overrightarrow{L_o}$	vector direction of L_o
L_x	range of points along the $x-z$ plane
L_y	range of points in the y-direction
n	mesh size of meshes in the $x-z$ plane (m)
p	mesh size of meshes in the y-direction (m)
P_n	point on grid
$P_n{}'$	point projected on plane S_p
r	wave roughness coefficient
R	solar intensity acting on PV panel at STC (W/m^2)
R_{STC}	solar intensity acting on PV panel (W/m^2)
s	wave steepness ratio
$\vec{S}$	solar vector
S_{sh}	shading factor
S_p	solar plane orthogonal to solar vector $\vec{S}$
V	voltage (V)
V_{OC}	open circuit voltage (V)
W	panel width (m)
x_n	x - coordinate of grid point at n (m)
$x_n{}'$	coordinate of x_n rotated by angle ϕ from north (m)
y_n	y - coordinate of grid point at n (m)
$y_n{}'$	coordinate of z_n rotated by angle ϕ from north (m)
z_n	coordinate of y_n rotated by angle ϕ from north (m)
$z_n{}'$	z - coordinate of grid point at n (m)

α	sun's altitude (°)
β	angle of inclination of plane (°)
γ_s	sun's azimuth (°)
ϕ	angle of the panel's direction (or wave propagation) with respect to north (°)
κ	shape constant
λ	wavelength (m)
ξ	shape constant
ρ	albedo coefficient
τ	shape constant
φ	shape constant

G_T	solar irradiance on PV panels $(kW.h.m^{-2})$
p	packing ratio
A	surface area (m^2)
η	PV panels efficiency *(%)*
L_m	miscellaneous system losses *(%)*
R	system rating *(kW)*
$\dot{R}$	system specific rating $(kW.m^{-2})$
K	annuitized capital cost *($)*
K_o	capital cost *($)*
i	discount rate *(%)*
n	project life
x	cost index
y_f	baseline year
y_c	installation year

1 Introduction

1.1 General Background

As of the latter end of 2011, the world was estimated to have reached a population of 7 billion. This trended growth in population has resulted in a relentless sustained demand for the energy industry. The limited availability of conventional natural energy resources, as well as their associated impacts on the environment due to the release of greenhouse gases (GHGs), has meant more focus being put on renewable energy sources which have the disadvantage of being land intensive. "Such changes in land use have enabled humans to appropriate an increasing share of the planet's resources, but they also potentially undermine the capacity of ecosystems to sustain food production, maintain freshwater and forest resources, regulate climate and air quality, and ameliorate infectious diseases" [1].

Large scale generation of electricity from solar photovoltaic (PV) technology is one of the renewable energy technologies which require a large land footprint in order to be effective, since the unobstructed surface area of the PV is directly proportional to how much electricity will be generated. This was one of the underpinning reasons for the development of the floating PV concept. All of the projects currently in existence (see Section 2.3), are mounted on a rigid pontoon structure, in small lakes, ponds or reservoirs. Engineering of these rigid pontoons for offshore environments, marine and lacustrine, would result in high costs of electricity generation (see Chapter 7). Another concern would be the reliability of the moorings and structure itself, which would have to sustain the force of the oncoming waves.

The solution proposed is to have a system which could readily deform to the shape of the water waveform and hence will yield to oncoming waves rather than try to withstand them. Existing thin film PV technology designed for land use, may offer such an alternative for the offshore environment, including lacustrine, marine and tailings pond environments. The rigidity of the structure can be altered by varying the materials used within the manufacture of the panels themselves. If the density of the structure is maintained lower than the density of the water, this would imply that the thin film PV array would be able to float without needing any extra buoyancy.

The ability of the system to float without the requirement of additional buoyancy allows the thin film array to be deployed in direct contact with the water surface and so provide an underlying heat sink (with heat capacity significantly higher than air). This allows the heat transfer between the PV panels and the surroundings to be rapid so that the panel's temperature assumes that of the water, typically cooler; this results in higher solar to electrical conversion efficiency, what is known as a negative temperature coefficient. A pontoon mounted array would not have this cooling benefit, but the PV panels could be tilted at an angle which would allow more direct sunlight to flood the panel's surface area.

The manufacturing process of the thin film PV laminates is a roll-to-roll process (Figure 1-1) which potentially allows long lengths of PV panels to be fabricated. This would make them more appropriate for large scale installations, since it would minimise the number of components (as well as connections) which would have to be installed and so increases the reliability of the system. The lamination process would also allow all connections of the array to be embedded

within the panels themselves, so limiting the exposure of the connectors/connections to the water.

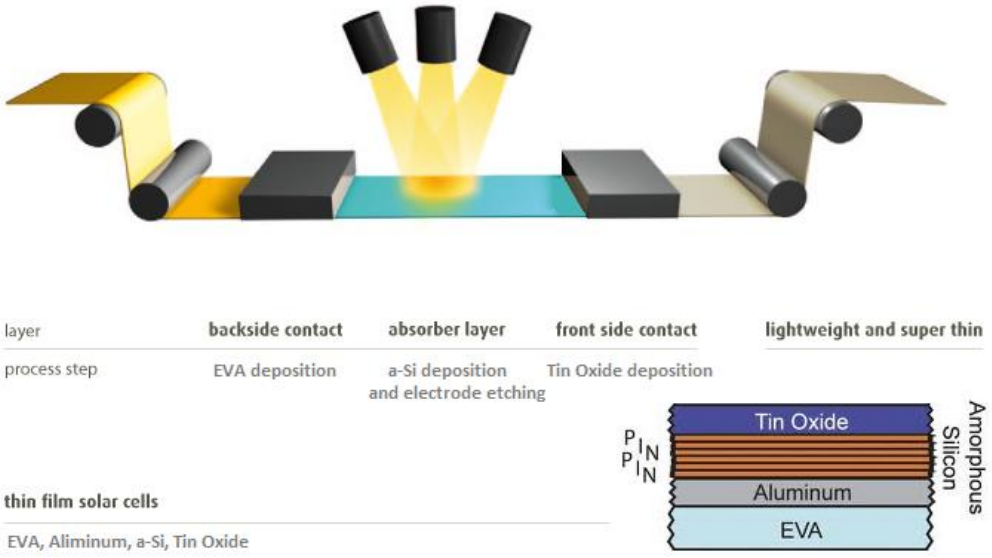

Figure 1-1: Roll to roll processing of a-Si solar cells (Adapted from **www.solarion.net**)

The technology being proposed is novel in nature and so will inevitably require a degree of feasibility analysis, modelling and testing. The feasibility analysis of the floating PV was determined through comparison with other offshore renewable energy technologies and taking case studies for the generation of electricity adopting the floating PV concept. Yield modelling was undertaken, to simulate the electrical yield of the array when it is deforming in regular water wave motion. A 500W prototype was developed and built to investigate and prove the concept of a floating thin film PV array. The results were then compared to a ground mounted control array which was installed with identical panels and was exposed to the same solar resource.

1.2 Objective and Scope

One of the main challenges in undertaking this research was the lack of literature and material available on the topic of floating PVs. The study objectives were to establish a database of existing floating PV applications, discuss the logistics and feasibility of a flexible thin film PV array, and develop (and proof the concept of) a floating PV prototype which could be scaled up to larger scale applications. The scope of the thesis can be described by the following two sections:

1. Application areas
    - Small water-bodies

      Developments in floating PV projects have been focussed on small water-bodies where the wave environments are mild and include only pontoon mounted systems. Literature on floating PV was very minimal and Section 2.3 aims to identify small water-body applications of this technology.
    - Lakes and marine environments

      The wave environments within a large lake are very similar to those in a marine environment, and this is because the large areas allow growth of wind waves. Techno-economic analysis was undertaken to compare the performance of large thin film PV with other offshore renewable energy technologies (Chapter 7). Case studies are given for both a lacustrine and marine application (Chapters 8 and 9).
2. Concept development
    - Modelling

The implication of an offshore environment is that the panels would be modulating in a quasi-sinusoidal motion; hence prediction of the yield is complicated by the motion, especially with high peaking waves with short wavelengths. A model based on a regular wave form was developed for theoretical predictions of the electrical yield from an offshore array (Chapter 4).

- Experimental testing

  One of the issues of concern at the outset of the research was that of potential water absorption within the PV panel due to the contact of the panel with water. If the water absorption is substantial it could lead to corrosion of the electrodes within the PV junction and hence loss of electrical connectivity within the panel. Quantitative analysis of the water absorption is given in Chapter 5.

- Prototype testing

  The testing of the prototype was mainly to prove the conceptual design and to assess the array's performance when in contact with a wet surface. Comparative testing with a land based similar system was performed, as well as prolonged testing of the array to trend any degradation in electrical yield. The results achieved from this testing are presented in Chapter 6.

Chapter 2 is the introductory outline to this research and gives a quantitative outlook on the materials used in thin film PV manufacture, optic variations and the current market and research in floating PV. Chapter 3 aims to identify the main force components onto a floating thin film PV system and compare it to a very large floating system (VLFS).

The main aim of this thesis was to assess the techno-economic feasibility of the thin film PV technology, not only with researched costs and modelled yields (Chapters 7 – 9) but also with actual results attained from a developed prototype (Chapter 6). Research in Chapters 5 – 6 is focussed on the implications of the PV panels being in direct contact with the water surface.

1.3 Thesis Outline

The introductory and concluding chapters to this work are in Chapter 0 and Chapter 11 respectively, with Chapter 0 introducing the concept and Chapter 11 summarising the results and contributions of the research, with indications of directions for future research. Chapter 2 presents a review of key technical aspects having a bearing on subsequent work. A general description of the floating PV precedent practice is made in Section 2.3. Chapter 3 gives an outlook of the basic hydrodynamics of the floating thin film PV and assesses the main force components acting on the floating body.

Chapter 4 details the methodology developed to predict the yield of an array of thin film PV in a marine environment – assuming sinusoidal waveforms. The issue of water absorption in the laminated PV is characterised in Chapter 5. In particular, its effects on the electrical and mechanical properties, and conversion efficiency. The electrical reliability is further verified in the consequent chapter. Here the specifics of the proof of concept prototype design, along with the yield results obtained are presented and compared with the performance of a ground-mounted control installation.

Chapters 7 – 9 highlight the techno-economics of such a project proposal for large scale applications. Chapter 7 compares the various offshore renewable energy technologies, including the thin film PV array, to show an economic standing of floating PV with other offshore carbon offsetting technologies. The costs realised for the floating PV (both flexible thin film and pontoon mounted) in Chapter 7 are used in the case studies in Chapters 8 and 9 that consider integration of floating PV systems with i) a remote mine and ii) within an islanded grid respectively.

Chapter 10 synthesises findings from the previous chapters in a discussion of the technology prospects. The final chapter concludes the research undertaken, highlights the list of original contributions associated with this work, and makes recommendations for future work and research.

2 Literature Review

Although the concept presented through this research is novel and unique in its nature, some related aspects within the research have been already explored by researchers in different fields and this chapter draws upon this existing knowledge. The first three sections within this review will address general issues with the development of the concept (material selection, moorings etc.), while the latter half will address direct research related aspects. The development of floating PV technology has been brought together in a separate section, 2.3, which looks at the existing technologies and what other commercial and research teams are proposing for large scale deployment of offshore PV.

2.1 Materials

The development of the concept undertaken is mainly focussed on generation of electricity from thin film PV arrays. The particular type of thin film PV, amorphous silicon (a-Si) being referred to, is a polymer laminated thin film which allows flexibility of the array. Other than the polymer lamination there are other components which make up the composite, namely the interface glue, conducting metal and the thin film PV deposition. The protection barrier for the encapsulation is offered by the polymer lamination and the contact adhesion so special attention has to be given to these materials.

2.1.1 Polymer lamination

Polymer lamination of the PV thin film panel was developed as a cheap and effective method of encapsulating the photovoltaic composite. The basic requirements of the polymer used to

encapsulate the PV material in such an application (floating directly on water) are that the material does not offer significant flexural rigidity when in wave driven motion, has high transparency and is waterproof. For typical PV applications "a transparency of at least 85 %, permeation values as low as 10^{-5} g/cm^2 day for water vapor transition (WVTR) and respectively 10^{-5} cm^3/m^2 day atm for oxygen transition (OTR) are needed" [2]. The polymers more commonly used for lamination of the thin film PV panels are *polyvinyl fluoride* (PVF), *ethylene tetrafluoroethylene* (ETFE) and *polyethylene terephthalate* (PET) [3]. Other polymers which have been used for this laminating process are *polytetrafluoroethylene* (PTFE), *fluorinated ethylene propylene* (FEP) and *perfluoroalkoxy* (PFA). The properties of each suitable polymer for lamination are given in Table 2-1.

Table 2-1: Polymer film properties (for lamination) collated from McKeen & Massey [4]

Polymer Film Type	**ETFE**	**FEP**	**PFA**	**PTFE**	**PVF**	**PET**	
PHYSICAL PROPERTIES							
Density (kg/m^3)	1,900	2,150	2,150	2,200	1,780	1,380	**Standard**
Elastic Modulus, MD/TD (MPa)	73,500/900	480	760/1400	760/1400	2068-2620	2,100/2,025	ASTM D882
Elongation at Break, MD/TD (%)	45/560	300	60/450	250	90-250	110/70	ASTM D882
Tensile Strength at Break, MD/TD (N/mm^2)	234/48	21	69/24	41.4	55.2-110.3	213/290	ASTM D882
OPTICAL PROPERTIES							
Refractive Index	1.407	1.341-1.347	1.358	/	1.46	/	ASTM D542
Light Transmission (%)	95	96	95	95	/	90	ASTM D424
PERMEABILITY PROPERTIES							
Moisture Absorption (%)	<0.02	<0.02	0.3	<0.01	<0.5	/	ASTM D570
Water Vapour Permeability (g/m^2.day.mm)	0.3	/	0.1	/	0.09-0.057	1.1	ASTM E96

MD-Machine Direction; TD-Transverse Direction

2.1.2 Interface glue

The interface glue is what creates the bond between the composite layers. This glue must not only create a strong bond, but it has to be compatible with the composite materials and ensure that the surface clarity of the PV panel is maintained. The products typically used for flexible thin film application are *ethylene-vinyl acetate* (EVA) and *polyvinyle butyral* (PVB) glue. Other products which could be utilised for this aim are *ethylene-methyl acrylate* (EMA), *thermoplastic polyurethane* (TPU) and Cytop™ [5]. EMA is comparable to EVA and its major benefits are thermal stability, chemical resistance and mechanical performance at lower temperatures. PVB is known for its reduced moisture permeation properties as well as its high clarity. TPU is a copolymer of polyurethane which is known for its waterproofing properties and is used for many marine applications. Apart from its waterproofing properties it is also a product which allows high flexibility in bonding. Cytop™ is another adhesive which provides a waterproof surface, mainly due to the material having hydrophobic properties. The other appeals of Cytop™ are that it too is flexible and commercially available.

In the development of the prototype undertaken, the manufacturer's panels used EVA adhesive. The waterproofing concern with floating PV arrays, indicate that Cytop™ and TPU adhesives would have favourable benefits in such an application. They would have been preferential in the manufacturing of the panels, although all of them still provide the essential transparency, adhesion and flexibility.

2.1.3 Anti-fouling and self-cleaning coatings

The reliability of the PV panel is compromised not only if water manages to penetrate to the p-n junction but also if light photons are deterred from reaching the cells and hence reducing the occurrence of the photoelectric effect. Light deterrence can be optical, through submersion of the panels (which is discussed in the following section), and physically by growth of algae on the top surface of the panels and accumulation of dirt. This implies that both self-cleaning and anti-fouling need to be considered for this application. Although proper self-cleaning would exclude the requirement for anti-fouling treatment since the surface would not be suitable for algal growth [5, 6], the underside would still have to be painted with a commercial marine anti-fouling paint.

Effective self-cleaning mechanisms which could be used for these purposes are coatings of materials which are either hydrophobic or hydrophilic photocatalytic coatings [7]. In the first case as the word ‘hydrophobic’ suggests, the material repels water droplets and this is due to the high water contact angles. When utilising superhydrophobic materials or even better ultrahydrophobic materials for the coating, this water contact angle is even greater almost forming a perfect sphere of the water droplet. The mechanism which allows the self-cleaning of the surface is the rolling of these droplets off the surface together with the dirt in the acting direction of gravity. So a perfectly smooth laminated surface (of the thin film PV composite) would be more effective with such a self-cleaning coating.

Transparent superhydrophobic with photocatalytic properties would allow the disintegration of any water stains which would be left behind [8]. For a relatively calm water environment the

wave motion might not be enough to supply water for the self-cleaning process. The other alternative would then be the utilisation of a hydrophilic photocatalytic coating. A hydrophilic photocatalytic coating does not rely on the flow of water to transport the dirt off the surface of the panels. Rather the photocatalyst in the coating chemically breaks down the dirt when exposed to light. Most commonly this photocatalyst is titanium dioxide (or titania) [7]. Titania has gained popularity because it is inexpensive, efficient and most importantly in this application, has high transparency.

So either self-cleaning mechanism could be utilised, although the benefits of either would be enhanced by having a smooth laminated surface rather than a textured surface. If water supply is limited only by rain availability a hydrophilic photocatalytic coating would be more suitable, otherwise a superhydrophobic surface would be better suited.

2.2 Optical variations for floating PVs

The light effective on the solar panels for generation of electricity through the photoelectric effect may depend on other factors rather than the radiating solar intensity. This could be through reflectance of the additional radiation from the surrounding, which is known as the albedo effect, or also in the case of a floating PV from reduction in the solar intensity due to a layer of water on top of the PV panels.

2.2.1 Albedo effect

The albedo effect is a measure of the optical reflectance of the solar radiation due to the surface properties. So a higher albedo would result in higher total solar radiation exposure of the PV

panels, since it signifies the fraction of solar radiation reflected from the ground. In an open sea environment this changes according to the wave motion (since this would change the angle of incidence), the water quality and also the sky conditions. A study by Payne [9] on the albedo of sea surfaces, gives albedo values of 0.061±0.005 for heavily overcast skies and 0.03 for high sun ranging to 0.45 at altitudes less than 10°.

Table 2-2: Colour and roughness coefficients for lakes and ponds, modified from Dvoracek & Hannabas [10]

Surface and condition	**Colour Coefficient** c	**Roughness Coefficient** r
Lakes and ponds, clear water		
waves, none	0.13	0.29
waves, ripples up to 2.5cm	0.16	0.70
waves, larger than 2.5cm with occasional whitecaps	0.23	1.23
waves, frequent whitecaps	0.30	2.00
Lakes and ponds,		
green water, ripples up to 2.5cm	0.22	0.70
muddy water, no waves	0.19	0.29

The model developed by Dvoracek & Hannabas [10] relies upon characterisation of the water body through the colour and roughness coefficient to estimate the albedo coefficient as follows:

$$\rho = c^{r \cdot \sin \alpha + 1} \qquad [2\text{-}1]$$

where c is the colour coefficient and r is the (wave) roughness coefficient, α is the sun's altitude and ρ is the albedo coefficient.

The model follows Payne's study that with lower altitudes the albedo effect is greater since the angle of incidence on the panel is more obtuse at those altitudes. The model suggests that a water surface with low clarity, either from whitecaps (higher albedo coefficient) or it being muddy (lower albedo coefficient), is a better reflector of the solar radiation. High ripples lead to lower albedo coefficients since they decrease the angle of incidence between the light waves and the water surface. Hence higher reflectance to the surrounding areas would be expected at lower solar altitudes, with darker water and relatively low wave heights.

2.2.2 Light intensity attenuation in submerged panels

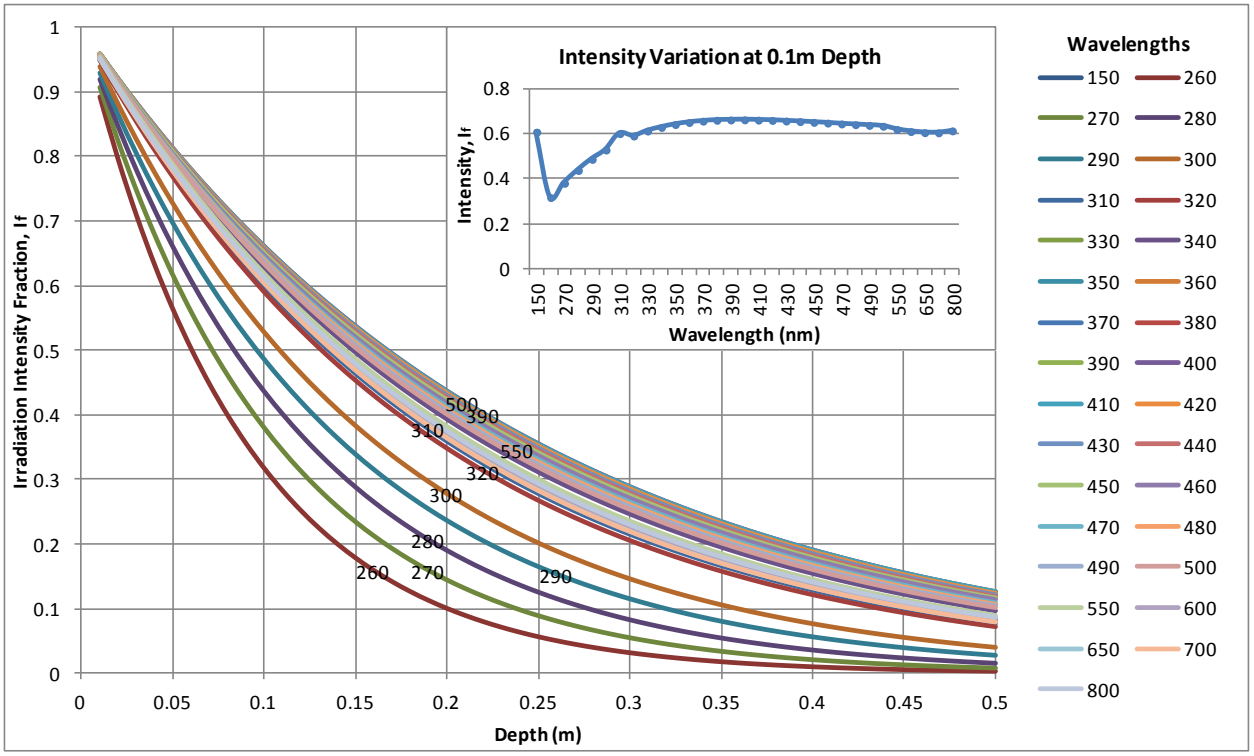

Figure 2-1: Theoretical spectral absorption of different light wavelengths in sea water according to model by Kopec & Pawlak [11]

The floating thin film PV array concept is not intended to be fully submerged at all times but inevitably it would experience some periods during which it would be somewhat partially/fully submerged by millimetres of water. This is predicted to attenuate the light intensity during those periods. A quantification of the decrease in solar intensity expected is given in Figure 2-1 which is derived from the model by Kopec & Pawlak [11]. This suggests a non-linear attenuation based on the wavelength of light and depth in the water column. Longer wavelengths have a higher attenuated fraction of solar intensity at a given wave depth than shorter wavelength. With 1-2mm of water coverage the light intensity attenuation should not exceed more than 10%.

This analysis can be confirmed through experimental results reported in the following literature [12-14] for the optical and electrical behaviour of a submerged crystalline PV panel. A relative increase in the electrical conversion efficiency of 11% was measured at a submersion depth of 4cm due to the cooling effect of the water (characteristic of the negative temperature coefficient of PV panels), while a decrease of 23% was measured at a depth of 40cm (in clear water).

2.3 A Review of Floating PV Installations

The existing floating PV projects include conventional PV arrays, as well as concentrated PV arrays which benefit from the surrounding water body to prevent overheating of the solar cells. The review given here within is limited to only conventional PV arrays for the novel floating application. The pre-mature stages of this technology application limit the projects which have been developed around the world. The following overview will aim to illustrate each of the projects in existence, and the installation and technological variations between each. For the most part, these installations are mounted upon a pontoon-based floating structure and are

installed in either reservoirs or ponds used mainly for irrigation purposes (motivated by increasing demand for energy in modern irrigation systems and agriculture). Common benefits from these installations was a reduction in water evaporation from the reservoir/pond [15] and decreased algal growth (due to the reduction in sunlight penetration within the water body)[16]. Also electrical yields were slightly improved, in most reported cases, probably due to the cooling benefit offered by the underlying water surface as illustrated by Bahaidarah *et al*. [17] while testing a photovoltaic panel which was in direct contact with water.

2.3.1 Existing PV Installations

The propriety nature of the technology somewhat limits the literature available on floating PV installations. Through online research and direct contact with the developers (commercial and academic) Figure 2-2 was compiled. This figure illustrates the floating PV projects developed worldwide to date solely for electricity generation, of which there are 19 in total.

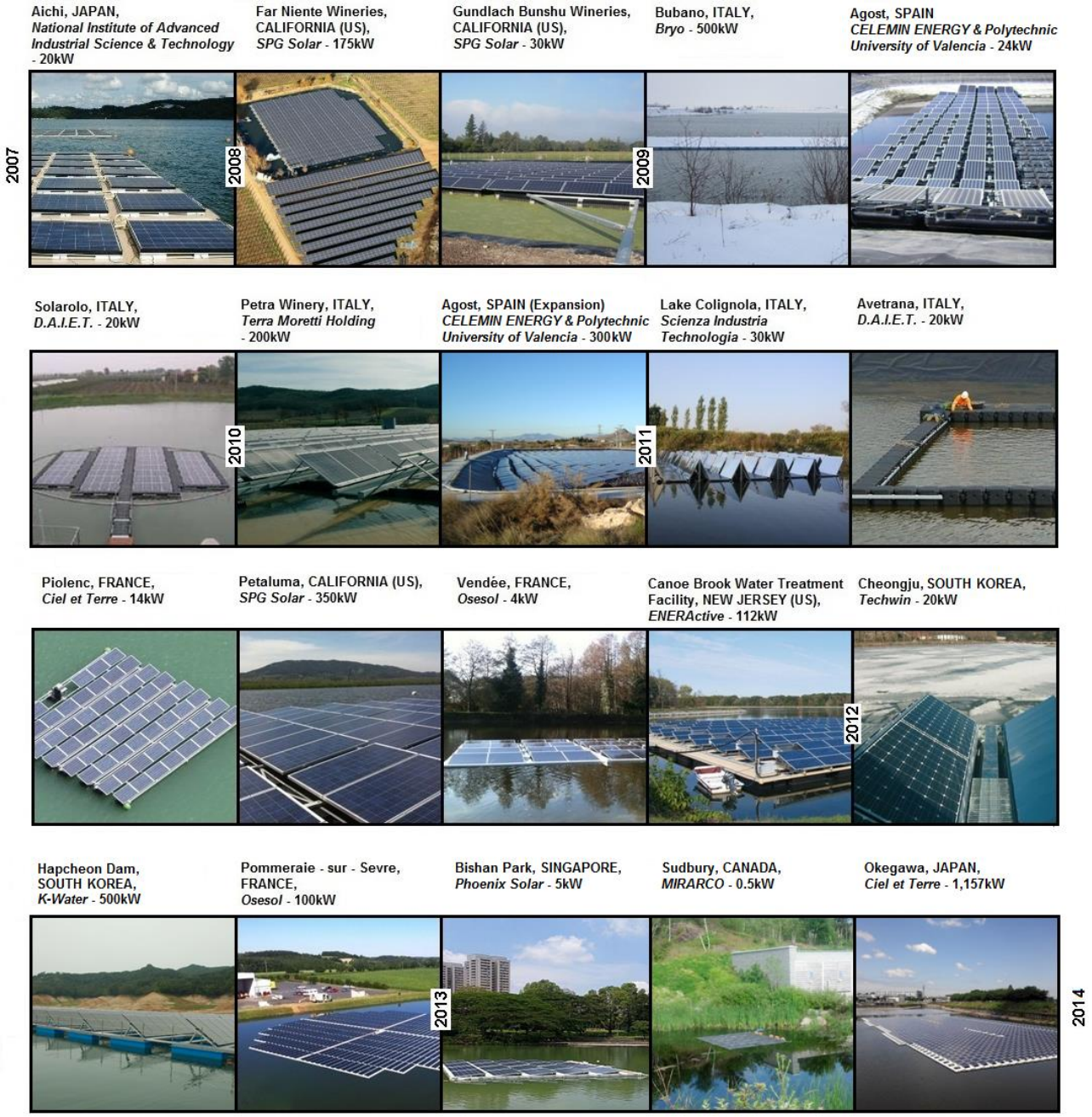

Figure 2-2: Floating PV projects timeline

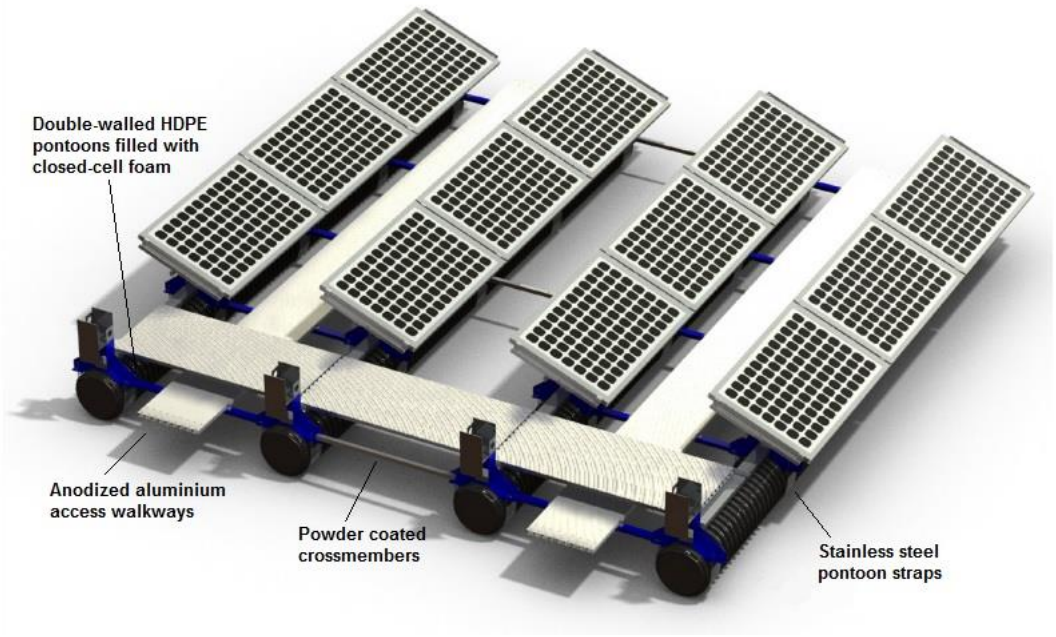

Figure 2-3: TTi's 'Floatovoltaic' product incorporated within the Far Niente floating PV project [18]

The project which has received most news coverage and is usually claimed as being the first floating PV project, although a floating PV project for research purposes had been installed the previous year in Aichi, Japan, was that of Far Niente wineries in California, USA. SPG Solar were contracted by the owners of the winery to install the array in 2008[19]. Their motivation for the deployment of the PV panels on top of their water reservoir was not to displace land which was used to grow the vines – and so a more precious resource for their business. The installation was based on modular crystalline PV panels which were mounted at an optimal tilt on top of individual pontoons. The mounting structure includes walkways between the rows of panels and along the sides to facilitate cleaning and maintenance of the panels. The array is based on TTi's 'Floatovoltaic' product (illustrated in Figure 2-3). Having this effective cover

from the pontoon and the PV panels on the reservoirs resulted in reduction of water evaporation from the reservoir, research in Australia suggests that 40% of open reservoir's water could be lost through evaporation [20]. This could be correlated to water loss in the Napa Valley region since world radiation maps indicate that they have similar mean solar radiation. So a significant reduction in water evaporation is definitely positive for the farming business.

The Aichi, Japan project, referred to previously, was developed by a research team from the National Institute of Advanced Industrial Science and Technology in Japan. The aim of their research was to compare the electricity output from an array which was water-cooled and another which was air-cooled [21]. The panels in this case were installed as an array lying at a slight tilt (1.3° south facing) on top of foam polystyrene board floating on top of the water body. The major variance in experimental results between the two systems was mainly due to the accumulation of bird dropping over the air-cooled PV system (where the water cooled system was kept clean due to the 10 minute regular water coverage). Hammond *et al.* [22] estimates an 8% reduction in efficiency due to surface solar radiation occlusion from the bird dropping, which could be recovered to a 3% loss after a heavy rainfall.

The installation in Gundlach Bunchu Wineries (2008) also in California is very similar to that in Far Niente (even in motivation, it being a winery too); the project was designed and executed also by SPG Solar. The main difference between the two is the array size, with that of Far Niente being much bigger at 175kW_p rated, while that of Gundlach Bunchu being just 30kW_p.

One of the biggest projects developed is that of Bubano, Italy at 500kW_p. This was realised by Byro, in 2009, which is a collaboration of four local companies which retain equal shares in the

project. This system is grid connected and takes revenue from the feed-in tariff. Prior to installation, a preliminary environmental impact assessment was required to outline any potential hazards to the ecosystem and lake fauna. The buoyancy for the installation is maintained with hollow polyethylene cubes at the two opposite edges and through which struts for the PV panel mounting are run through (Figure 2-4). The array is modular with four buoyancy cubes of either side holding 4 PV panels mounted at a slight incline. An interesting feature of this project is that, this was the first floating PV project which was exposed to snow and ice. The impact was only to the surface panels, since the climate it was set in was not cold enough for the surrounding waters to freeze. Thus consideration for the mooring and structure, for the thaw/freezing conditions did not need to be taken into consideration. The developers claim a 20-25% increase in electricity output due to the cooling effect from the water, consistent with the negative temperature coefficient performance for PV modules (higher temperatures leading to lower efficiencies and lower temperatures leading to higher efficiencies).

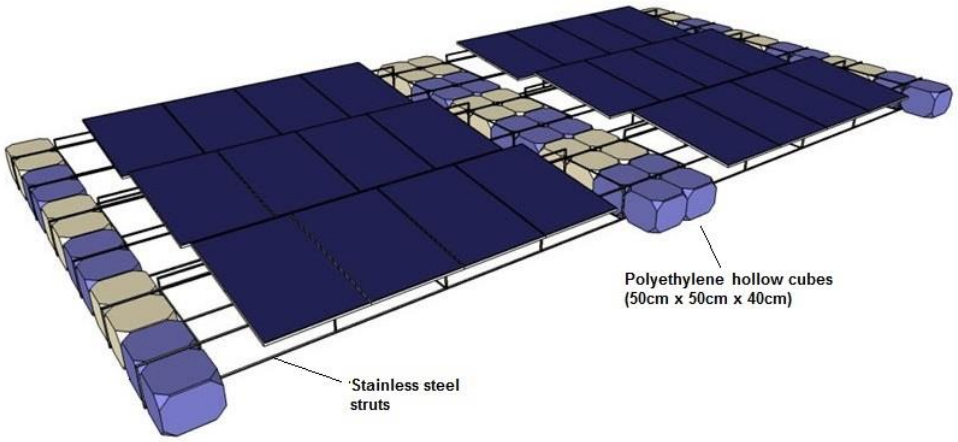

Figure 2-4: Schematic design of the floating PV installation in Bubano [23]

On the topic of evaporation of water reservoirs, a research team in Spain developed a 24kW$_p$ floating PV array on a water treatment reservoir in Negret, in 2009 with the primary objective of reducing water evaporation. This was expanded to a 300kW$_p$ array later the following year due to its good performance. This project is a collaboration between the Polytechnic University of Valencia and the company CELEMIN ENERGY. The array is made up of a number of modules each holding 2 panels, tilted at 10° (facing south) and fabricated by rotomoulding using medium density polyethylene [24] (refer to Figure 2-5). The platform has inserts for the electrical cables and the metal struts from the top. Its base is smooth and rounded to protect the reservoir's geomembrane and each of the modules are connected together with metal pin links, creating a flexible elastic system able of deforming to the concave profile of the reservoirs according to the changing water levels. Recorded annual electrical yield for the Negret PV array averaged at just under 30GWh since 2009 [15], at a capacity factor of approximately 13.5%. Economics given by Ferrer-Gisbert *et al.* [15] indicate that almost 45% of the costs were pontoon associated costs. The economic analysis highlighted in the same paper indicates profitability for the array installation at the Negret site, with an internal rate of return of 12.65%, which does not include any economic savings from the reduction in water loss.

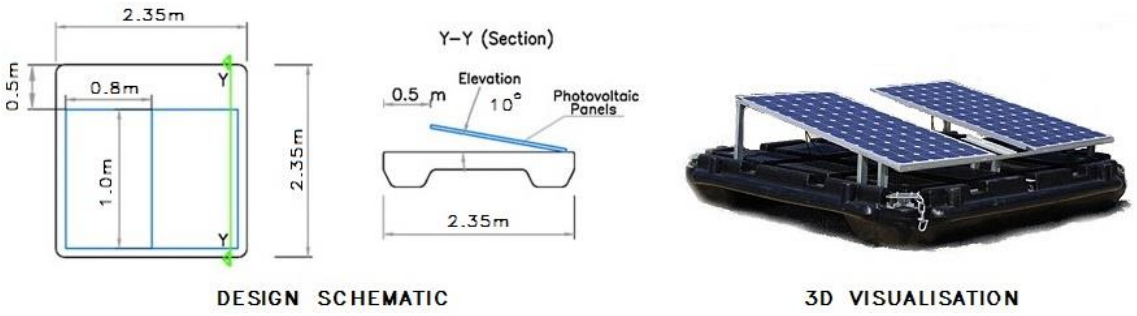

Figure 2-5: Polytechnic University of Valencia and CLEMIN ENERGY floating PV design [15]

The Solarolo project (2009), also in Italy, was designed by D.A.E.I.T. on top of an irrigation pond where they elected to only tilt them at 8° to maximise the power density output (by minimizing footprint of the array). The design realised by D.A.E.I.T. consisted of a modular array unit, of 20kW_p. The array unit construction is very similar to the structure in Bubano. The design logic behind this (and the installation in Bubano) is to minimise the structure components and also to create a channel through which the panels can be air-cooled from underneath (since there is no gap behind the panels, as those by SPG Solar, by which the panels can be air-cooled). Also the buoyancy at the sides rather than underneath allows a channel by which any individual panel can be physically reached. At the Solarolo site the cubic buoys are extended to the edge of the reservoir, as a platform, to allow continuous access to the installation (access to the Bubano site is solely by boat).

In 2010, the only project realised was that at Petra Winery in Italy, which was grid connected later in 2011. A special feature of this installation is that it includes a tracking system which rotates the system according to the sun`s motion. This was designed and constructed by Terra Moretti Holdings, while the research group at *Scienza Industria Technologia* (SCINTEC) were responsible with the tracking and safety systems. The motivation for this installation is similar to that Far Niente, since it is also situated in a winery. The structure of the array is made almost entirely of metal struts, with buoyancy (and integrated tracking system) underneath maintaining the whole structure afloat. The structure is designed to hold the crystalline panels at an optimal orientation of 40°, while tracking the solar motion.

The same group, SCINTEC, also developed the installation at Lake Colignola in 2011. This was developed at a prototype scale, 30kW_p in size, and similar to the Petra Winery installation, with a motor running the tracking system and was constructed entirely of metal struts with low lying tabular buoyancy keeping it afloat. The interesting aspect of this development was the utilisation of mirrors to reflect additional solar radiation onto the PV panels (similar applications with ground-mounted installations are reported in [25, 26]). The Lake Colignola's project PV panels are mounted horizontally rather than tilted, with mirrors positioned on the south and north face of the panel. The mirrors were placed at an angle of 60° and -60° respectively [27] and this is expected to double the solar radiation effective on the PV panels. This implies higher operational temperatures, so the proximity of the PV panels to the water is key in cooling the array in order to maintain the panel`s efficiency. Testing estimates a 60-70% increase in annual yield compared to a conventional fixed-ground mounted installation [28].

SCINTEC's next contribution to the field of floating PV was thanks to their partnership with the French company Osesol. Osesol have installed a 100kW_p floating PV array at Pommeraie-sur-Sevre (2012), in France, following the initial success they had with their 4kW_p prototype in Vendée (2011), also France. The Osesol installations are mounted on a structure constructed entirely from PVC, which resulted in some cost savings compared to the installations in Italy which required metal struts for the PV panel mountings. The other project SCINTEC helped design was in Korea, Cheongju (2012), built by Techwin in collaboration with Koinè Multimedia and SCINTEC. This project was especially challenging because of the climatic conditions the project was set in, with the waters surrounding the project subject to freezing temperatures during the winter months. Special consideration was taken in the choice of the individual

components within the installation, so that they were able of withstanding the seasonal freezing and thawing.

In 2011, D.A.E.I.T. and SPG Solar added two new projects to their portfolio. D.A.I.E.T. installed a replica of their Solarolo project in Avetrana, also in Italy, at the same 20kW$_p$ scale. In the case of SPG Solar they changed their design to accommodate the larger installation scale at Petaluma, California with an installed capacity of 350kW$_p$. Instead of the modular design used at Far Niente, they adopted a singular large pontoon structure on which the tilted PV panels were mounted and were installed with on-board inverters. The pontoon was tension tied to four buoys at each side of the rectangular floating structure, which were moored to the reservoir's bottom.

The majority of the projects discussed are installed in ponds and reservoirs used for irrigation, while a couple are in small lakes. The PV project in Canoe Brook Water Treatment Plant in New Jersey, USA, as indicated by the name was installed floating in a water treatment reservoir (like the Negret reservoir in Spain). This is a 112kW$_p$ installation designed by ENERActive and their main challenge was to adjust the mooring (which was subcontracted to Seaflex) to the changing levels in water within the reservoir and keeping the polystyrene floating structure (holding the tilted array of PV panels) in place during the freezing/thaw cycles.

Moving on to the Ciel et Terre development (installed in 2011) at the Piolenc site, in France, this was originally an abandoned quarry which has since been flooded. The PV panels are held tilted towards the sun with metal struts, which also links the array together, and is kept afloat with buoyancy underneath each row within the array. The site developers, Ciel et Terre, have submitted an application for a 12MW installation at the same site which would make it the

largest installation to date. Ciel et Terre have also established bases in other countries, mainly Japan and India and have submitted application for multi-megawatt installations in those countries on top of dams and lakes. Their last accomplishment was in Okegawa, Japan (2013) which holds the title for the largest floating installation at almost 1.2MW_p. The array is the similar to that in Piolenc and was constructed as modular panel units (consisting of 4,530 260W solar panels) in France and then delivered to site.

To match the installation at Bubano, is the 500kW_p installation at Hapcheon Dam, South Korea in 2012. This project is the first of a planned series of investments by Korea Water Resources Corporation (K-Water), who plan to build an installed capacity of 1,800MW_p by 2022 jointly with private companies. One of the motivations for the project was the lack of available ground and rooftop spaces for the large scales of photovoltaic installations envisaged and in the case of the ground installations also the limitations due to environmental planning. The crystalline PV panels of the arrays are mounted on metal struts which are tilted at the optimal solar radiation angle and kept afloat by mini-platforms. The materials chosen in the design had enhanced water and moisture resistance to decrease the chances of freezing and cracking.

On smaller scales in 2013 there were two additional projects one in Singapore and the other in Canada, both for research purposes. The one in Canada, presented herein, is discussed through the following research, because in contrast to all the other projects it is not mounted on a rigid pontoon but mounted directly onto the water surface while utilising a laminated thin film PV product. The project in Singapore is located in Bishan Park and was developed by Phoenix Solar as a test project, being monitored for one year, with data being recorded for research. The

outcome of this project could potentially lead to larger installations in Singapore. The panels here are mounted on a single pontoon with the crystalline panels at a slight incline, due south.

2.3.2 Floating PV Concepts

The projects realised throughout the 2007-2013 period are exclusive to self-contained water environments such as reservoirs, ponds and small lakes. This means that the requirements for the structure and mooring do not have to withstand harsh conditions of a marine (or large lacustrine) environments, characteristically including tides (not in lakes), high winds and large waves. The two concepts which have been proposed for such offshore environments have a similar logic in design and in contrast to existing floating PV installations, which incorporate mainly crystalline PV panels which are rigid, they utilise flexible thin film PV (Figure 2-6) to generate electricity. This is so that the structure can yield with the wave motion, rather than withstand its force, and hence allow the moorings to be subjected to significantly less loading force (which are a huge issue in reliability of offshore structures) [29].

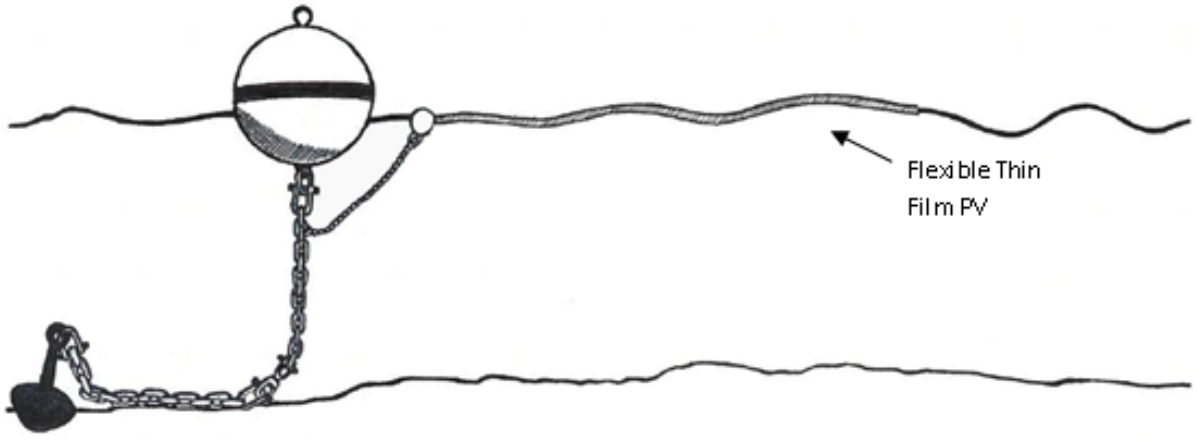

Figure 2-6: Schematic of the thin film floating PVs

MIRARCO's Floating PV Project

Figure 2-7: MIRARCO's Floating PV Prototype (Left) and the control ground mounted nearby panels (Right) – Sudbury, Canada

The first of these offshore floating PV concepts discussed here within was developed at MIRARCO (2010), a mining research company in Sudbury, Canada, with the aim of providing an alternative method for electricity generation for remote mines. This concept features a single scalable array (either with larger panels and/or a greater number of panels). The system is designed to have the terminal connectors connected to each other within the array, with the number of panels connected in series and parallel depending on the required output voltage. Buoyancy is designed to be potentially incorporated within the laminated thin film PV panels themselves with air pockets trapped within the lamination. The design is aimed to decrease the number of components within the project to maintain procurement and O&M (operations and maintenance) costs low and also increase the project's reliability (with less components prone to

failure). Also the aim is to have the panels in direct contact with the water surface to enhance the direct cooling by the water and allow self-cleaning.

MIRARCO have recently launched a 0.5kW$_p$ test project on a small pond in Sudbury, Canada (as featured in Figure 2-2) for data collection and analysis. For this prototype it was not feasible to integrate the buoyancy within the laminate, so thin strips of neoprene were glued to the back of the array. The neoprene strips allowed the panels to be linked together into an array; hence no further components for linking of the panels were required. Identical PV panels were installed as a control on the ground nearby in order to allow comparison between the two setups (Figure 2-7).

DNV's Floating PV Project

The other flexible floating PV concept is called SUNdy (2012), realised by DNV – Det Norske Veritas. The overall design is as described by Figure 2-8, and consists of a series of thin film PV panels connected together and then onto the electrical bus lines running through the hexagonal vertices. The panels themselves are envisaged to be laminated and adhered to a flexible foam surface which would give the panels buoyancy and structure. The panels are each rated at 560W and embedded within the underneath flexible foam is a 3 phase micro-inverter which converts the electricity from dc to ac directly. At the edge of the float embedded is also a marine grade connector which allows the panels to be connected to each other both mechanically and electrically. A transformer is located at the center of the hexagonal structure from which the electricity is delivered to shore. Plans are for walkways and water cannons, for the cleaning of the panels, to be located between the center and the vertices to allow access to the equipment.

The structural design is inspired from a spider web and is designed to be compliant with the waves while still being structurally strong and capable of maintaining its shape. The whole structure is designed to be kept in place thanks to catenary mooring at each of the vertices.

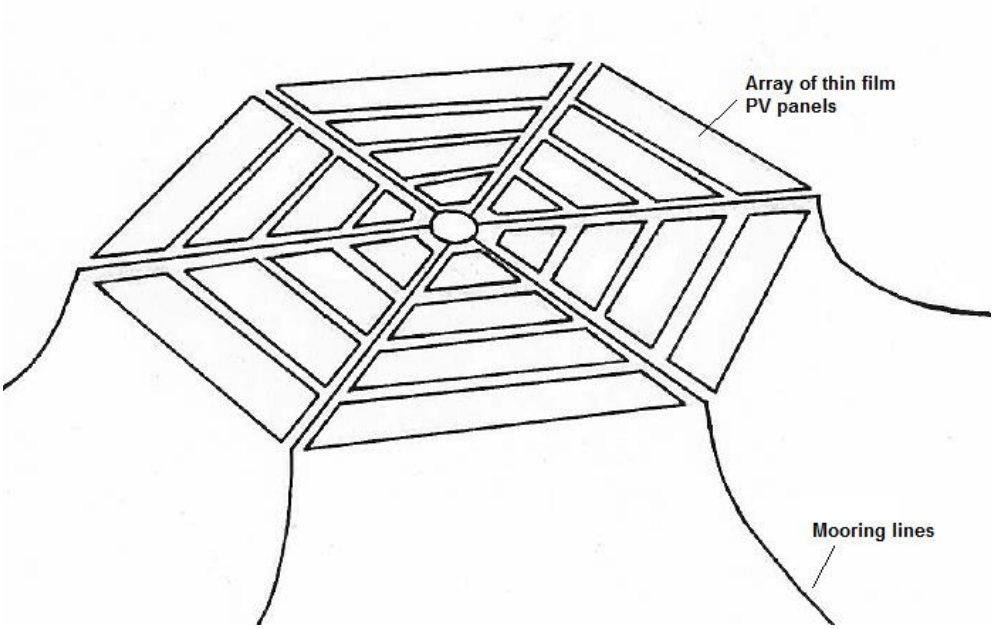

Figure 2-8: Schematic of the $2MW_p$ SUNdy concept, the hexagonal design consisting of 4,200 individual panels

Submerged PV Concept

The invention by M. Rosa Clot, P. Rosa Clot and S. Carrara [30] (SCINTEC) has some elements from both the existing projects (pontoon mounted projects) and the floating concepts being developed. This is since it utilises a rigid concept which is also in direct contact with the water as illustrated in Figure 2-9. The system cannot undulate with the oncoming waves due to it being rigid, so instead to withstand rough sea conditions it is designed to be able to submerge up to 2m.

The submersion and floating of the array is achieved by pumping in and out water respectively in surrounding enclosed buoys. For normal operating conditions the array is designed to be under just 0-2mm of water which according to research undertaken by SCINTEC would not deter the solar radiation effective on the PV panel's surface [12], while it would aid with the cooling of the panels to improve its electrical efficiency.

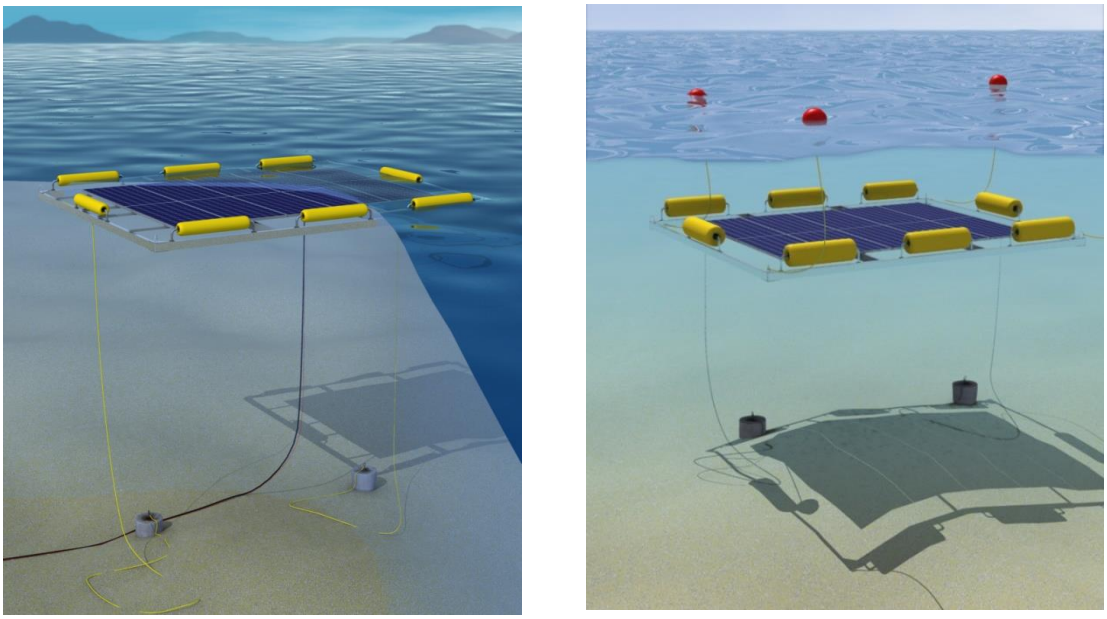

Figure 2-9: SCINTEC submergible floating PV concept [Copyright: Prof. Marco Rosa-Clot]

Concepts for future developments are aimed to exploit larger expanses of water on which to introduce this technology. This would mean that such an installation would be subjected to larger loads by the harsher sea wave environments. The concepts proposed for such environments envisage a flexible thin film structures able of undulating with the waves or else conventional rigid PV arrays which could be submerged in rough water conditions. The trend exposed by the projects timeline has indicated significant research towards the establishment of the floating PV

technology and the development of multi-megawatt scale floating PV arrays. Interest and current negotiations mostly in Asia indicate that we will be seeing larger installations in the near future. Floating PV arrays could become a front runner in renewable energy technology installations.

3 Hydrodynamics of large scale floating PV arrays

The motion of a floating thin film PV array should not vary significantly from those of the oncoming waves, this is because the laminates are not designed to harness mechanical energy from the waves and because they low have flexural rigidity. As will be set out, any floating thin film array mooring system would only be affected by a small load due to the array. Somewhat similar systems are the VLFSs (very large floating structures), which are also flexible arrays which occupy large expanses of the sea area – although flexible their flexural rigidity is significantly higher since their application is for airports, bridges, emergency bases and terminals.

There are numerous theories relating to the hydrodynamics of such large flexible floating bodies. Chen *et al*. [31] gives a detailed review ranging from theories developed as early as 1959 to 2003. They are classified into: two-dimensional linear theory, two-dimensional nonlinear theory, three-dimensional linear theory and three-dimensional non-linear theory. The literature review includes a large number of the Chinese and Japanese publications which due to language barriers are not generally acknowledged worldwide. The theories are mostly developed and widely accepted when dealing with linear responses, but not as much with nonlinear responses. Frequency domain methods are used to predict linear and partially nonlinear dynamic responses, while time domain methods are applicable to fully nonlinear interactions.

3.1 Hydrodynamic comparison of VLFSs and floating thin film PV arrays

The focus on the hydrodynamics of such floating structures is primarily due to their effect on the wave environment, which implies additional loading on the mooring systems due to these interactions. An analysis to prove the low energy interaction on the waves by the floating thin film PV array, draws a comparison with similar interactions between waves and VLFSs. This methodology is based on the equation of flexural rigidity for a plate. The flexural rigidity, D is defined as the force couple which is required to bend a non-rigid structure to a unit of curvature,

$$D = \frac{E_y h^3}{12\left(1-v^2\right)} \qquad [3\text{-}1]$$

where E_y is the Young's modulus, h is the thickness and v is the Poisson's ratio of the thin film array composite.

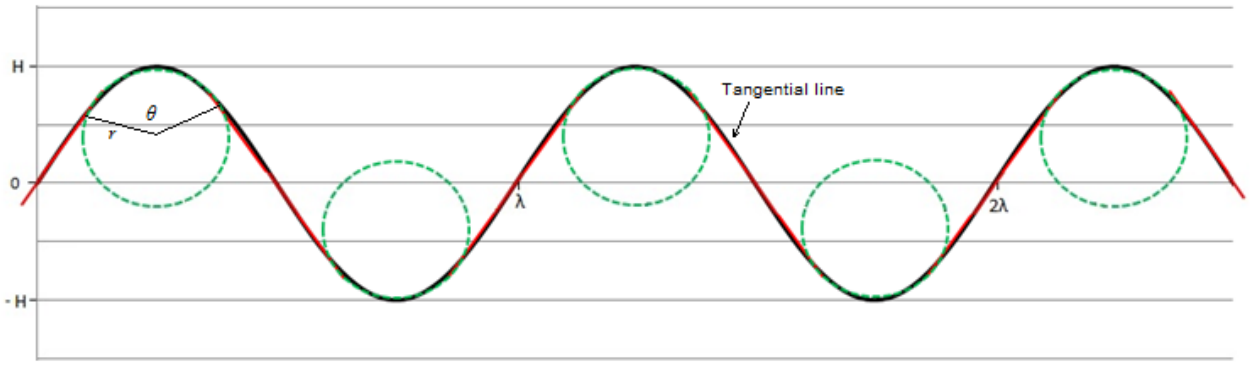

Figure 3-1: Illustration of the sinusoidal shape form in linear and circular segments

Considering the motion of the array in regular waves, would imply that the motion is sinusoidal. So the bending motion of the thin film PV array could be approximated to the same sinusoidal motion. Since a sea wave can in nature only exist at a steepness ratio (wave height to wavelength) of 0.141 [32], before the wave breaking, the wave can be reduced to a sequence of linear and circular segments as indicated in Figure 3-1.

The angle of curvature, θ (°) and the radius of curvature, r, were determined through the tangential lines with the curve intersecting the curve at the x-axis and which have a gradient equal to the differential of the wave curve at that point.

The energy extracted from the waves or required to bend the array when it is modulating according to the oncoming wave fronts can be calculated as a factor of the force:

$$E = \frac{Ld}{\lambda} 2F \qquad [3\text{-}2]$$

where

$$F = \frac{D}{r}\left(\frac{\theta}{360°}\right) \qquad [3\text{-}3]$$

and L is the length of the array, d is the width of the array, λ is the wavelength of the waves, r is the radius of curvature and θ is the angle of curvature.

Table 3-1: Physical properties for a VLFS (data from [33]) and a T3F-PV array (data recorded experimentally from a sample section of the array). Results are based on a wave environment of

λ = 212.2m, θ = 21.93°, H = 7.4m and r = 184.06m. (In shorter wavelengths the resulting wave height would be close to zero for VLFSs and still negligible for the T3F-PV).

Physical Property	Unit	VLFS	Thin Film Flexible Floating PV (T3F-PV)
Young's Modulus, E_y	*Pa*	1.19 x 10^{10}	2.29 x 10^{9}
Poisson ratio, v		0.13	0.40
Thickness, h	*m*	2.0	0.00044
Length, L	*m*	300	300
Width, d	*m*	60	60
Bending energy, E	*J*	4.53 x 10^{8}	1.09 x 10^{-3}

The decrease in energy from the waves due to the floating arrays can be summarised as follows, from the combination of equations [3-1], [3-2] and [3-3]:

$$E = \frac{1}{6} \cdot \left(\frac{E_y h^3}{1 - v^2} \right) \cdot \left(\frac{Ld}{\lambda \cdot r} \right) \cdot \left(\frac{\theta}{360°} \right) \qquad [3\text{-}4]$$

So for a VLFS system and a floating thin film PV array in the same wave environment with λ = 212.2m, θ = 21.93°, H = 7.4m, r = 184.06m and physical properties given in Table 3-1, the energy reduction in the waves would be equal to 4.53 x 10^{8}J for the VLFS and 1.09 x 10^{-3}J for the floating thin film PV system. Taking into consideration the energy embedded within the waves, $E = \frac{1}{16} \rho g H^2$ where ρ is the density of the water (taken to be 1025kg/m^3 in this analysis), g is gravity (9.81m/s^2) and H is the wave height, would result in a totally negligible percentage reduction of H for the floating thin film PV system (of 8.77 x 10^{-11}%), in comparison with a

reduction of 48.18% for the VLFS. In shorter wavelengths (~10m) the resulting wave height would be close to zero for VLFSs and still negligible for the T3F-PV. The low impact of the floating thin film PVs on the wave environment supports the hypothesis that its hydro-dynamical motion would be almost equivalent to that of the waves.

3.2 Review of forces acting of the floating thin film PV

This section aims to outline each of the forces acting on an array of floating thin film PV, in order to clarify the typical loads that may be expected on station keeping mooring loads. This material does not aim to undertake a detailed hydrodynamic analysis.

The external forces acting on a floating thin film PV array are wind, wave motion, and tidal current. The forces dependant on the floating body and mooring configuration are the buoyancy (B), weight (W), surface tension (S), and mooring tension (T). Figure 3-2 illustrates the main forces acting on the floating thin film PV array. Other forces which are usually considered in wave hydrodynamics [34] are the wave, tidal and wind inertia. The wave and tidal inertia are considered by Morrison's equation [35] for the wave excitation force, F_H which considers the tidal drag and the wave and tidal inertia, as follows:

$$F_H = \frac{1}{2}\rho_w C_{d\,water} A_w \left|u - \dot{X}\right|\left(u - \dot{X}\right) + \rho_w C_m V_w \dot{u} - M_a \ddot{X} = D_{tide} + I_{tide} + I_{wave} \qquad [3\text{-}5]$$

where u is the tidal velocity, V_w is the volume of array in water, $C_{d\,water}$ is the water drag coefficient and M_a is the added mass coefficient. The added mass coefficient can be equated to $\rho_w(C_m - 1)V_w$, where C_m is the inertia coefficient. $\dot{X}$ and $\ddot{X}$ are the velocity and acceleration of

the floating thin film PV array. D_{tide}, $I_{tide}$and I_{wave} are the resultant tidal drag, tidal inertia and wave inertia forces in the water fluid. The other force which would need to be considered is the downward force arising from tidal drag, N_{tide} acting perpendicularly to D_{tide}.

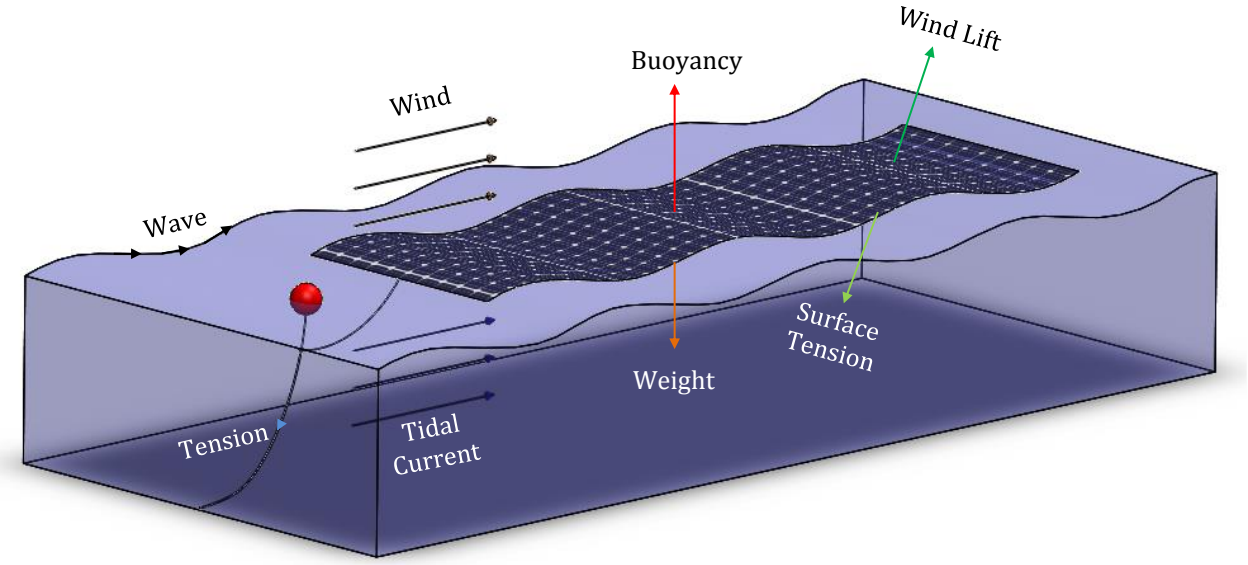

Figure 3-2: 3D schematic diagram of forces acting on the floating thin film PV array

The inertial components within the wave excitation force equation [3-5] depend on the volume of the array submerged in the water and it's mass. The structure being a thin film and having a low density of the material would suggest that these force components would be small. Determination of the energy required to overcome the flexural rigidity, undertaken in the previous section, 3.1 also supports this assertion, as the proportion of energy absorbed by the floating PV array was shown to be less than 0.1%.

The other main external force is an aerodynamics force, F_W and is a combination of the wind drag, lift and aerodynamic moments, represented by:

$$F_W = \frac{1}{2}\rho_a C_{d\,air} A_d \left(U - \dot{X}\right)^2 + \frac{1}{2}\rho_a C_L A_L \left(U - \dot{X}\right)^2 + \frac{1}{2}\rho_a C_a A_L \left(U - \dot{X}\right)^2 = D_{air} + L + I_{air} \quad [3\text{-}6]$$

where ρ_a is the density of the air, $C_{d\,air}$ is the air drag coefficient, A_d is the surface area of drag, U is the wind velocity, C_L is the lift coefficient, A_L is the lift surface area and C_a is the aerodynamic moment coefficient. D_{air}, L and I_{air} are the resultant forces due to air drag, air lift and aerodynamic inertia respectively in the air fluid medium.

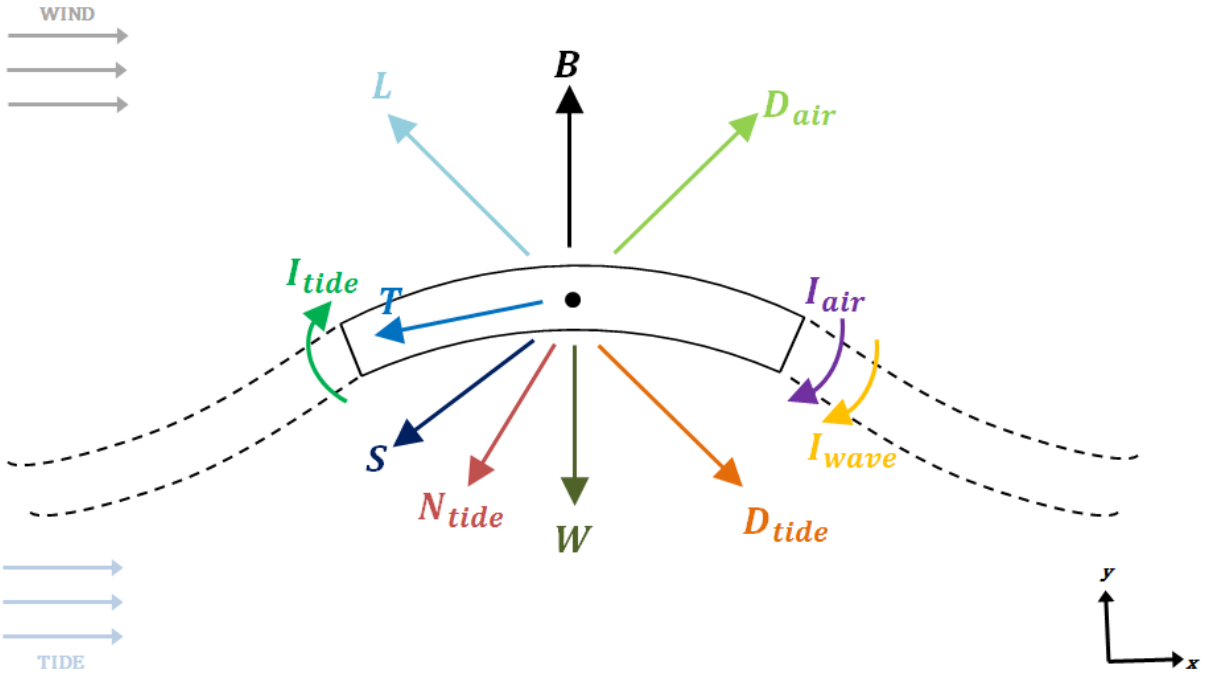

Figure 3-3: Free body diagram of a floating thin film PV array

Figure 3-3 shows a free body of a representative section element of the floating thin film PV array. The following equations highlight the force components acting in the vertical and horizontal direction:

$$\uparrow \quad B + L_y + D_{air\,y} + I_{tide\,y} - D_{tide\,y} - W - N_{tide\,y} - I_{wave\,y} - I_{air\,y} - S_y - T_y = 0 \qquad [3\text{-}7]$$

$$\rightarrow \quad D_{air\,x} + I_{tide\,x} + D_{tide\,x} - L_x - N_{tide\,x} - I_{air\,x} - I_{wave\,x} - S_x - T_x = 0 \qquad [3\text{-}8]$$

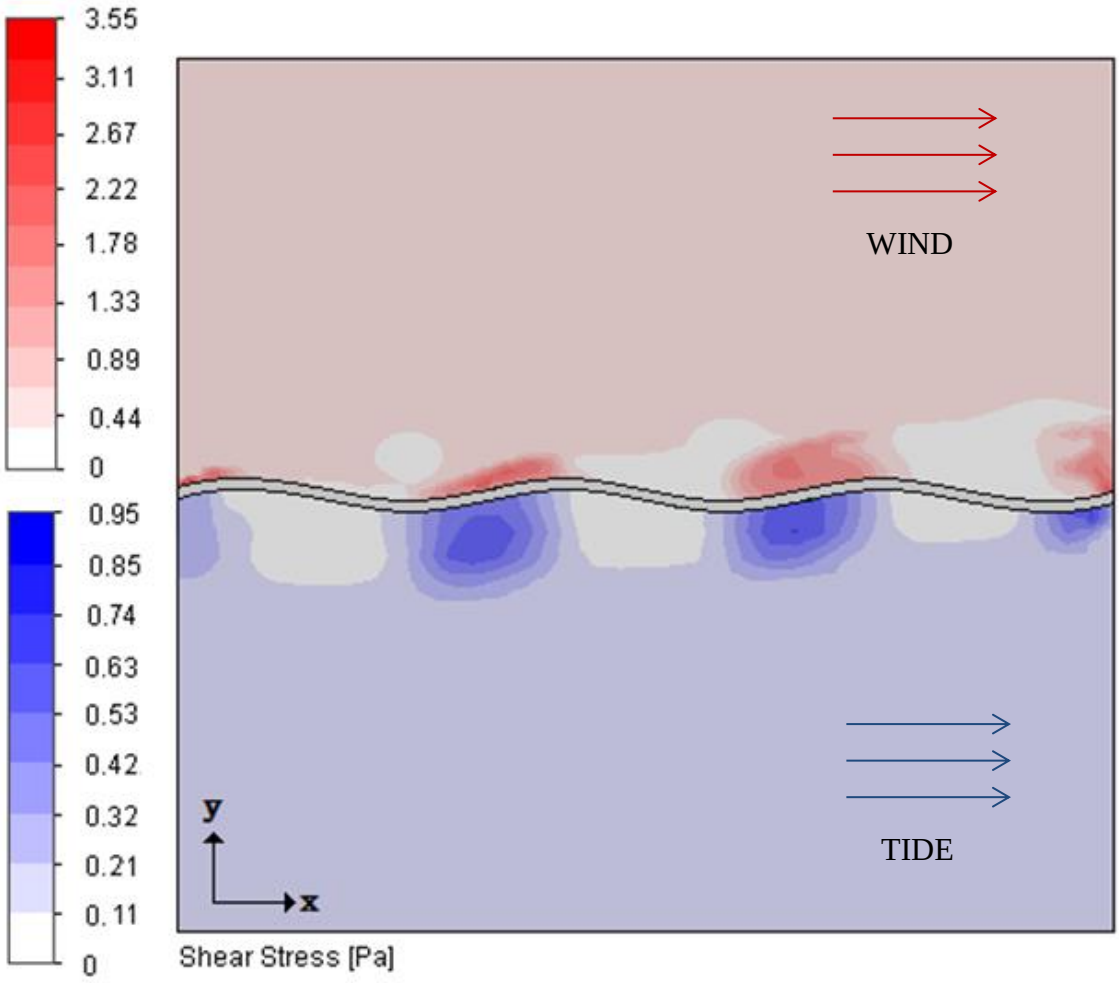

Figure 3-4: Shear stress acting horizontally on a floating thin film PV array (600m x 200m), with a wind speed of 25m/s and 0.5m/s, as produced a 3D CFD model [36].

In order to assess the resultant mooring load T, an estimate of each of the forces was made using numerical, analytical or computational fluid dynamics (CFD) methods; with T being the resultant

of all the acting forces remaining in equations [3-7] and [3-8]. The CFD simulation model was conducted using Solidworks Flow Simulation [36] for a 600m x 200m floating thin film PV array deforming with oncoming waves. The latter were taken to have a wavelength of 212m and wave height of 14.8m, according which to Garrison [37] are typical ocean waves. For a near shore environment, were the floating PV arrays are predominantly envisaged for deployment, 14.8m is an extreme wave height. The CFD modelling was simulated with a wind speed of 25m/s[1] and tidal current of 0.5m/s, acting in the same direction, to represent a challenging operating environment and subsequently at a wind speed of 50m/s and tidal current of 3.5m/s, to consider extreme conditions. Figure 3-4 shows the resulting shear stress acting on the top and underside of the thin film array, for the first case.

The lift, drag and inertia for the wind and tide were also determined from the CFD results to permit estimation of the horizontal and vertical forces acting on the floating thin film PV array. These are compiled in Table 3-2, which includes estimates of the remaining forces obtained as indicated.

Inspection of Table 3-2 reveals that the magnitude of some of the force components is negligible such that, equations [3-7] and [3-8] may be simplified to:

$$\uparrow \quad B + L_y + D_{air\,y} + D_{tide\,y} = W + N_{tide\,y} + T_y \qquad [3\text{-}9]$$

$$\rightarrow \quad D_{air\,x} + D_{tide\,x} = L_x + N_{tide\,x} + T_x \qquad [3\text{-}10]$$

[1] At such wind speeds wind turbines reach their cut-off speed [38] G. Boyle, O. University, Renewable energy: power for a sustainable future, Oxford University Press in association with the Open University, 1996.

Hence, the resulting mooring tension for equilibrium is:

$$\uparrow \quad T_y = B + L_y + D_{air\,y} + D_{tide\,y} - W - N_{tide\,y} \qquad [3\text{-}11]$$

$$\rightarrow \quad T_x = D_{air\,x} + D_{tide\,x} - L_x - N_{tide\,x} \qquad [3\text{-}12]$$

Table 3-2: Estimate of forces acting on a thin film PV array (600m x 200m)

	Name	Symbol	Quantification Method	Force per m^2 of thin film surface area	
				Challenging	Extreme
Vertical Forces	Buoyancy	B	Numerical: $B = \rho_w V_w g$	0 – 60N (varying with max. V_w)	
	Lift	L_y	CFD Modelling	6N	35N
	Air Drag	$D_{air\,y}$	CFD Modelling	0.07N	0.3N
	Air Inertia	$I_{air\,y}$	CFD Modelling	~0N	
	Weight	W	Numerical: $W = mg$	55N	
	Tidal Inertia	$I_{tide\,y}$	CFD Modelling	~0N	
	Tidal Drag	$D_{tide\,y}$	CFD Modelling	0.03N	1.1N
	Tide Normal	$N_{tide\,y}$	CFD Modelling	3N	130N
	Wave Inertia	$I_{wave\,y}$	Numerical: Flexural rigidity*	~0N	
	Surface Tension	S_y	Numerical: $S_y = \gamma \cdot p \cdot cos\theta$†	~0N	
	Mooring Tension	T_y	/	*Resultant*	
Horizontal Forces	Air Lift	L_x	CFD Modelling	1.2N	6.4N
	Air Drag	$D_{air\,x}$	CFD Modelling	0.8N	2.5N
	Air Inertia	$I_{air\,x}$	CFD Modelling	~0N	
	Tidal Drag	$D_{tide\,x}$	CFD Modelling	0.3N	10N
	Tidal Inertia	$I_{tide\,x}$	CFD Modelling	~0N	
	Tide Normal	$N_{tide\,x}$	CFD Modelling	0.5N	26N
	Wave Inertia	$I_{wave\,x}$	Numerical: Flexural rigidity*	~0N	
	Surface Tension	S_x	Numerical: $S_x = \gamma \cdot p \cdot sin\theta$†	~0N	
	Mooring Tension	T_x	/	*Resultant*	

* Numerical modelling conducted in Section 3.1

† γ, p and θ represent the surface tension (N/m), perimeter of the thin plate (m) and pull angle (°) respectively [39]; with γ taken to be 60mN/m and θ, 30°.

The magnitude of the tension components was assessed in Table 3-3. The resulting force $T = \sqrt{(T_y)^2 + (T_x)^2}$ was calculated accordingly for the two environmental conditions described. Results show that for the first condition (challenging) the tension forces in the *y*-direction balance, due to the buoyancy, while in the *x*-direction there is tension in the mooring line resulting in an overall 72kN of mooring load when considering the entire array. For the second condition (extreme environment), the down force from the tidal current is so great that it causes the panel to submerge. This combined with the large horizontal component due to drag, results in the total mooring load exceeding 10,000kN.

Table 3-3: Predominant force components acting on floating thin film PV structure at wind speed of 25m/s and tidal current of 0.5m/s (challenging) and at wind speed of 50m/s and tidal current of 3.5m/s (extreme), according to equations [3-11] and [3-12] with forces estimated in Table 3-2.

Challenging Conditions	*Extreme Conditions*
Wind Speed – 25m/s Tidal Current – 0.5m/s	Wind Speed – 50m/s Tidal Current – 3.5m/s
T_y = 52 N/m^2 + 6 N/ m^2 + 0.07 N/ m^2 + 0.03 N/ m^2 + -55 N/ m^2 + -3 N/m^2	T_y = 60 N/m^2 + 35 N/ m^2 + 0.3 N/ m^2 + 1.1 N/ m^2 + -55 N/ m^2 + -130 N/m^2
0 N/m^2 of thin film PV area	**-89** N/m^2 of thin film PV area
T_x = 0.8 N/m^2 + 0.3 N/ m^2 + -1.2 N/ m^2 + -0.5 N/ m^2 +	T_x = 2.5 N/m^2 + 10 N/ m^2 + -6.4 N/ m^2 + -26 N/ m^2 +
-0.6 N/ m^2 of thin film PV area	**-20**N/ m^2 of thin film PV area
T **= 72kN**	***T*** **= 10,950kN**

The wave rider buoy deployed by PRIMaRE [40] is reported to withstand a resultant 3.5kN mooring load. Consequently, the number of moorings of this type and rating required to maintain the 600m x 200m thin film PV array, is approximately 21. Depending on the mooring configuration their rating may have to be doubled to deal with the predominant drag directions. Higher rated mooring lines, such as those for wave energy converters, have mooring ratings upwards of 500kN [41]. On such a rated mooring line, an area of 900m x 900m of floating thin film PV array could be deployed, under these challenging conditions. The installed capacity of thin film PV is estimated to be 16MW and having a capacity factor of 0.25% at the equator, according to Table 7-8 and considering additional area for the mooring spacing.

The extreme case condition is extreme. The down force noted for the tidal drag is of interest. Once the array is submerged with the tidal current passing above and below the panels, tidal down force will be balances by tidal life and the mooring tension would be substantially reduced (aerodynamic lift will then be zero). Such an observation needs to be substantiated with, for example, testing of individual modules in a tidal flume with a load cell in line with the mooring.

3.3 Station-keeping

There are two main types of moorings: surface and subsurface [42]. The surface type has a floating buoy, while the subsurface moorings have a submerged buoy (as illustrated by Figure 3-5). The surface type mooring has to be more heavily designed since it would be exposed to rougher wave conditions. In the case of the floating thin film PV array a surface mooring type will be considered, since a subsurface mooring type would induce a downwards load onto the array which could result in partial submersion in some wave conditions. The moorings can be

further categorised according to their mooring arrangements, which are catenary or tension moorings for spread moorings applicable to such a system (Figure 3-6).

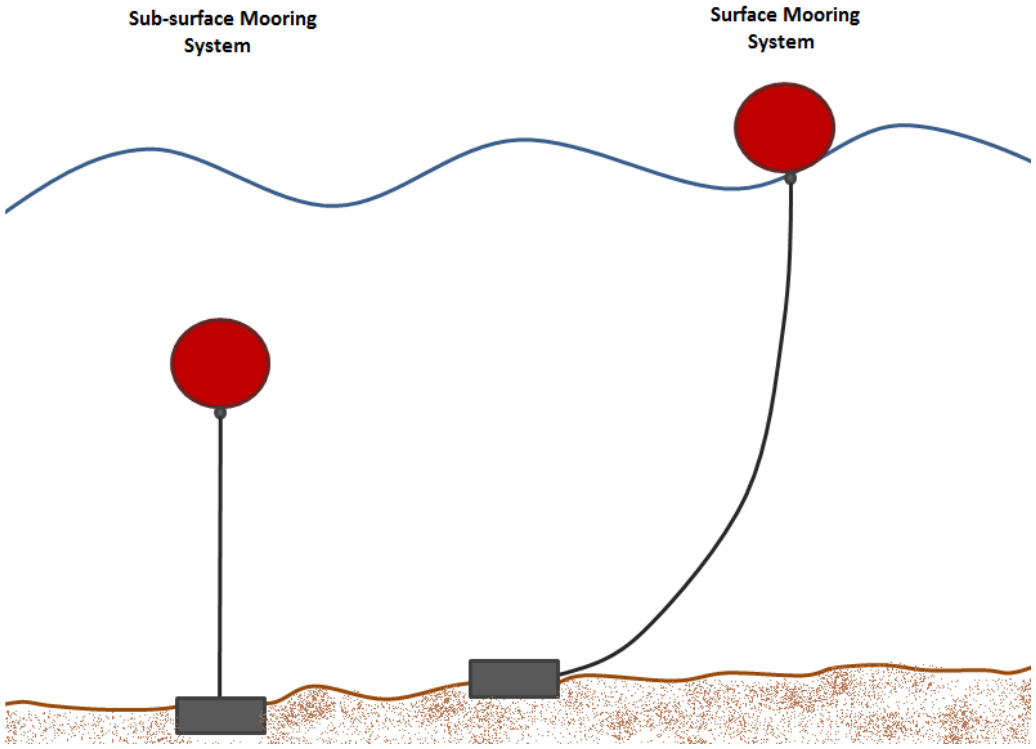

Figure 3-5: Diagram of a surface and subsurface mooring system

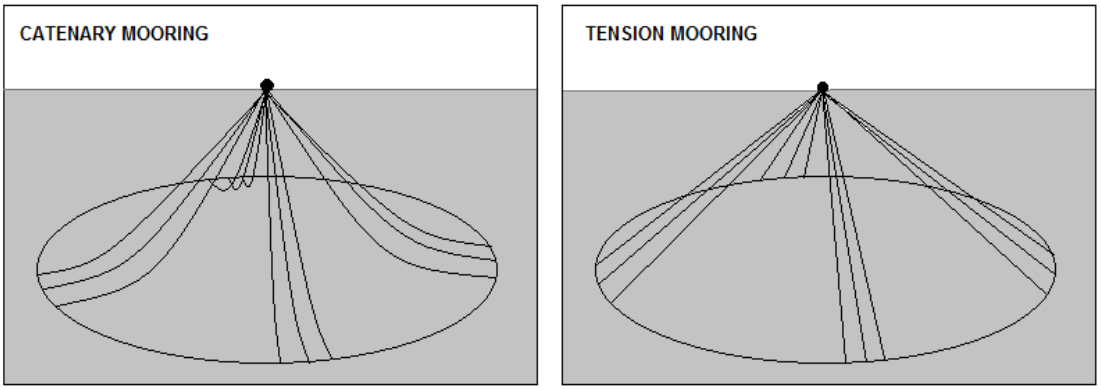

Figure 3-6: Illustration of a catenary and a tension mooring system

Table 3-4: Anchor type characteristics, compiled from [43] and [44].

	Drag	Deadweight	Pile	Plate
Description	Anchor embedded in seabed with mooring loading being parallel to the ground.	Mooring loading is horizontal to ground and due to friction provided by the seabed and deadweight loading.	Vertical drilled pile into the ground, with vertical loads due to the friction along the pile and the mooring line.	Vertically driven plate which has vertical and horizontal forces acting on it from the mooring line and due to the weight of the ground above it.
Cost	Medium	Medium	High	High
Pros	Developed anchoring technique, able of withstanding high loads (>100,000lbs). Various types and sizes available. Anchor is recoverable.	Can be constructed on site, and material economical if available. Reliable over hard ground with thin sediment coverage.	Withstands uplift. Relatively short mooring line. High capacity (>100,000lbs) possible. No potential for dragging. Suited for hard grounds and coral.	Withstands uplift. Relatively short mooring line. High capacity (>100,000lbs) possible. No potential for dragging. Suited for hard grounds and coral. Relative light weight structures and does not protrude from seabed.
Cons	Long mooring lines. Anchor not suitable for vertical loads. Is not suitable for hard ground conditions. Could damage other utilities such as pipelines, cables, etc.	Low opposition to horizontal loads, in comparison to other anchoring types. Expensive due to requirement of large load handling equipment and vessels.	Cost depends on water depth and availability of pile driving machinery. Requires site data to design pile anchoring.	Cost depends on water depth and availability of plate driving machinery. Requires site data to design plate anchoring. Anchor is not recoverable. Anchor cable susceptible to fatigue failure.
Catenary	Primary choice for sediment seafloors. Broad experience use.	Primary choice for limited sediment or rock ground. Needs larger load handling equipment.	Applicable but expensive.	Applicable but expensive.
Multi-catenary	Suitable if used with sinkers to reduce uplift forces. Limited to sediment bedding.	Practical option for limited sediment or rock ground. Handling equipment will drive cost.	Applicable but expensive, unless a large number of piles are being considered.	Applicable but expensive (less than piles though), unless a large number of piles are being considered
Tension	Cannot handle uplift loads	Applicable in limited sediment grounds but costs could be high in deep waters.	Suitable, although more costly than plates in deep sites. Required site knowledge.	May be the least cost option for sediment seafloors but not appropriate for rock.

Focussing on a surface mooring, the tension moored system is constricted in movement and so occupies a small surface area whereas catenary mooring has longer mooring lines (approximately 3 times the depth) which allows the surface mooring buoy to move over a greater area, corresponding to the length of the mooring line. Either tension or catenary mooring could be employed based on area limitations, seabed conditions and costs (since the anchoring system would have to be designed accordingly). The anchoring characteristics by type are given in Table 3-4, and are compared according to mooring type. The other major component making up the mooring system is the mooring line.

Mooring line material is typically from wire rope, chain and synthetic rope (with their costs increasing from low to high respectively) [43]. Chain is good for catenary moorings as its weight helps to keep the mooring in touch with the seabed near to the anchor, and also it has good abrasion and bending properties. Wire ropes have good elastic properties and so are ideal for high tension systems. Similarly synthetic ropes also have good elastic properties but they are virtually weightless, so they are utilised as tethers especially in deep water applications [43].

Depending on the type of mooring required a combination of the three mooring line types could be used. This ensures that the line has the elasticity, flexibility and abrasion properties as needed. Connecting elements would be required to ensure proper connections between each of the materials; these include swivels, links, winches and shackles, according to DNV standards for long-time mooring systems [43]. An example of a typical mooring configuration is given in Figure 3-7, this various type of mooring lines being used within the single mooring system along with other components, such as shackles.

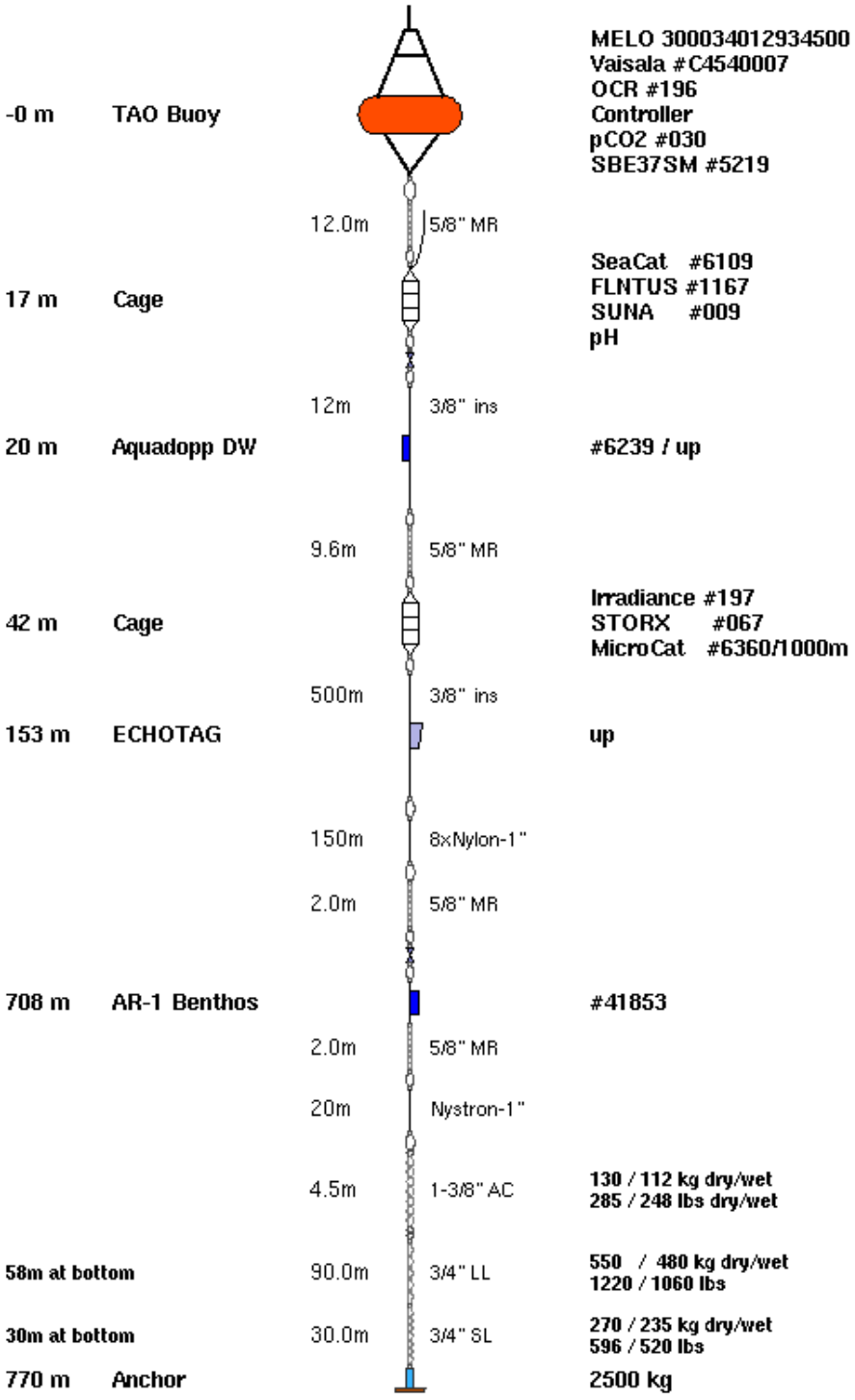

Figure 3-7: CCE-2 mooring configuration [45]

4 Electrical yield modelling of a sinusoidal thin film solar array for offshore applications (floating thin film PVs)

The objective of this part of the research were to model the yield output of a solar PV array in wave motion and compare the output to that of a panel lying perfectly horizontal. For this study a sinusoidal model was utilised to represent the panel's shape floating on top of the water, which would imply that this model would only be applicable to regular wave front environments. Also the solar exposure of the array when static in a sinusoidal shape was taken to be representative of the solar exposure on the panels when they are moving dynamically with sinusoidal form. This can be justified for large arrays where the ratio of array length to wavelength is very large.

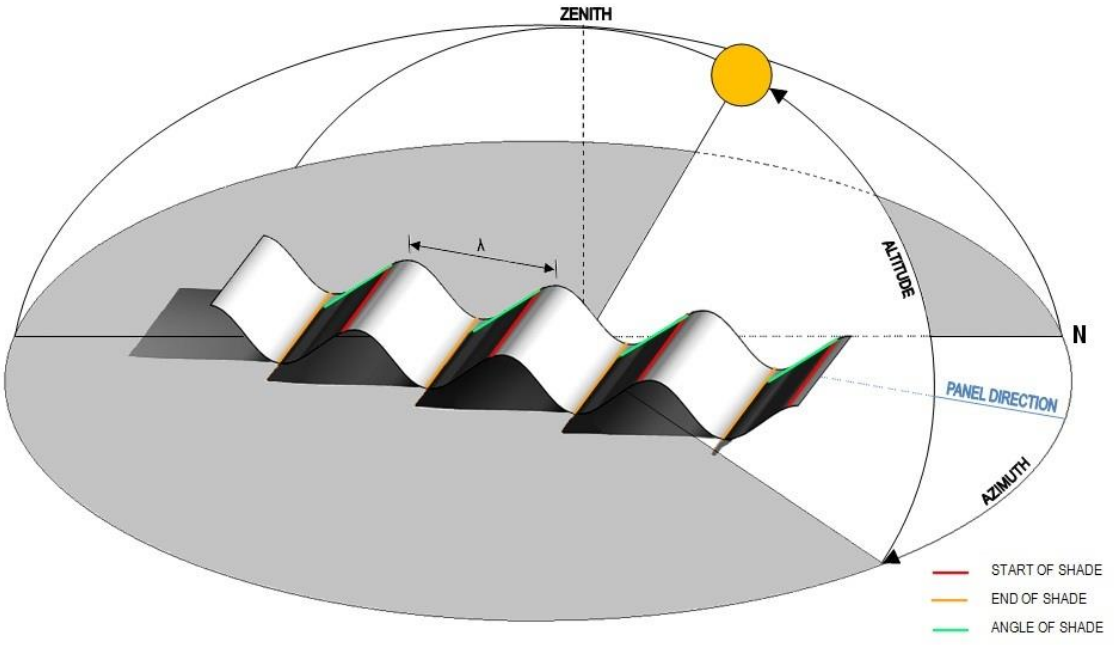

Figure 4-1: Diagram showing the different parameters taken into consideration for the estimation of the solar intensity and illustrating the shadowing effect from each sinusoidal peak.

The methodology applied required discretization of the PV array surface in a meshed grid, with the mesh size equivalent to each PV module within the PV panel, in order to determine if the mesh was shaded or not (from the peak of the wave form, Figure 4-1). The yield was determined for each PV module within the mesh based on the orientation and the shading ratio. Shaded PV modules not only reduce yield, but can act as a resistance, reducing net output of the entire PV panel. Since the overall electrical output from the array (refer to Figure 4-2) results through i) the optimised output of the series connected modules (considering by-pass diodes) with the individual PV panels, ii) the series connection of each PV panel within the row, and iii) the parallel connection of each row of panels.

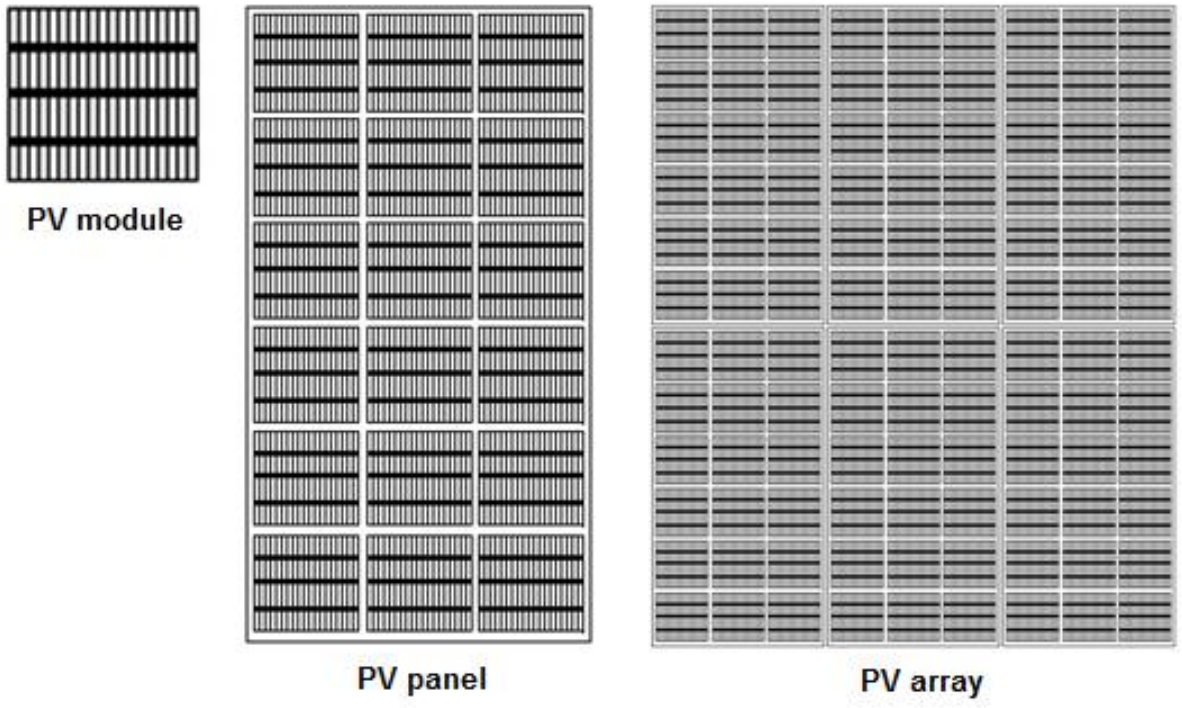

Figure 4-2: Representation of a PV module, PV panel and a PV array

4.1 Methodology

The electrical yield output from the solar thin film PV array depends upon i) the curvature of the array and hence the effective solar radiation incident on a panel of the array, ii) the shading by the peak of the wave form and iii) the electrical connections between the modules within the array. In order to evaluate the electrical output, the array had to be discretized into a grid, so that the effective solar radiation could be estimated for each mesh/PV module within the grid.

4.1.1 Grid Generation

The grid for the discretized mesh of the array was first generated at an angle of 0° away from the north and then rotated horizontally to consider the different propagation direction of the floating thin film PV array on the sea surface. The unit mesh area was taken to be of size L_x by L_y (see Figure 4-3). The deformation was taken to be acting in the x-z plane, in accordance with the equation:

$$z_n = A \cdot \cos\left(2\pi \cdot \frac{x_n}{\lambda}\right) \qquad [4\text{-}1]$$

where A is the amplitude of the wave height, λ is the wavelength, z_n is the z-coordinate at n and x_n is the x-coordinate at n.

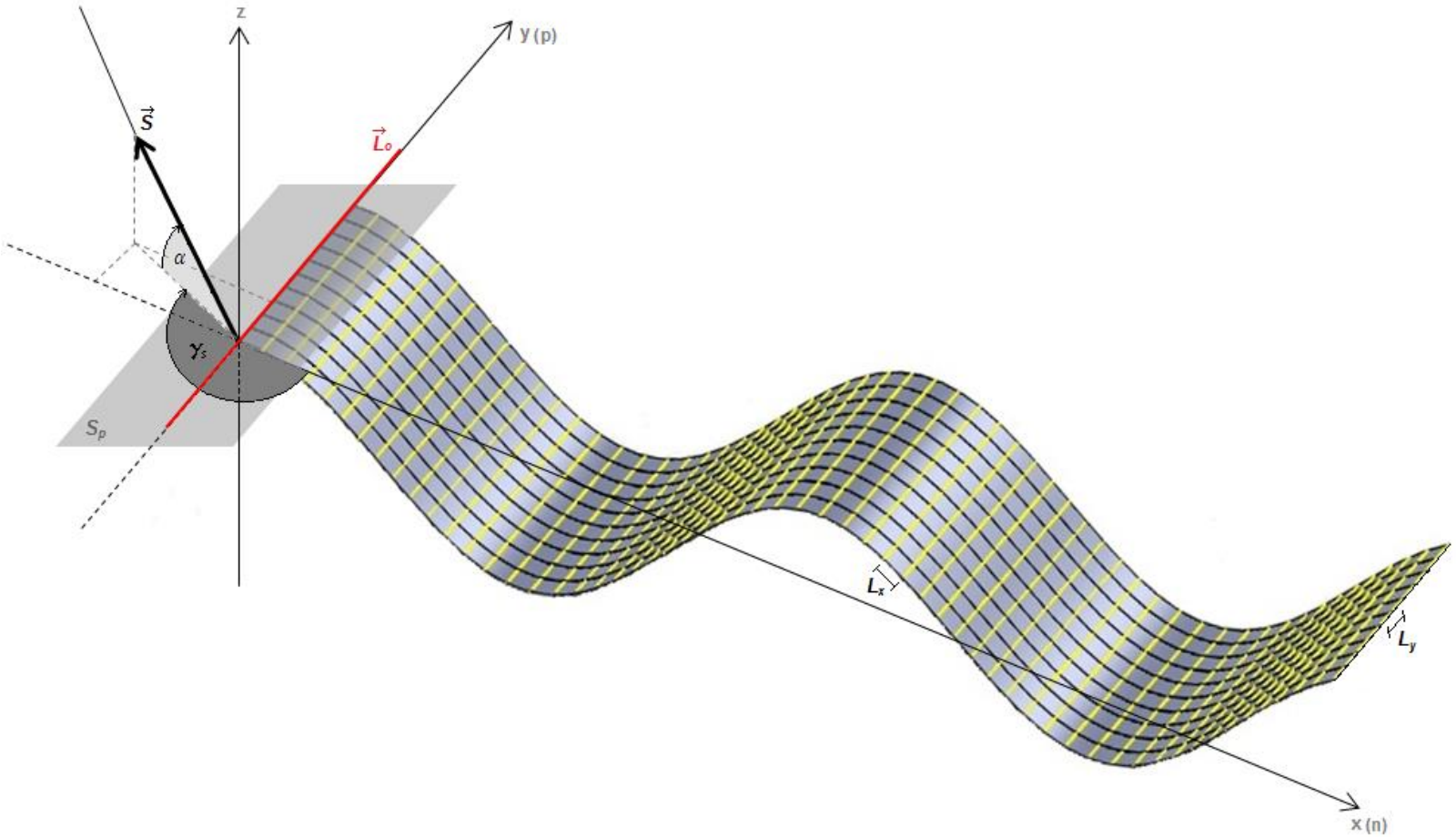

Figure 4-3: Discretized PV panel, L_x indicates the mesh size along the x-z plane while L_y shows the mesh size in the y-axis. Vectors and planes used in the shading derivation are highlighted.

The value for any point, P on the grid is (x_n, y_p) where y_p is directly proportional to the mesh size in the y-direction and x_n varies according to the deformation, and so is a function of solved z_n which could be solved iteratively from the simultaneous solution of equation [4-1] and the Pythagorean equation, where ${L_x}^2 = ({x_n}^2 + {z_n}^2) - ({x_{n-1}}^2 + {z_{n-1}}^2)$. Hence:

$$y_p = p \cdot L_y \qquad [4\text{-}2]$$

and

$$x_n = \frac{1}{2} \cdot \frac{1}{\pi} \Bigg\{ 2\pi \cdot x_{n-1} + \Bigg[{L_x}^2 \cdot \lambda^2 - A^2 \cdot \lambda^2 \cdot \cos\left(2\pi \cdot \frac{x_n}{\lambda}\right)^2 + 2A^2 \cdot \lambda^2 \cdot \cos\left(2\pi \cdot \frac{x_n}{\lambda}\right) \cdot$$

$$\cos\left(2\pi \cdot \frac{x_{n-1}}{\lambda}\right) - A^2 \cdot \lambda^2 \cdot \cos\left(2\pi \cdot \frac{x_{n-1}}{\lambda}\right)^2 \Bigg]^{1/2} \Bigg\} \qquad [4\text{-}3]$$

These x, y, z coordinates for the grid points as mentioned previously are only relevant if the panel is at a 0° angle from the north. The following matrix shows the equations by which the x, y, z coordinates are rotated to the x', y', z' coordinates at an angle ϕ from the north according to the direction of wave propagation.

$$\begin{pmatrix} x' \\ y' \\ z' \end{pmatrix} = \begin{pmatrix} x_n \cdot \cos(\phi) + y_p \cdot \sin(\phi) \\ -x_n \cdot \sin(\phi) + y_p \cdot \cos(\phi) \\ z_n \end{pmatrix} \qquad [4\text{-}4]$$

4.1.2 Shading Characterisation

The methodology in determining the shaded areas of the grid was developed by the concept given by J. G. Corripio [46] for digital elevation models (DEMs). This takes a plane orthogonal

to the solar vector and projects the normal from the points to the plane. The distance from the line of origin, L_O (shown in Figure 4-3) to the projected points can then be used to determine whether that point is shaded by another point or not.

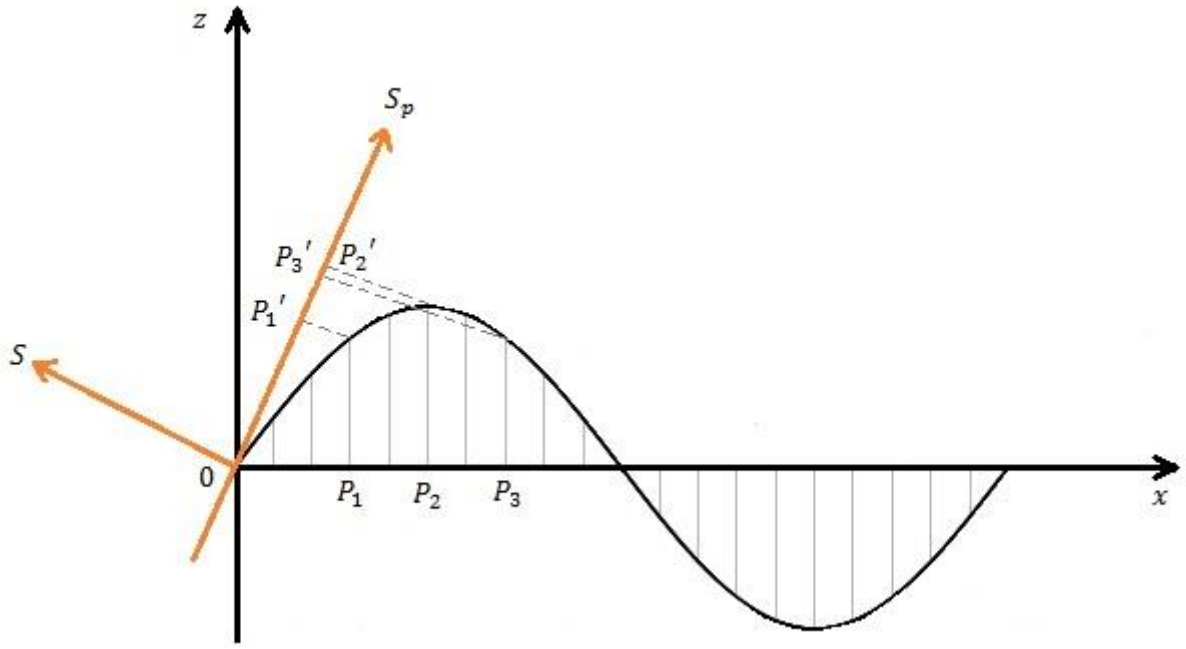

Figure 4-4: Graphical representation of the shading methodology

As illustrated in Figure 4-4 the grid points are projected onto the plane orthogonal to the solar vector, S_p and the distance from P_n' to the line of origin, L_O is indicative of whether the point is shaded. The solar plane, S_p can be calculated as follows since it passes through the point of origin $\langle 0,0,0 \rangle$ and is normal to the solar vector $\vec{S}$.

$$S_p = \begin{pmatrix} x \\ y \\ z \end{pmatrix} \cdot \vec{S} = \begin{pmatrix} x \\ y \\ z \end{pmatrix} \cdot \begin{pmatrix} \cos(\alpha) \cdot \cos(\gamma_s) \\ \cos(\alpha) \cdot \sin(\gamma_s) \\ \sin(\alpha) \end{pmatrix} \quad [4\text{-}5]$$

where α is the sun's altitude and γ_s is the sun's azimuth.

The line vector $\overrightarrow{L_O}$ passing through the origin, parallel to the plane S_p and perpendicular to vector $\vec{S}$ can be determined by taking the cross product of the vector normal to the plane $x - y$ and $\vec{S}$. Hence:

$$L_O = \begin{pmatrix} -\cos(\alpha) \cdot \sin(\gamma_s) \\ \cos(\alpha) \cdot \cos(\gamma_s) \\ 0 \end{pmatrix} \quad [4\text{-}6]$$

from which the distance from the projected point, $P_n{}'$ to the line, L_O be evaluated as:

$$D = \sqrt{\left(\frac{|P_n \times V_L|}{|V_L|}\right)^2 - \left(\frac{|P_n \cdot \vec{S}|}{|\vec{S}|}\right)^2} \quad [4\text{-}7]$$

The grid was analysed for the range of n values in the $x - z$ plane. If the distance $P_n{}'$to L_O is smaller than the highest preceding distance of $P_{n-1}{}'$to L_O, then the point P_n was shaded, and if it was greater than the point P_n was not shaded and becomes the highest preceding distance to be considered for the next point. A value of zero was assigned to the shading factor, S_{sh} if the grid/mesh was shaded at that point and a value of $S_{sh} = 1$ if it was not shaded.

---

* P_n was considered rather than the vector P_n to origin point, because the origin point of the grid is at ⟨0,0,0⟩, thus making the vector equal to P_n.

4.1.3 Variation in solar energy intensity according to mesh tilt

The solar energy intensity for the tilted meshes can be calculated using the equation for the effective solar energy intensity on a tilted plane:

$$I_{t\beta} = S_{sh} \cdot I_{B\beta} + I_{D\beta} + I_{R\beta} \quad [4\text{-}8]$$

where $I_{t\beta}$ is total solar energy intensity on the plane inclined at an angle β, and $I_{B\beta}$, $I_{D\beta}$ and $I_{R\beta}$ are the direct, diffuse and reflected components of the sunlight respectively acting on a plane with tilt β.

The direct solar energy intensity on the tilted plane can be calculated using data on direct solar energy intensity on a horizontal plane, I_{BH} and knowledge of the sun's position (altitude and azimuth), at the time of evaluation, with respect to that of the panel.

$$I_{B\beta} = I_{BH}\{\sin\alpha \cdot \cos\beta + \cos\alpha \cdot \sin\beta \cdot \cos(\gamma_s - \phi)\} \quad [4\text{-}9]$$

where α is the sun's altitude, γ_s is the sun's azimuth and ϕ is the angle of the panel's direction with respect to the north.

Liu and Jordan's [47] model, which assumes that the two components of diffused radiation (background diffused radiation and ground reflected radiation) are isotropic, is used to determine the conversion factors for evaluation of the two components of diffused radiation at the tilted plane, β.

The conversion factor for the sky diffused radiation, assuming a sky of uniform intensity, is $\frac{1+\cos\beta}{2}$. For the reflected diffused radiation, with the ground approximated as an infinite plane, the conversion factor is $\frac{\rho\cdot(1-\cos\beta)}{2}$, where ρ is the albedo coefficient. Hence the total incident solar energy on a tilted plane is:

$$I_{t\beta} = I_{BH}\cdot\cos(90-\alpha) + I_{DH}\left(\frac{1+\cos\beta}{2}\right) + \rho(I_{BH}\cdot\sin\alpha + I_{DH})\left(\frac{1-\cos\beta}{2}\right) \quad [4\text{-}10]$$

where I_{DH} is the diffused component of the solar energy intensity on a horizontal plane.

The albedo coefficient is estimated from the model of Dvoracek & Hannabas [10] which predicts the albedo for water bodies. This model relies on the data from Table 2-2 and adoption of the Equation 2-1.

4.1.4 Estimation of the Electrical Yield Output

The electrical output from a PV panel depends not only on the magnitude of solar intensity effective on the panel, but also on how the solar cells are connected together within the panel (in series, in parallel or a combination of both). The simplest cell connection configuration is one with all the cells connected together in series (minimising connections), although with such a connection, if a cell in a series string was not exposed to any solar radiation, then the entire string would produce no electric power. To mitigate this, by-pass diodes can be introduced within the panels.

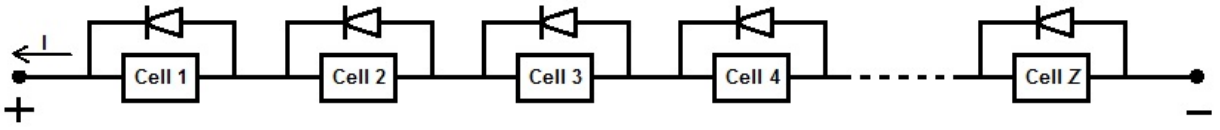

Figure 4-5: Electrical schematic of a Uni-Solar ePVL-136

For the research conducted herein the specifications of a Uni-Solar ePVL-136 panel (Figure 4-5) were considered. The IV curve for the Uni-Solar ePVL-136 was modelled through the following equation for a range of voltages ranging from 0V to V_{OC}:

$$I = I_{SC}\left\{1 - \exp\left(\frac{-\tau^2}{\varphi}\cdot\left[100\cdot\tau\cdot\frac{V_{OC}-V}{V_{OC}}\right]\right)\right\} \quad [4\text{-}11]$$

where I is the is the panel's current at a specific solar intensity, R for which I_{SC} is the short circuit current and V_{OC} is the open circuit voltage. The constants τ and φ are shape parameters within the equation, which have been fitted to the IV curve specifications of the Uni-Solar ePVL-136.

The I_{SC} and V_{OC} were derived from the following equations, which take into consideration the solar intensity, R_{STC} and short circuit current, $I_{SC_{STC}}$ at STC[2] (Standard Test Conditions) and the shape constants κ and ξ:

$$I_{SC} = \frac{R}{R_{STC}}\cdot I_{SC_{STC}} \quad [4\text{-}12]$$

[2] Radiation intensity of 1000W/m^2, temperature of 25°C and an air mass of 1.5AM

$$V_{OC} = \sqrt[\kappa]{\frac{R}{\xi}} \quad [4\text{-}13]$$

The maximum power point for each individual solar cell within the panel can be determined from the IV curve, plotted according to equation [4-12]. The electrical output from the entire panel considers the usage of by-pass diodes at each module to allow optimisation of the electrical output from the serially connected string of PV modules, forming the group of PV modules within the PV panel.

4.2 Modelled Results

The visual basic (VBA) code developed from the methodology described in Section 4.1 was applied to a 500m x 500m thin film array which was modelled at the three wave steepness ratios, $s = \frac{H}{\lambda}$ given in Table 4-1.

Table 4-1: Conditions necessary for a fully developed sea, modified from Garrison [37]

Wind Conditions			**Wave Size**			**Wave Steepness**
Wind Speed in One Direction	Fetch	Wind Duration	Average Height, $H = 2A$	Average Wavelength, λ	Average Period	s
km/hr	*km*	*hr*	*m*	*m*	*sec*	
19	19	2	0.27	8.5	3.0	0.0159
56	518	23	4.1	76.5	8.6	0.0268
92	2,627	69	14.8	212.2	14.3	0.0697

Each of the wave steepness ratios were modelled at 2 wave propagation directions $\phi = 0°$ (in the north/south direction) and $\phi = 90°$ (in the east/west direction) with hourly solar radiation data

for latitudes -50° to 50° at a longitude of 0°. The results were obtained using an Intel Core i7 CPU at 2.93GHz and 4GB of RAM, with hourly time series used within the model taken from satellite derived solar radiation data [48].

Table 4-2: Electrical yield from floating array under a sinusoidal waveform, propagating N (0°)

	Wave Height, H (m)	0	0.135	2.05	14.8	0.135	2.05	14.8
	Wavelength, λ (m)	/	8.5	76.5	212.2	8.5	76.5	212.2
	Wave Steepness, S	/	0.016	0.027	0.070	0.016	0.027	0.070
Latitude (°)	50	101630	108752	98613	90120	7.01	-2.97	-11.33
	30	158221	159360	152992	138389	0.72	-3.30	-12.53
	0	175221	203552	197585	176488	16.17	12.76	0.72
	-30	155826	173991	168194	151191	11.66	7.94	-2.97
	-50	103404	86715	80373	75556	-16.14	-22.27	-26.93
		Electrical Yield (W/m^2/annum)				Electricity Yield Change (%)		

The results obtained from the execution of the described model show variances in electrical output both with regards to project location (i.e. latitude) and the wave propagation direction. Analysis of the hourly electrical yield from the array demonstrates that impacts of shading are mainly in the early and late hours of the days, as expected, and this is also when the solar radiation intensity is low. In the cases were the panels were oriented east/west, the effects of shading were more prominent, especially in the higher and lower latitudes. This is because at these latitudes at the time of the peak solar radiation (mid-day), the sun is not high enough to produce a shade on the array surface. On the other hand, for the panel directed north/south, the tilt on the sinusoidal shaped array allowed higher levels of direct radiation which resulted in higher yields compared to the east/west direction.

Shadowing and mismatched electricity output from different modules had greater influence on the electrical yield of the array in higher and lower altitudes than in central latitudes (as indicated in Table 4-2 and Table 4-3). Analyses of the solar radiation yields effective on the array were less impactful, indicating the significance of energy conversion and connectivity between the modules. In central latitudes the deformation of the thin film PV resulted in higher electricity conversion yields, than if considering a flat array, due to the higher elevations of the sun.

Table 4-3: Electrical yield from floating array under a sinusoidal waveform, propagating E (90°)

	Wave Height, H (m)	0	0.135	2.05	14.8	0.135	2.05	14.8
	Wavelength, λ (m)	/	8.5	76.5	212.2	8.5	76.5	212.2
	Wave Steepness, S	/	0.016	0.027	0.070	0.016	0.027	0.070
Latitude (°)	50	101630	97630	85981	75423	-3.94	-15.40	-25.79
	30	158221	146278	139831	140394	-7.55	-11.62	-11.27
	0	175221	181031	173558	148137	3.32	-0.95	-15.46
	-30	155826	157838	150951	130079	1.29	-3.13	-16.52
	-50	103404	83519	76756	70505	-19.23	-25.77	-31.82
		Electrical Yield (W/m^2/annum)				Electricity Yield Change (%)		

4.3 Results Overview

4.3.1 Static vs. Dynamic Wave

When considering a thin film solar PV array which is floating in direct contact with water waves, as the waves are in continuous, dynamic motion so are the panels floating on top of them. The research conducted considered a static sinusoidal surface for the estimation of total annual solar yield, which is assumed to result in identical yields for a surface in motion. This was assumed because the wave form of a surface wave on a body of water at a fixed point in time has the same

form as the wave form of the same surface wave passing through a fixed point in space (as shown by Figure 4-6).

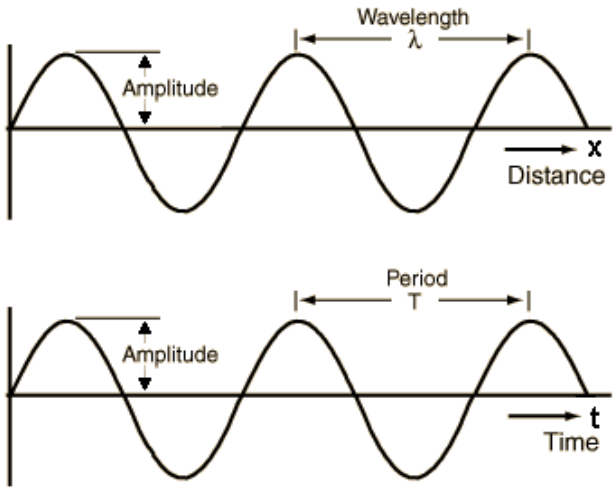

Figure 4-6: Displacement versus time plot for an idealised ocean wave passing through i) top – fixed point in time and ii) bottom – fixed point in space [49]

For long wavelengths, such as 212.2m wavelengths considered in Table 4-2 and Table 4-3, the length of the individual panels is small in comparison and so the variance in the effective solar intensity at each cell would be small and have no significant effect on the overall yield output. At smaller wavelengths, less than the panel's length, the propagation of the wave would have an effect on the estimated output electrical yield provided that the variation in overall solar intensity is significant. Since maximum wave steepness is *circa* 0.141, this would imply at these smaller wavelengths the wave would be just a ripple. Such a wave would not have a wave height high enough to alter the solar intensity significantly from mesh to mesh, since its profile would be

almost horizontal (especially when considering the damping the solar PV array would provide to the oncoming wave ripples).

4.3.2 Regular vs. Irregular Wave

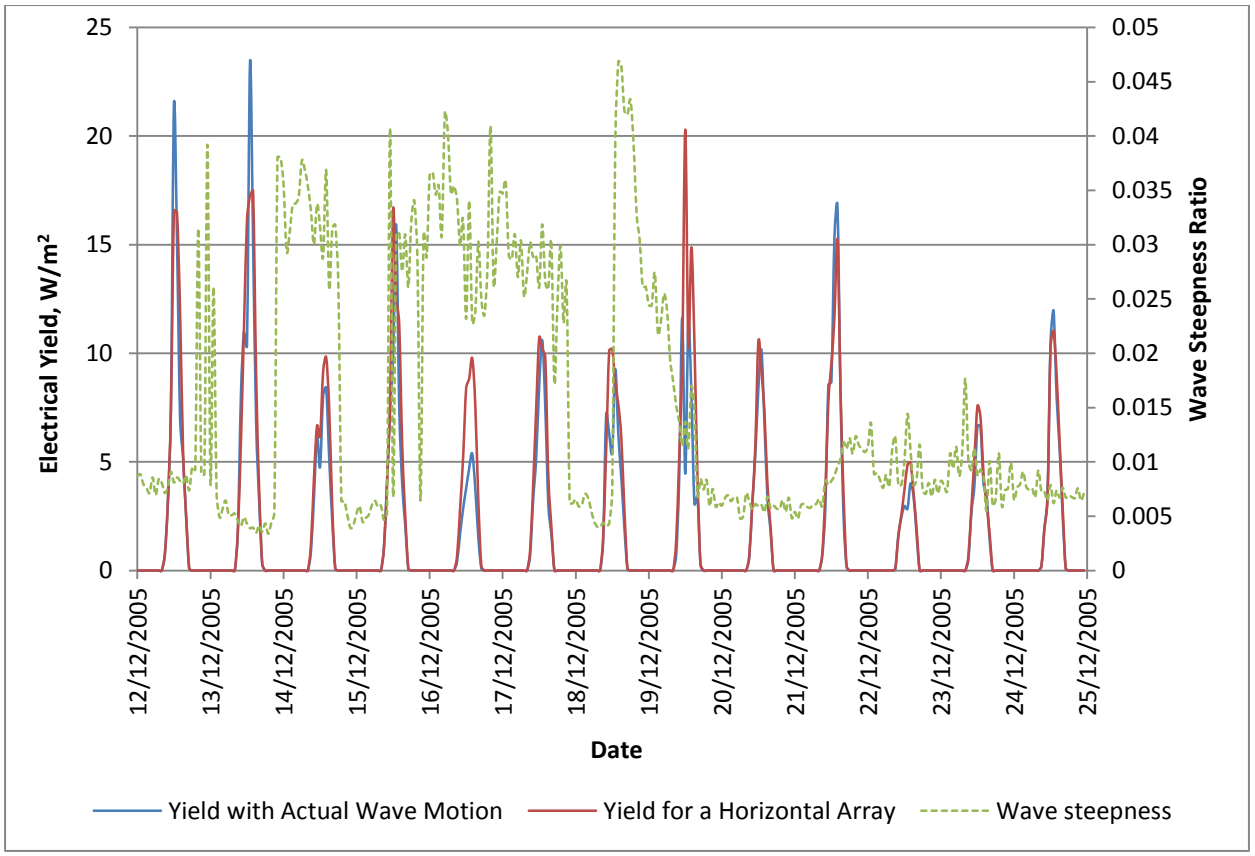

Figure 4-7: 13 day electrical yield output from modelling of a floating PV array moving according to actual wave motion and comparing the output from a horizontal array

Ocean and sea waves are not sinusoidal, but irregular due to numerous non-linear effects that affect the waveform. A so-called 'fully developed sea' [49] is frequently conceived as a superimposition of sinusoidal wave forms with varying amplitudes and frequencies. Typically

wave data is presented as a scatter diagram which shows the frequencies, throughout the monitoring period, for which various sea states occur. Since the electricity output is correlated not only to the wave state but also the position of the sun, time series wave data has to be considered for the electrical yield model of a thin film PV array in irregular waves. The interval of the data has to be such to allow solar variations to be modelled.

Hourly time series data recorded from a wave buoy, located at 50°21.29'N, 5°4W with a sea depth of 52m, from 11/12/2005 to 10/04/2006 was integrated within the model to estimate the electrical yield of a flexible floating PV array moving according to actual wave motion, and compared with a horizontal array. The wave form motion was taken to be a changing sinusoid based on the significant wave heights and periods recorded from the wave buoy on an hourly interval.

The modelled results showed a variation of 0.3% in electrical yield output between the two scenarios, with the summative yield (for the period of wave data available) being 18,253W/m^2 and 18,309W/m^2 for the array moving according to the wave motion and horizontally respectively. A sample graphical data of the results are represented in Figure 4-7, it shows that for higher wave steepness ratios (hence where shadowing is more prominent on the moving array) the output from a horizontal lying array is higher. For lower wave steepness ratios the output from either array is generally similar, while for mid to lower steepness ratios depending also on the wave direction the electrical yield output from the array moving according to the wave motion was slightly higher.

4.3.3 Temperature Effect

In the research undertaken temperature was not taken into account when estimating the electrical yield output. Temperature is an important factor in power output of a PV panel and one of the reasons for deploying a panel in direct contact with the water level is that it can benefit from the cooling effect of the water. This is due to the negative temperature coefficient of PV panels, which dictates that for every °C increase from the temperature at STC, being 25°C, the efficiency of the PV panel decreases by a certain percentage. For the panel taken into consideration in this study, the Uni-Solar ePVL-136, this is -0.21%/°C.

A study conducted by the The Nara Institute of Science and Technology [50], shows that the temperature of a ground mounted PV panel was an average of 13°C in February and 44°C in July. Satellite data [48] for the same year gives the average air temperature to be 4.3°C and 25.2°C for February and July respectively. Assuming that the air temperature and water temperature are equivalent, although realistically the temperature of an open water body would be expected to be lower in July and slightly higher in February, the temperature of the PV module can be taken to be 4.3°C in February and 25.2°C in July since water is a good heat conductor and will maintain thermal equilibrium of the panel with the water body. The cooling could result in a decrease of 8.7°C and 18.8°C in panel temperature for February and July respectively; this would be equivalent to an increase of 1.8% and 3.9% respectively in overall efficiency.

Hence for a better prediction of the electrical yield output it would be sensible to account for the variation of the air temperature (or better, water temperature) from the STC temperature of 25°C. This is for consideration in future research.

5 Water absorption characterisation, electrical reliability and mechanical testing of a submerged laminated a-Si thin film photovoltaic (PV) cells

Uptake of floating PV solutions [51], for increased availability of space requirement for renewable electricity generation, includes additional environmental parameters which need to be considered for wide spread implementation. This is especially the case if the floating PV array is in direct contact with the water surface (Figure 5-1); potentially leading to water absorption and issues is the PV's microelectronics reliability. Study more focussed on the electrical degradation of the a-Si PV cells due to humidity has been conducted by Tan et al. [52].

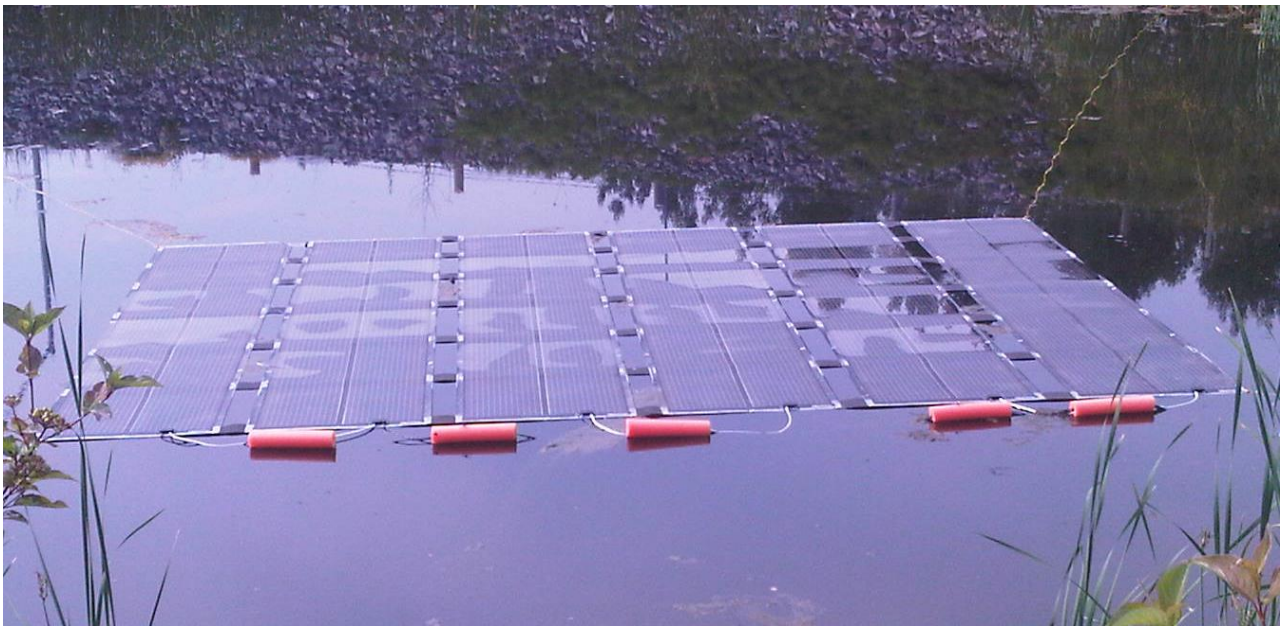

Figure 5-1: Floating thin film PV array prototype in Sudbury, Canada

The research conducted in Chapter 5, is targeted towards the characterisation of water absorption (according to ISO 62 [53]) for a-Si ETFE laminated thin film PV (with EVA lamination adhesive and stainless steel backing). Load testing of samples cut from the floating array after the 45day testing was performed (according to ASTM D882 for tensile testing of thin plastic sheets [54]) to observe any changes in the material's stiffness.

5.1 Outline of Experimental Testing

5.1.1 Water Absorption Characterisation

Table 5-1: Chemical composition of the fresh water and saline solution (diluted by a factor of 1000, with and hence with results multiplied by 1000).

	Detection Limit	Fresh Water	Saline Solution
Al	0.60	<DL	1460
As	1.00	1.53	10.4
B	1.00	15.2	0.001
Ba	0.87	16.9	15.1
Ca	10.0	19800	<DL
Cd	0.80	<DL	<DL
Co	0.60	<DL	<DL
Cr	0.06	0.334	<DL
Cu	1.80	162	538
Fe	4.00	<DL	<DL
K	6.00	1740	<DL
Li	0.40	0.804	31.8
Mg	1.00	5820	9850
Mn	0.20	<DL	<DL
Mo	0.40	<DL	<DL
Na	2.00	65.4mg/L	1.27%
Ni	0.40	35.3	<DL

Results are in µg/L (ppb) unless otherwise stated

The focus of this part of the research was mainly to determine the water absorption in fresh water conditions, although lab testing was conducted in a salt solution too to assess any variations in

results. The chemical composition of the water solutions in which the laminated thin film PV panels were submerged is given in Table 5-1, measured by a Varian Quadrupole ICP-MS (inductively couples plasma mass spectroscopy).

The submerged samples were put in water baths of the two water solutions, and testing was conducted at four temperature ranges (23, 35, 50 and 68°C with ± 2% accuracy). A schematic of the experimental rig is given in Figure 5-2. The moisture gains within the samples (after initially being left in the oven at 50°C overnight) were recorded at 24, 48, 96 and 192hr intervals. The samples at room temperature (23°C) were maintained submerged to verify water saturation of the laminates. The samples were 7.5cm x 7.5cm (± 1mm) and 0.85mm thick, a photographic image is given in Figure 5-3.

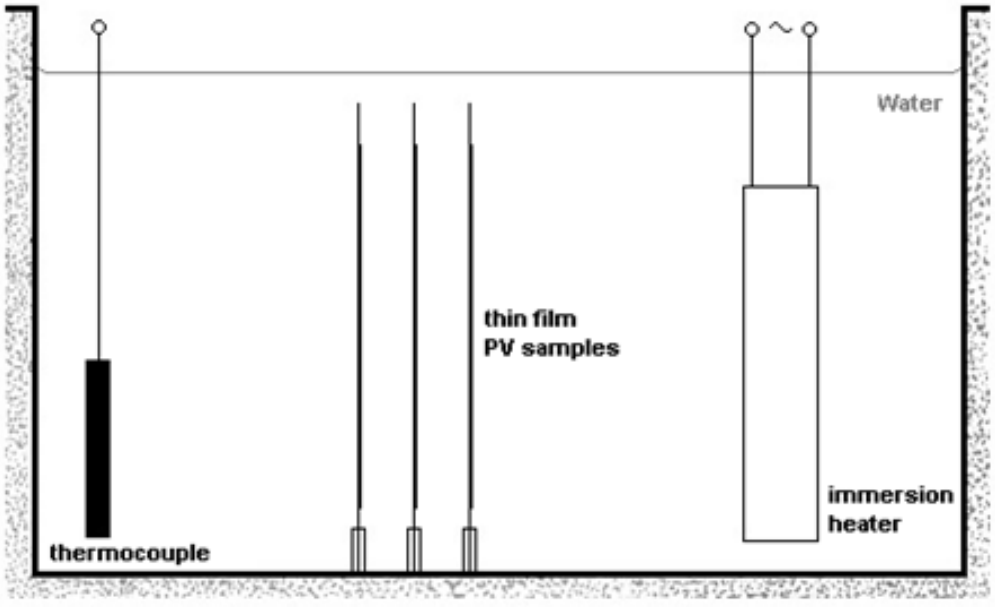

Figure 5-2: Experimental rig schematic

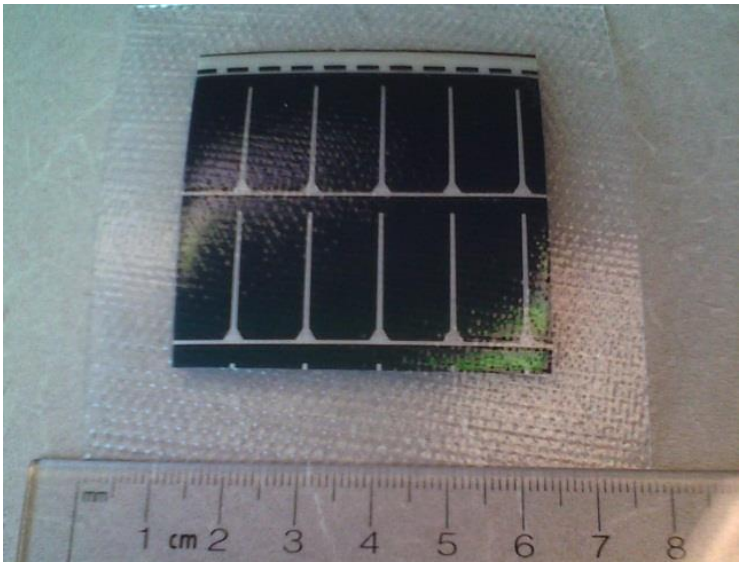

Figure 5-3: Sample thin film PV panel

5.1 Tensile testing

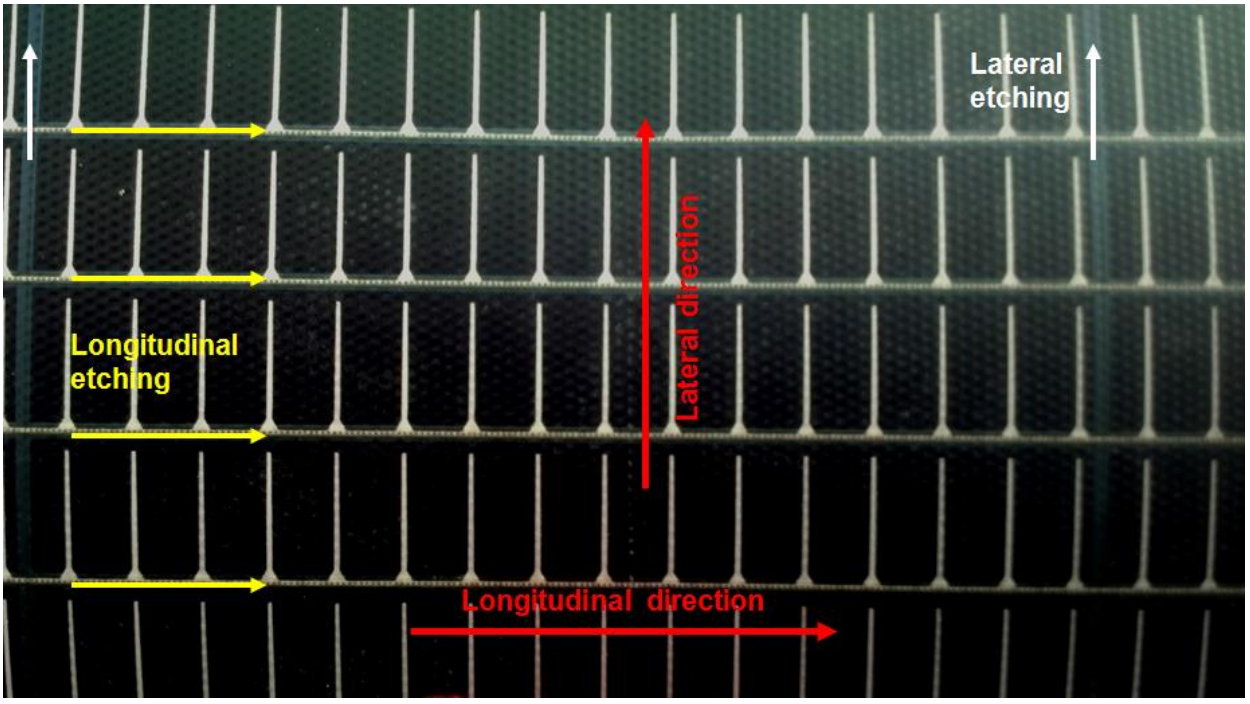

Figure 5-4: Highlight of key features of the thin film PV panel

The tensile testing was performed to determine the stiffness of the material accounting for the water absorbed within the laminate. Testing was conducted using a Tinius Olsen load frame test rig, with displacement control which was measured digitally through a pressure sensor feeding directly into the computer and calibrated through the manufacturer's software. Samples from identical panels: i) dry and ii) subjected to water absorption (cut after absorption), were cut along the longitudinal and lateral direction of the panels (indicated in Figure 5-4) and effective load withstood to failure was calculated. Custom grips (Figure 5-5) were then glued onto the specimen samples, to ensure proper load transfer and fitting between the load frame and the samples.

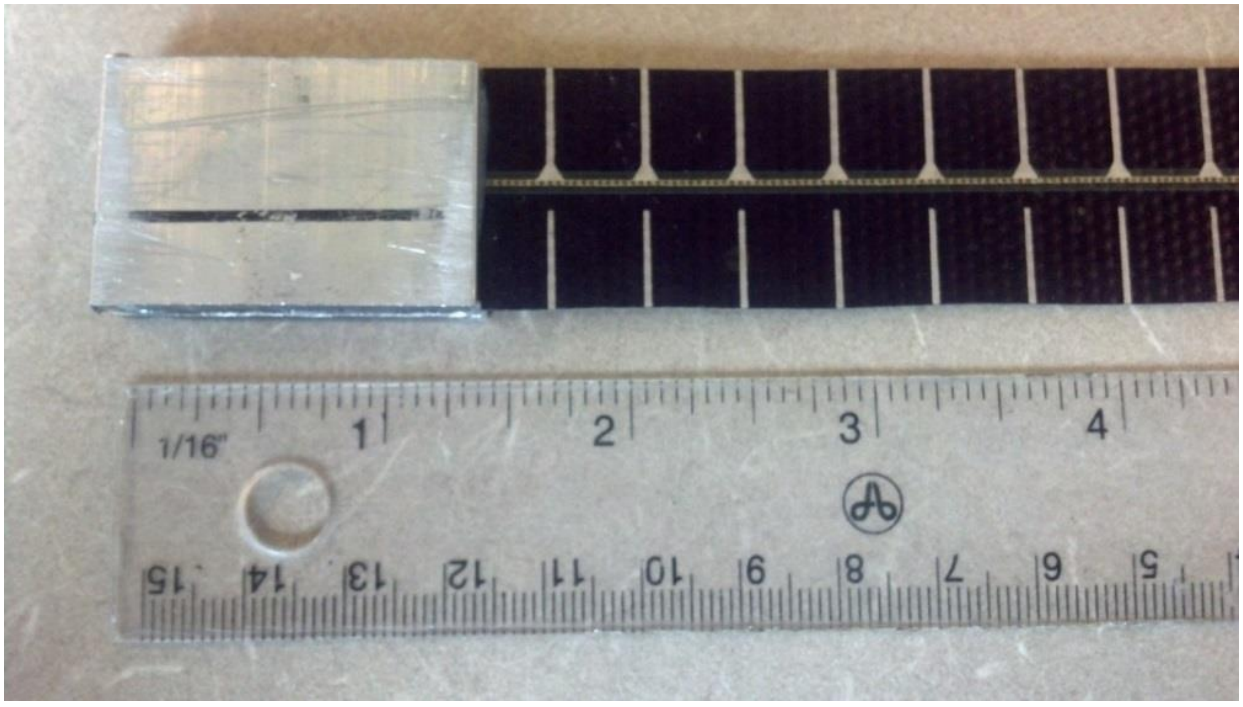

Figure 5-5: Laminated thin film PV sample with ends gripped and glued to 2 aluminium bars for proper load transfer

5.2 Water absorption

5.2.1 Results

The results from the water absorption testing are illustrated in Figure 5-6 and Figure 5-7, for ETFE laminated thin film PV samples submerged in a fresh water and salt solution respectively. These figures also include the curves of best fit according to Chen, Zhai and Zhao's model [55] derived from the experimental results:

$$M_t = M_\infty \left\{1 - \frac{8}{\pi^2} \exp\left[-\frac{\pi^2 D t}{h^2}\right]\right\}, \quad [5\text{-}1]$$

where M_t is the percentage mass absorption at time t, M_∞ is the percentage mass at absorption saturation, D is the diffusion coefficient (mm^2/s) and h is the thickness of the sample (mm).

The diffusion coefficient derived for each of the average temperatures, according to equation [5-1] is plotted in Figure 5-8. Results show that although the water absorption appears to be greater in the fresh water samples (comparing Figure 5-6 and Figure 5-7), the diffusion coefficient (illustrated in Figure 5-8) implies that water diffusivity rate is lower in fresh water than in the salt water. Meaning that the water saturation mass is reached relatively faster in the salt water solution than in the fresh water one, this can be noted from the saturation points (or point of plateau, within the first 11-12 days) in Figure 5-6 and Figure 5-7. Similar results were achieved by Chin et al [56] for another polymer, exhibiting lower absorption and higher diffusion coefficient in salt solution.

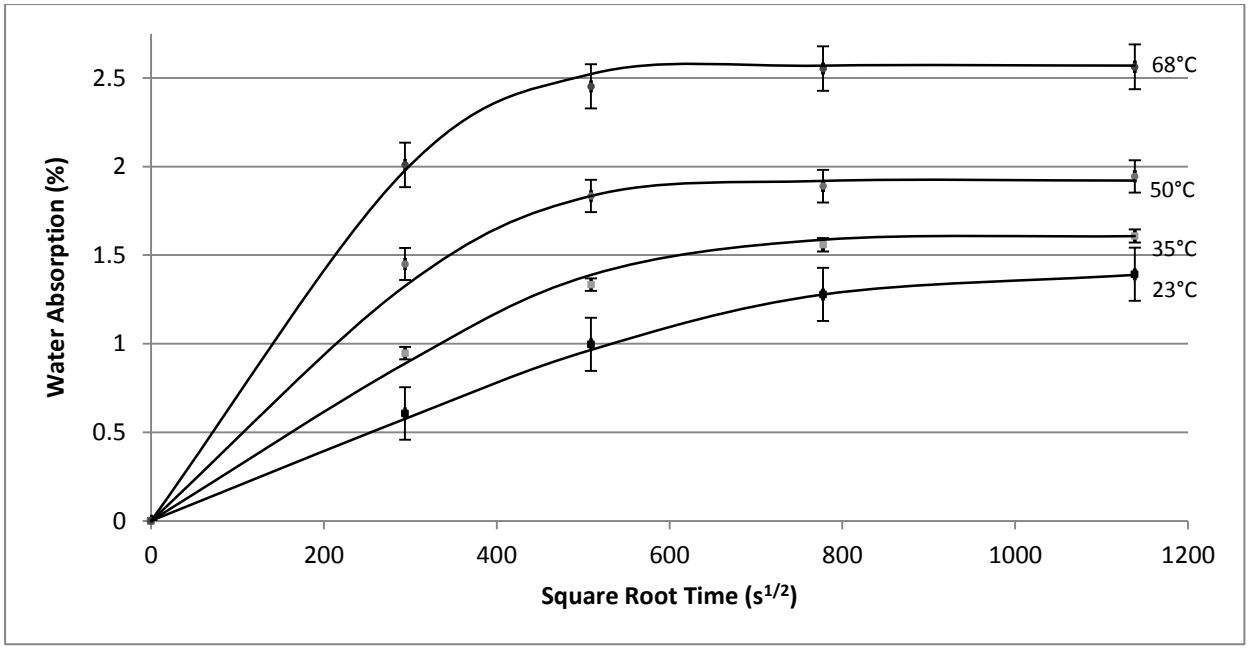

Figure 5-6: Water absorption (%) within an s-Si ETFE laminated thin film PV in fresh water

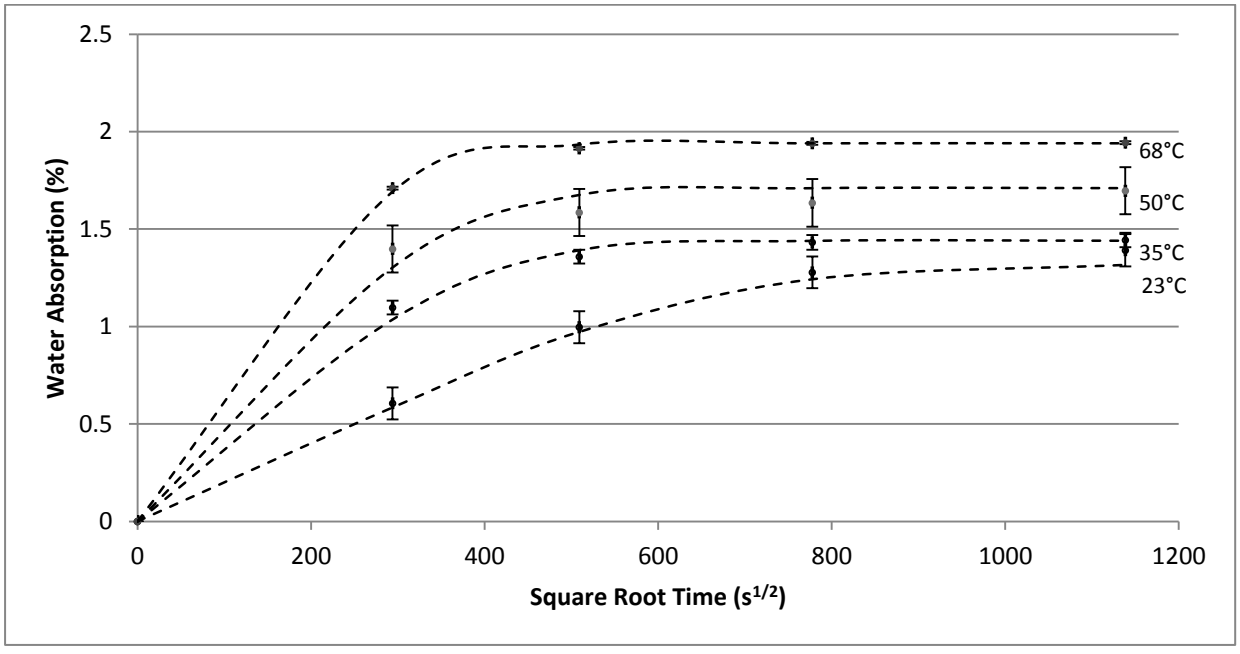

Figure 5-7: Water absorption (%) within an s-Si ETFE laminated thin film PV in a salt solution

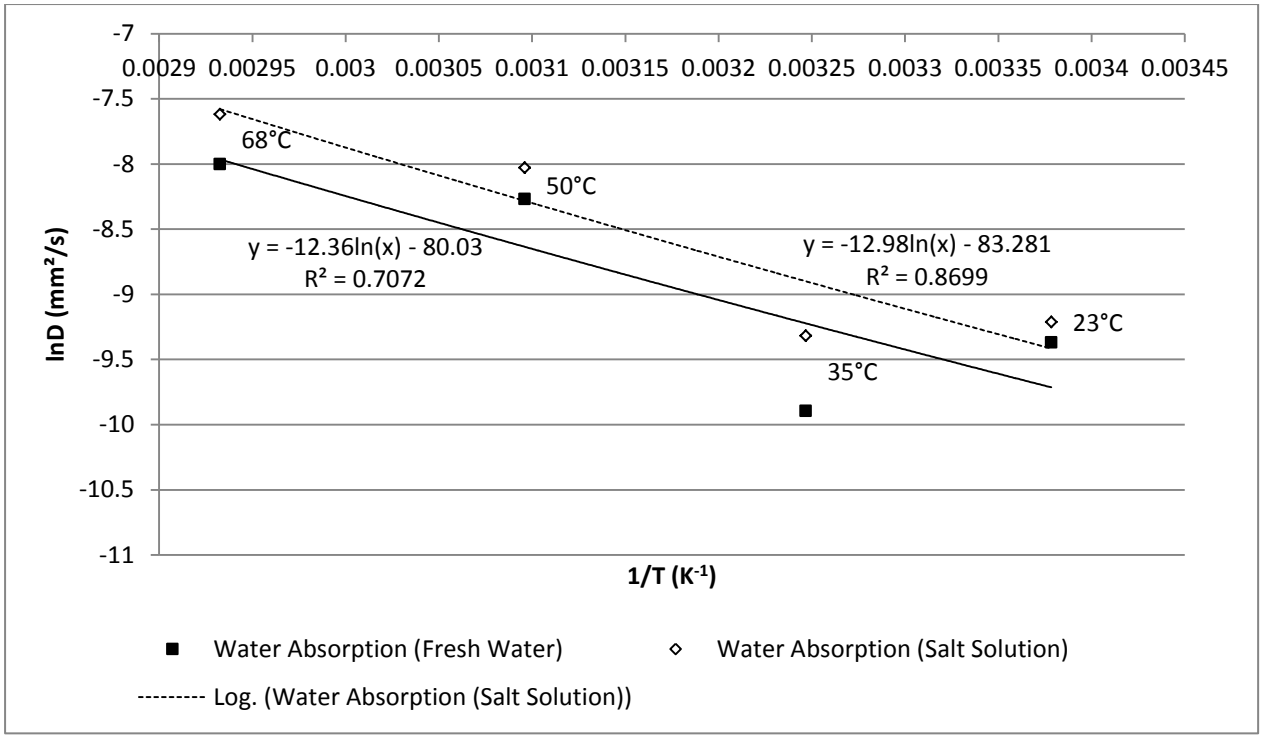

Figure 5-8: Diffusion coefficient versus temperature (lnD vs. 1/T) for the water absorption uptake at the various temperatures considered for the two water solutions

5.2.2 Observations

For all the tested samples (at 23°C, 35°C, 50°C and 68°C) no apparent degradation, delamination or discoloration was experienced. Although for samples tested at 50°C and higher tightening of the polymer around the thin film composite was more prominent. Further testing was conducted with the temperatures ranging from 70-100°C for which some effects of water damage could be noted. These included: i) discoloration (a change to a more yellowish colour) and ii) degradation of the thin film PV (breakage in the printed thin film material) was apparent in 4 out of the 6

samples for which the water temperature was allowed to exceed 70°C (as highlighted by Figure 5-9).

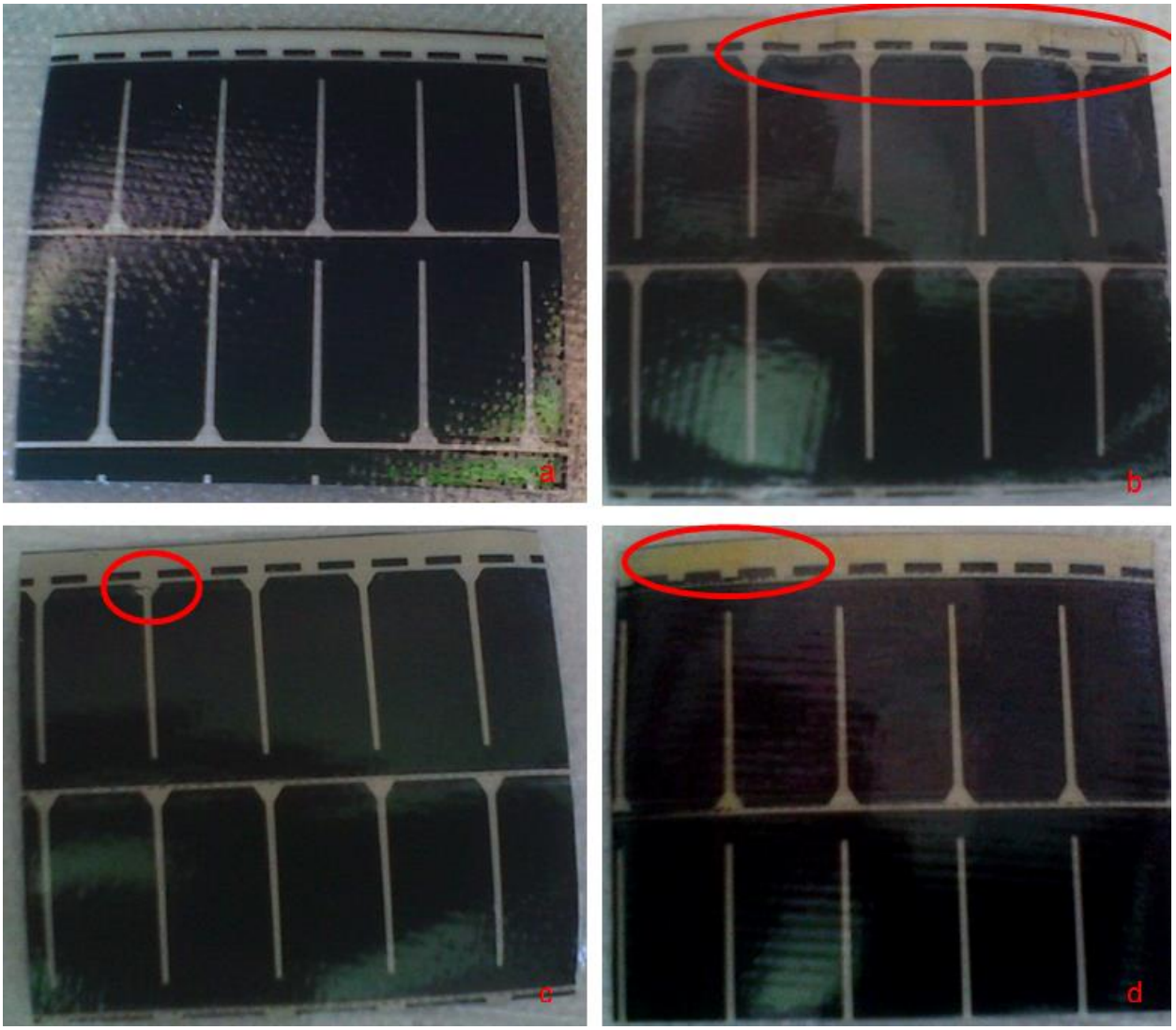

Figure 5-9: Signs of water damage and thin film degradation in modules exposed to 70°C and higher temperatures – a) thin film PV sample which has not been submerged in water; b) thin film degradation and discoloration; c) minor degradation; d) discolouration.

The other observation made throughout the testing was an apparent temporary white clouding of the ETFE in the samples subjected to the fresh water solution. This disappeared within the next day, after removal from the water. Further analysis with a Zeiss EVO-50 scanning electron microscope with an EDS spectrometer showed higher calcium content in the 'whitened' samples compared to the ones in the salt solution which did not experience any change in transparency. This would explain the perceived higher water absorption in the fresh water samples, with the molecular mass of the calcium substituting the H_2O water content being almost double in weight.

5.3 Stiffness Testing

Table 5-2: Summary of tensile testing results, conducted for 10 samples for each direction and condition (testing conducted at room temperature for dry and water saturated samples)

		Dry Samples		**Saturated Samples**	
		Lateral	Longitudinal	Lateral	Longitudinal
Deformation Stiffness (*GPa*)	Max.	2.87	2.74	2.43	2.23
	Min.	2.22	2.05	2.27	2.16
	Variance	0.09	0.07	0.02	0.05
	Average	2.50	2.36	2.42	2.21

The stiffness testing was conducted on two set of thin film PV samples (one which was subjected to water absorption till saturation at room temperature and the other with the samples maintained in dry conditions). Samples from each set were tested using both longitudinally and laterally cut samples, see Figure 5-4. Results from the testing are given in Table 5-2, sample profiles for the stress versus strain curves for the two tested directions are given in Figure 5-10 and Figure 5-11.

Data recorded from the testing, Table 5-2, indicate minor change in the averaged Deformation Stiffness from the samples tested when dry or fully saturated. Thus the effect on mechanical reliability of the PV panels from water absorption is not significant.

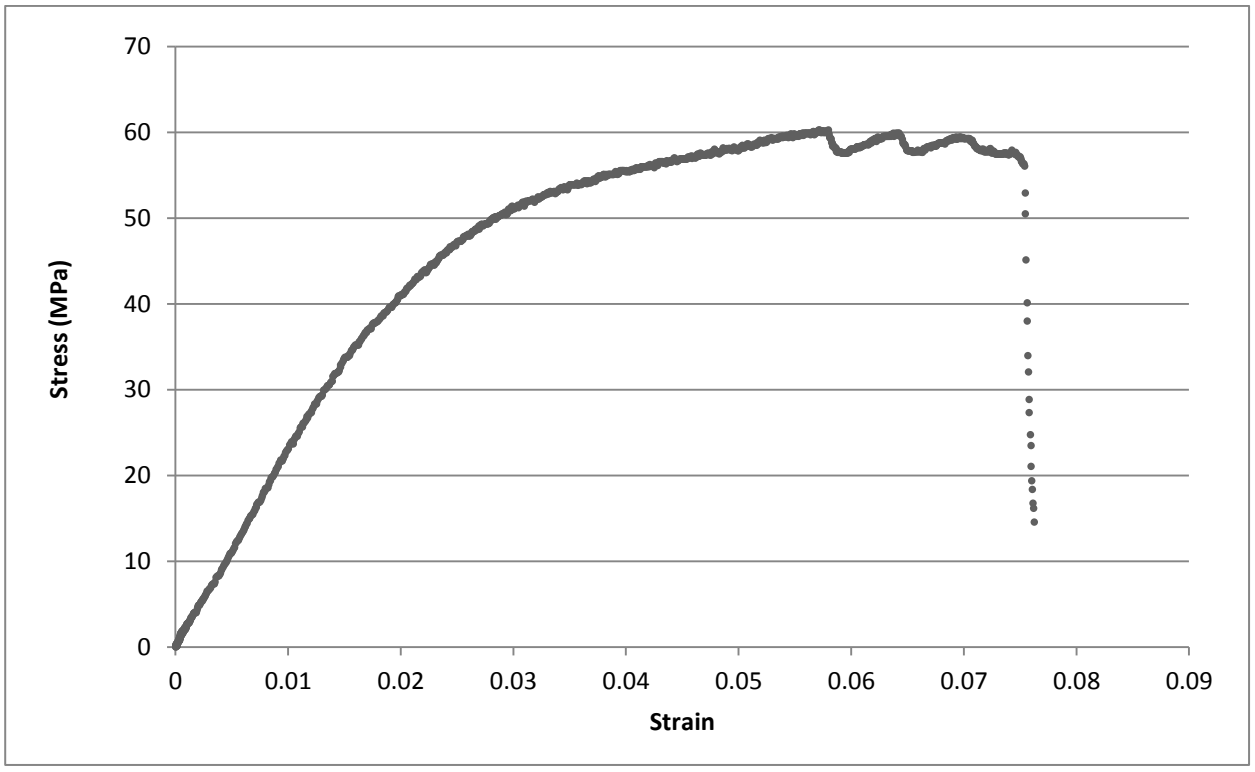

Figure 5-10: Load/elongation graph for a lateral sample of the thin film PV composite

The typical graph profiles recorded showed that the composite material was ductile in nature. Differences in the nature of the failures created was observed and recorded for the laterally and longitudinally directed samples. As can be noted from Figure 5-10, for samples with lateral direction following the point of maximum strength, a sequence of raptures occurred before breaking. While for the longitudinal direction (Figure 5-11) there was a single rapture with much

larger loss of strength after maximum strength, than in the lateral direction, before the ETFE lamination broke also.

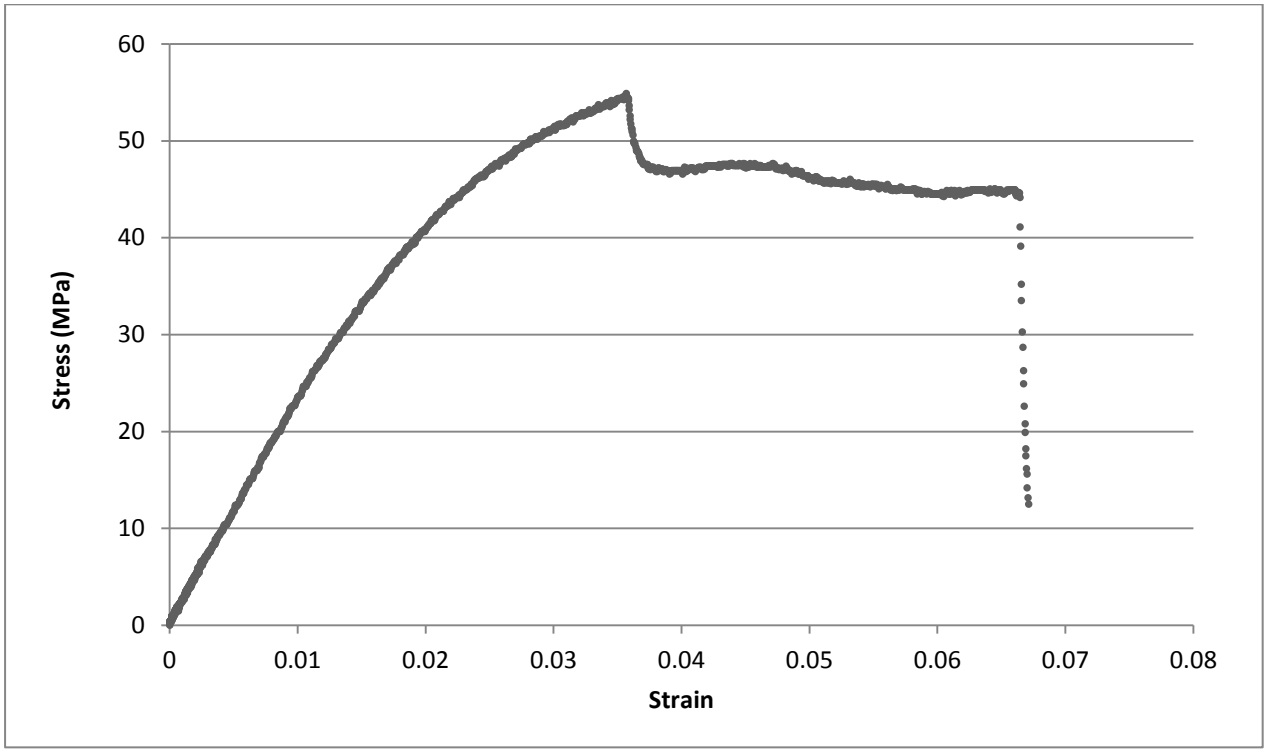

Figure 5-11: Load/elongation graph for a longitudinal sample of the thin film PV composite

Figure 5-4 also notes the manner in which the laser etching was performed on the steel backing within the composite. When cut, the samples in the lateral direction had 11 etch marks running across each of the samples, this created multiple areas of weakness at which could result in a break and hence the number of breaks in the composite as recorded by Figure 5-10. On the other hand, the samples which were cut in the longitudinal direction had only one etch mark from the laser and may so explain the single rapture for samples in the longitudinal direction and multiple raptures for samples in the lateral direction.

A simple experiment was conducted to assess whether or not saturation leads to substantial difference in deformation, using self-weight as the load. This involved laser profiling (±1cm) a saturated and dry PV panel, both lifted equally at mid-point. The results are reported in Figure 5-12, tabulation of the results and consequent determination of the area under the curves gave an insignificant variation between the two (0.5% difference). This showed that no significant variation in compliance could be made between the saturated and dry PV panels.

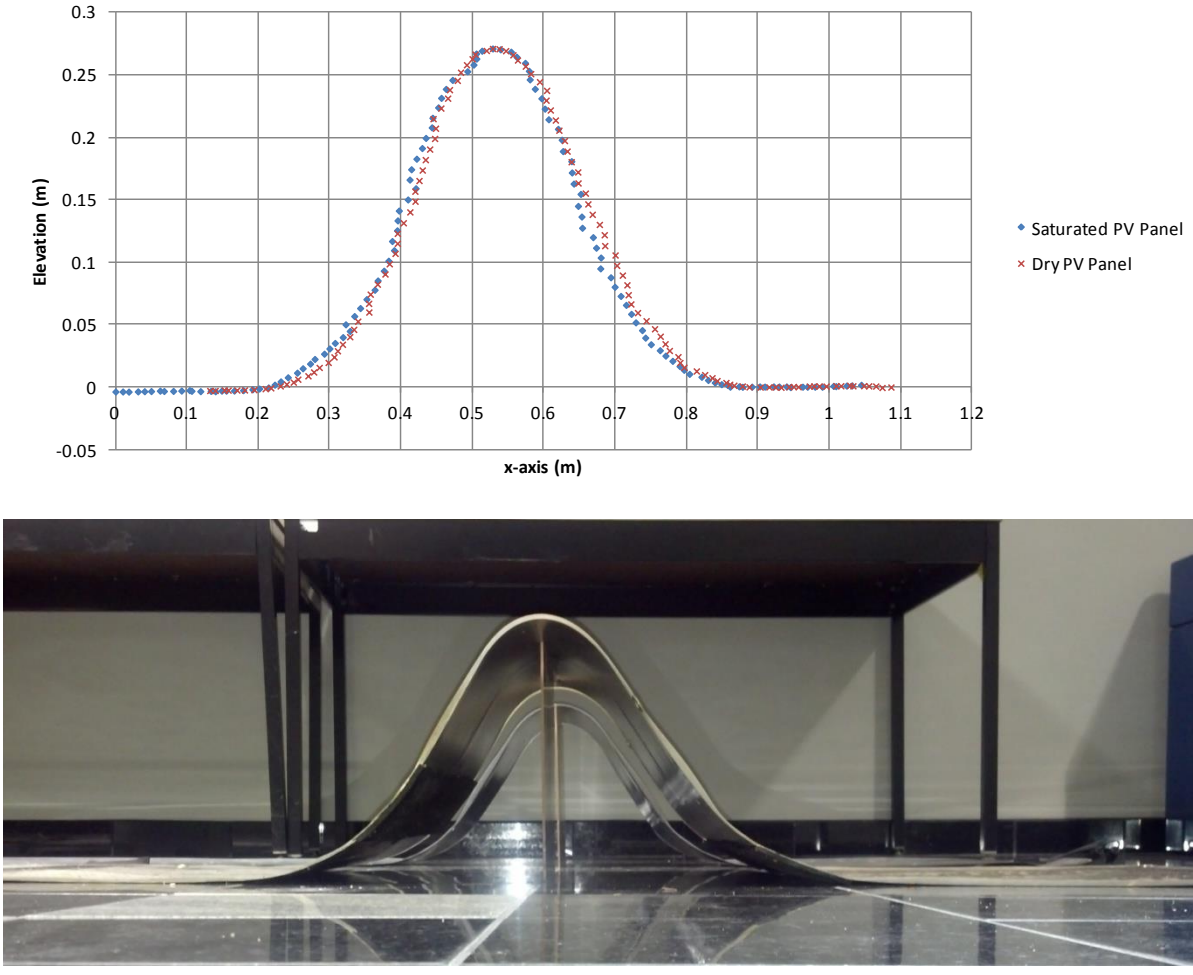

Figure 5-12: Profile testing of dry and fully saturated PV panels to show differences in mechanical compliance (top: graphical data and bottom: photographic representation)

6 Thin film flexible PV (T3F-PV) array: the concept and the development of the prototype

The objects of the work presented in this chapter, are to i) describe the design of such a floating thin film PV array for large scale electricity generation, ii) report on the development of a prototype, being the world's first deployment of a floating thin film PV, and iii) outline the performances and costs of the prototype. The primary motivation in manufacturing and deploying the array was to prove the floating PV concept. This was easily done through observation of the array and the continued electrical generation from it. The other things which had to be considered were its electrical reliability after the initial deployment, to verify a previous hypothesis of the research which indicated that there might be reduction in yield after the thin film PV laminate was fully saturated, and the electrical output variation between a ground mounted and a floating array.

6.1 Design elements

The concept of the thin film flexible floating PV (T3F-PV) array was motivated mainly by reliability issues in WECs which imposed relatively high loads on its mooring (and so failure probability) due to it interacting with the waves to harness the wave power. The key design element of T3F-PV was to develop a design which was flexible so as to allow the system to yield to the oncoming waves while not being significantly impacted in its electrical performance. The obvious choice for the PV selection was laminated thin film PV as this allowed selection of the

lamination material to suit the marine application. Also finishes on the laminate could be applied to combat fouling and allow self-cleaning.

In order for the system to be able to deform with the wave motion the PV structure had to compliant, as is the case with the T3F-PV. With a deformable surface, solar irradiance exposure occurs at several angles of incidence rather than a signal angle if a flat, resting surface is considered. Having the PV array mounted in direct contact with the water surface may lessen the engineering since compared to, for example an offshore platform, as the required infrastructure may be appreciably diminished. Forces to consider are a constant wind drag. Also the phenomenon of surface tension may help maintain the array in close contact with the water surface [57]. Other potential benefits of having the thin film PVs in direct contact with the water surface will be discussed in the subsequent sections.

6.1.1 Geometry of the array

The geometry of the array is an important consideration because it not only affects the dynamics of the system but also the system's reliability and the associated manufacturing costs. This was mainly focused on the minimisation of electrical connections between panels and electrical cable runs. Adaptability of the electrical network was still required, as it is important to avoid any situation of total failure of the system, just because one of the panels within the network failed.

Several design configurations were considered before selecting the geometry in Figure 6-1, which was not only motivated by the minimal electrical connections but also the ease of deployment of the array. The design selected allows scalability of the array without major

changes to the mooring design (since the array itself does not offer much resistance according to modelled hydrodynamics).

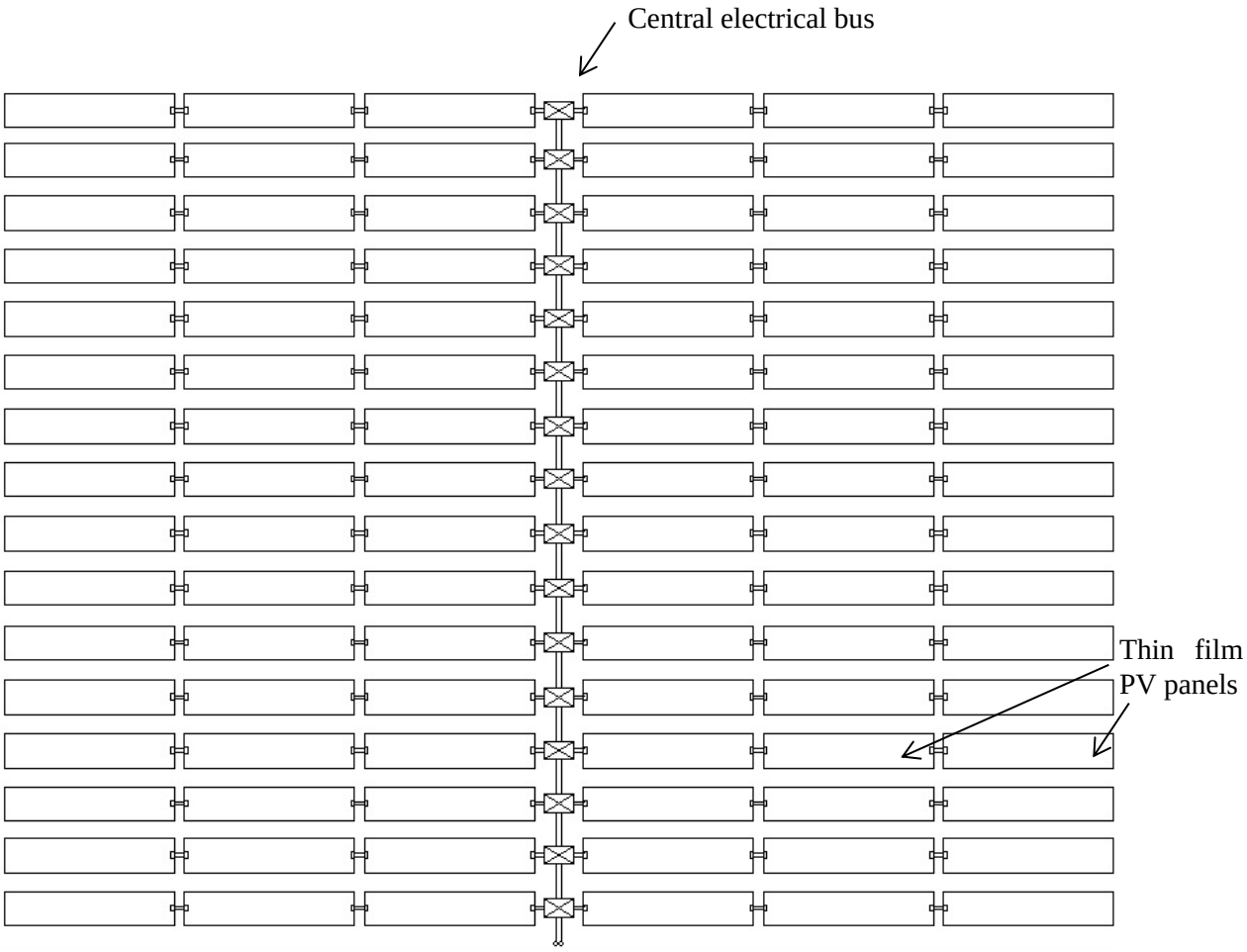

Figure 6-1: Schematic of a large scale installation of the thin film flexible floating PV (T3F-PV) array with availability to expand the array by adding more panel rows onto the central bus. The central bus comprises a string of dual micro-inverters that are cable of dealing with the electrical output of the 3 panels on either side of the central bus, in order to minimise losses and increase array efficacy.

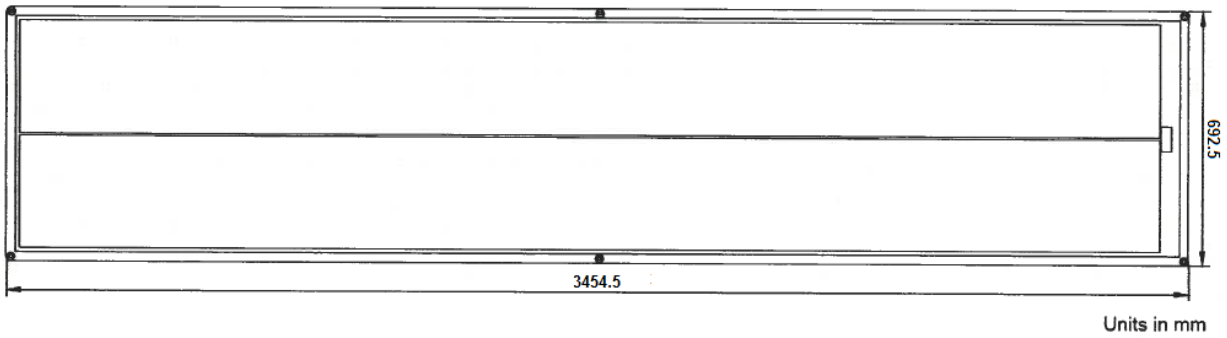

Figure 6-2: Schematic of the $94W_p$ panel

The array comprised a series of panels measuring 3.45m x 0.69m rated at $94W_p$ (Figure 6-2). To minimise the cable runs the panels could be manufactured with electrical connectors at either end; in the prototype reported only one such connector was used due to the small scale of installation. The electrical coupling also provides the mechanical coupling between each of the panels, and so has metal mesh around the conductor's insulation, below the polyurethane jacket. The electricity is delivered from the panels, connected in series (with by-pass diodes) to the micro-inverters on the central electrical bus and then is delivered to shore. The panel coupling arrangements are designed upon the currently available manufacture's maximum thin film panel's lengths; longer panels would be used in preference. Reducing the number of connections will increase the reliability, especially for offshore environments.

6.1.2 Array cooling

PV panels are characterised by a negative temperature coefficient, meaning that with higher temperatures the solar to electrical conversion efficiency of the PV panels reduces. By maintaining the panels at a lower temperature through direct contact with water the electrical

yield would be expected to be higher than an onshore system of the same capacity. On ground, on a sunny day, the PV panels could reach temperatures above 40°C whereas the water temperature would rarely exceed 20-25°C depending on the water body and its location. If the floating PV array is designed to be in thermal equilibrium with the water, then the panels would be approximately 20°C less in temperature than a similar array on ground. For a CdTe thin film panel with -0.21%/°C temperature coefficient [58], the 20°C change in temperature would imply an improvement in efficiency of over 4%.

The density of the panels is around 1050-1100kg/m^3, mainly due to the steel backing in the manufacturing of the thin film PV. Density of water is around 1000-1025kg/m^3 depending on salinity, so unless the fabrication of the panels is modified to incorporate less dense materials (and hence result in higher buoyancy) then buoyancy has to be added to the panels. In calculating the required buoyancy, the added mass from water retained on top of the floating array was also considered. 1/8^{th} inch thick neoprene sheet was estimated to be required to provide the appropriate buoyancy to the structure. The buoyancy has to be distributed uniformly at the back of the array to ensure that no part of the array is totally submerged. A thin layer of water on the surface (<2mm) will not have impact on the solar radiation, and would enhance the thermal contact of the panels [13].

6.2 Prototype

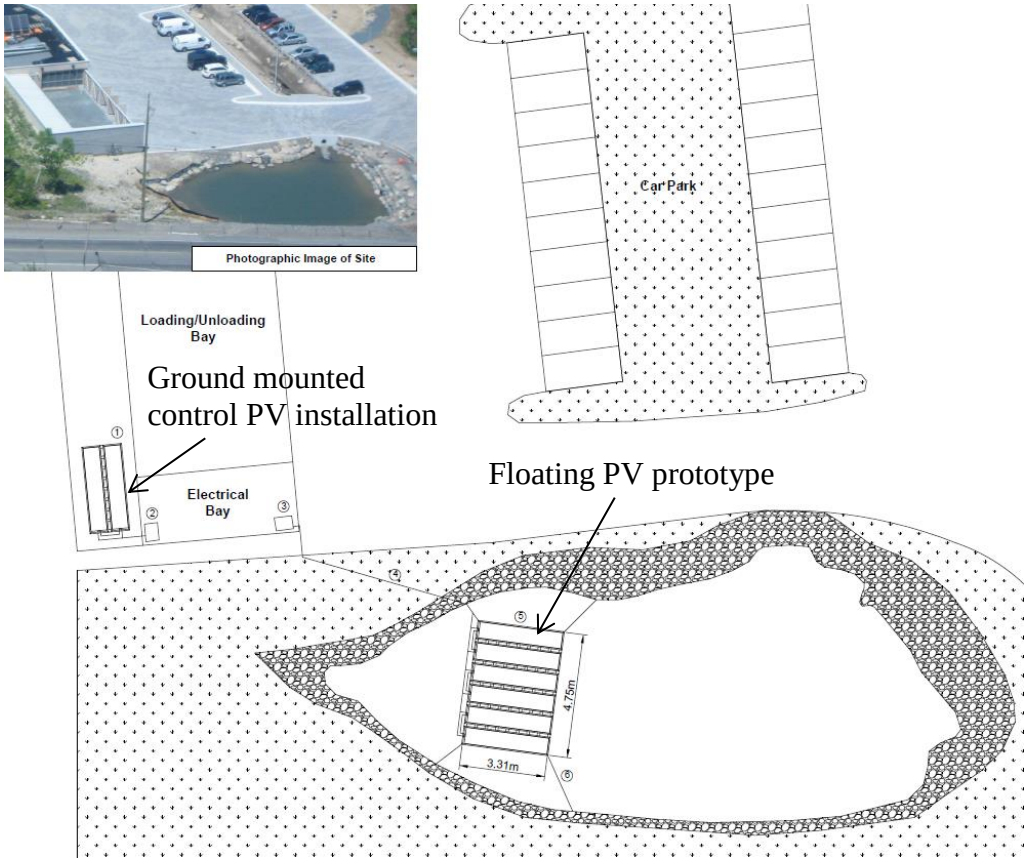

Figure 6-3: Layout schematic of prototype project location at the Vale Living with Lakes Centre, Sudbury (Canada)

A 570W_p prototype was developed for the purposes of i) proof of concept and ii) to verify the predicted performance of the floating PV array relative to the ground mounted installation. The prototype was installed in a small pond at the Vale Living with Lakes Centre, in Sudbury, ON, Canada. The pond is used to store rainfall water for grey water use within the research centre. Figure 6-3 shows a schematic of the prototype installation as well as that of a 1/3rd size ground

mounted PV array (control array) which is used to compare performance results. Photographs of the prototype and control installations are shown in Figure 6-4. The electricity generated from either system was disposed of through a dump load after being recorded by the monitoring equipment.

Figure 6-4: 570W_p floating PV array (left)[3] and 190W control array (right)

6.2.1 Manufacturing and deployment

The PV panels were manufactured by Power Film Inc. [59] and were designed specifically for this project, maximising the lamination width their machinery could deliver. The result was a double width PV panel measuring 3.45m x 0.69m and rated at 94W_p. The panels were laminated with sheets of ethylene tetrafluoroethylene (ETFE), resulting in a composite which is less than

[3] The two floating panels on the left hand side have full neoprene backing (1/8" thickness), while the remaining four panels have distributed buoyancy from 7 strips of 1/8" thick neoprene, 7" wide.

1mm thick. The choice of lamination using ETFE was mainly due to its self-cleaning properties and high transparency. The a-Si PV material was printed onto a steel sheet and then laser etched to create the p-n junctions, with each cell of $2cm^2$. EVA adhesive was used in the lamination process to enhance the panel`s waterproof qualities.

The array was pre-assembled prior to deployment with all electrical connections pre-fitted and water proofed. The cabling used was polyurethane (PU) cased to ensure no permeation of water into the electrical wiring. The electrical contacts and joins were connected and enclosed in a PU fast set solution. Any exposed electrical components, such as the PV`s junction box, was sealed with marine grade silicon. The neoprene mesh was bonded to the back of the panels, using Blanke's Aqua Seal Waterproof Polymer Adhesive chaulk, and so coupled the panels together to form the array. Finally all electrical connections, especially the PU cased joints, were enclosed in polystyrene casing to give them buoyancy (visible in orange in Figure 6-4). The array was then rolled up after assembly, and unrolled at location using the connected station keeping lines. The final step in the installation was connecting the electrical output cables with MC4 connectors to the dump loads and monitoring equipment.

6.2.2 Control station

The control station as described previously consists of a 2 panel array with identical panels to those used in the floating PV array. These panels were staked into the ground as shown in Figure 6-4. No extra waterproofing measures were undertaken in assembling the electrical connectors and conventional MC4 connectors were used. This array was similarly pre-assembled offsite and then installed as is on site and connected to the dump load and monitoring equipment.

6.2.3 Monitoring and dump load

The monitoring station included equipment which was required to monitor the electrical output from the PV panels as well as environmental characteristics such as the solar radiation and the temperature (installation circuit diagram in Figure 6-6). The sensing electronics and data logger were powered through a 12V battery which was charged by the PV array and which was prevented from becoming over charged with a charge controller. All the equipment (including the dump load) was enclosed in a heavy duty polymer box, with fans installed to cool the box (Figure 6-5).

The data logger used was an 8 port digital and analogue input with access through Serial RS232 commands over TCP/IP network using its integrated Wi-Fi 802.11 b/g module. Due to the restriction in analogue inputs to 8 ports the current and voltage could not be recorded from every panel, so the output was connected serially between the two adjacent panels and parallel between the three groups. Hence six analogue ports were taken up for the recording of the three voltage and current sensors corresponding to each of the grouped panels from the floating array. The last two analogue inputs were used to record the solar radiation and the water temperature. The dump load used was two resistive loads rated at 300W maximum loading.

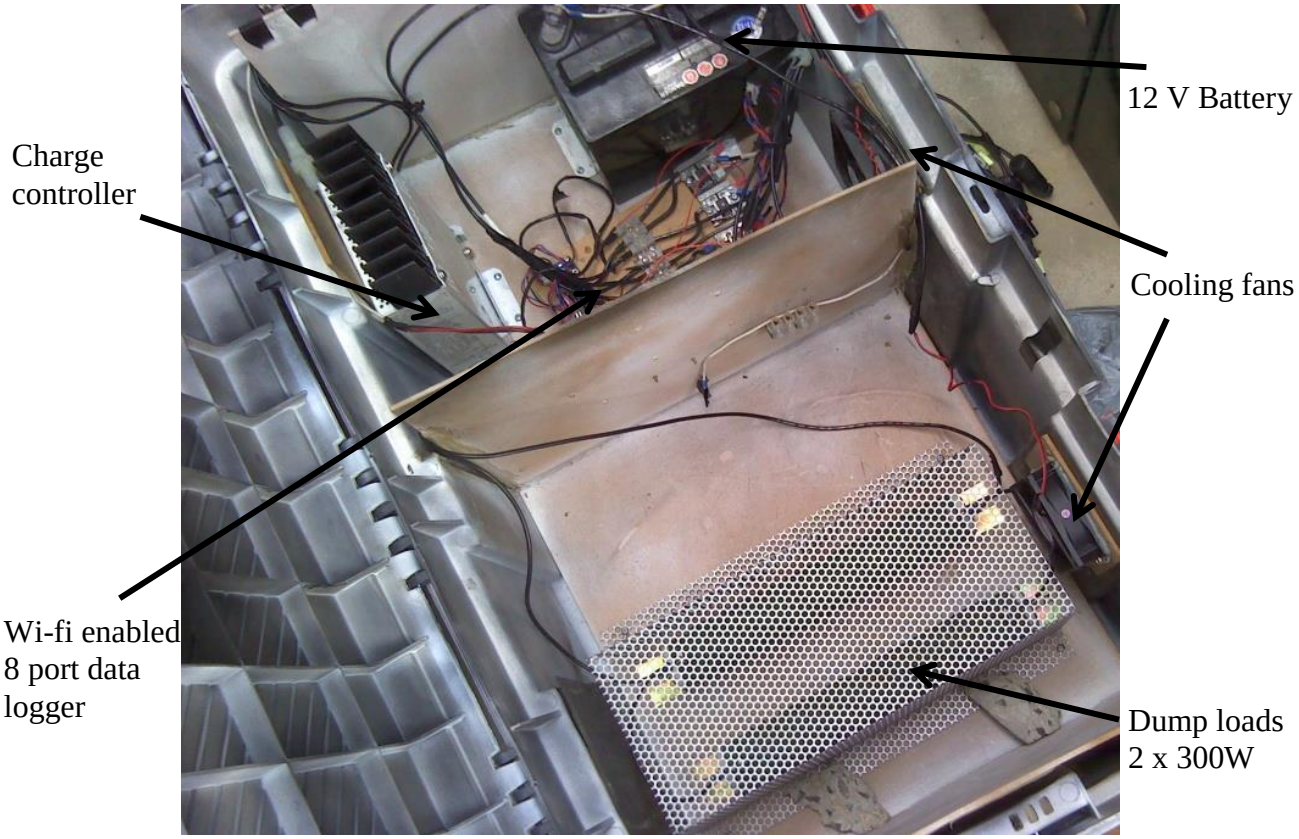

Figure 6-5: Monitoring and dump load box

The accuracy of the data recorded (current and voltage) was at ±5%, electrical sensing equipment was calibrated through a regulated electrical supply, while the temperature and radiation sensors were calibrated through comparison of data with other calibrated equipment. The logging data was set to record at minute intervals to capture environmental variations, such as changes in cloud formations. The length of cable from both installations, floating and ground mounted, to their respective monitoring equipment was of the same length to ensure same voltage losses.

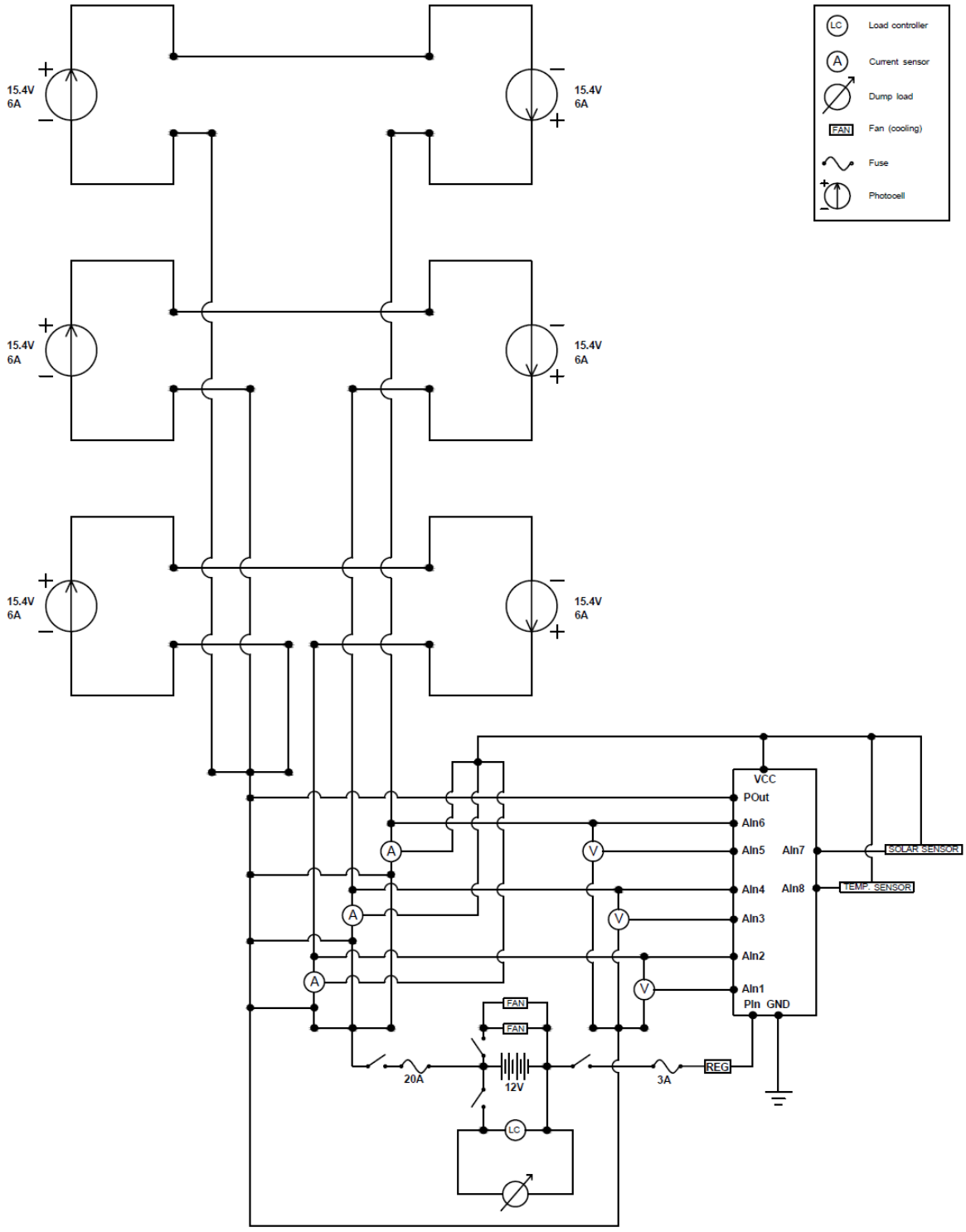

Figure 6-6: Circuit diagram for the floating PV prototype and its monitoring station

6.2.4 45 day monitoring of the floating PV prototype

The electrical data from the floating PV array was logged at minute intervals for 2 months continuously. Midway through the data collection 2 panels (comprising 1 logged group) was attached with more buoyancy to prevent it from being submersed with the added mass from rain water. This was primarily due to the concern that water coverage was affecting the electrical yield, especially since because of lower quality of the water.

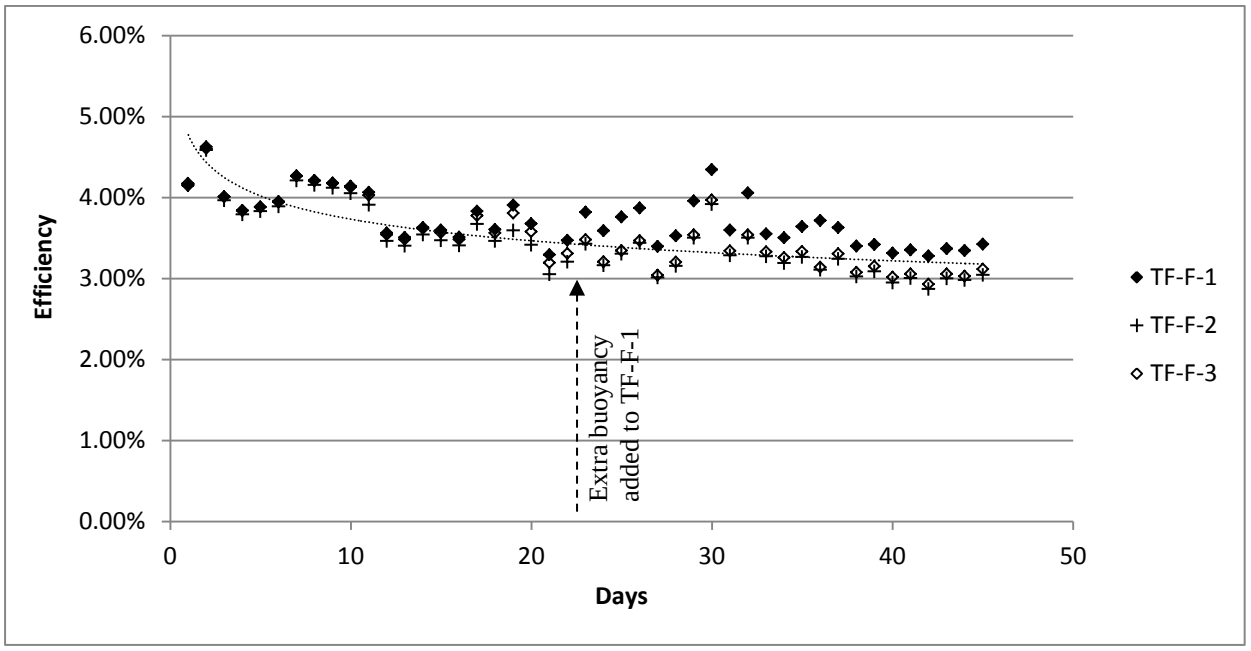

Figure 6-7: 45 day performance data from the 3 sets of floating PV array, with TF-F-2 being the central 2 PV panels, and TF-F-1 and TF-F-3 being the outer groups of panels.

The trend of electrical efficiency recorded is downwards over the first 15 days of operation of the floating PV array. Visual inspection of the system indicated that during those days there was significant accumulation of sediment on top of the panels, which remained for the subsequent

testing thereafter. This would be indicative of why the efficiency of the panels decreased as much in the initial days of electricity generation. The quantity of water which was retained on top of the thin film PV arrays also had significant effect on the electrical output; this was evident when comparing the efficiencies of the panels before and after the extra buoyancy was added underneath one of the groups of panels. A clear improvement in efficiency can be noted, representative of a 0.3% average improvement in efficiency throughout the recorded remaining datasets.

6.2.5 Ground mounted versus floating array

The two systems were installed to experience identical diurnal and environmental parameters throughout the complete testing period. Thus, the main difference between the ground mounted PV array and the floating PV array was predicted to be their operational temperature. This is because the floating PV is maintained at close to thermal equilibrium with the water body (if the array is in adequate contact with the water), while the ground mounted array depends on the air flow to cool down the panels. So the solar radiation and the wind speed have a big effect on the temperature of the ground mounted PV panels, unlike the floating array which will be more dependent upon the temperature of the water.

This is a relevant issue in this context because temperature plays an important role in the efficiency conversion solar energy to electrical energy in PV panels. A higher temperature will reduce the efficiency of this conversion, since it will lead to more losses. A thermal scan of the two PV arrays (Figure 6-8) at approximately the same time, just as the sun set, shows an 8°C difference in temperature.

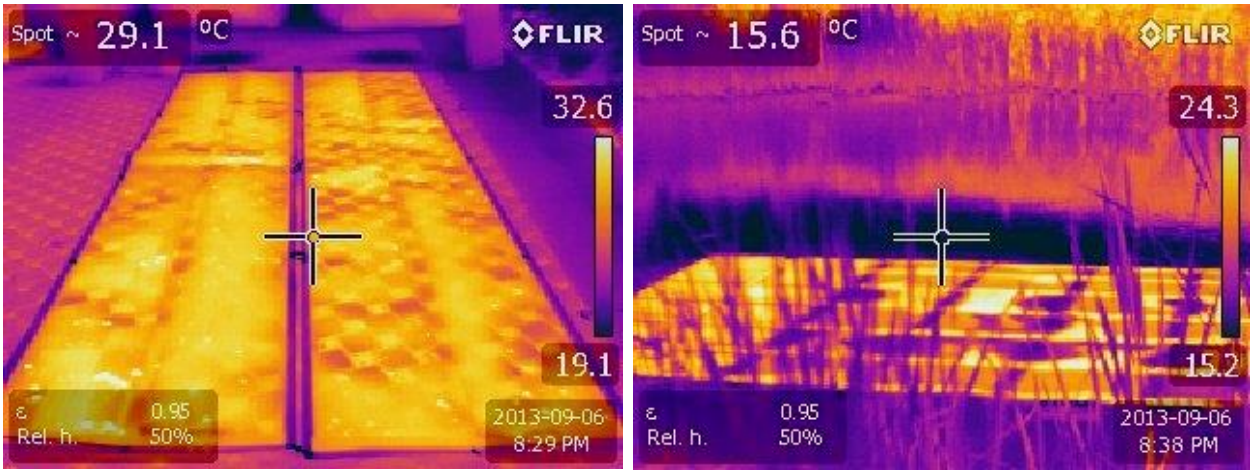

Figure 6-8: Thermal scans of ground mounted (left) and floating arrays (right)

A 3 day comparison of the operational performance between the ground mounted 2 panel array, the 2 floating panels with added buoyancy and 2 of the remaining floating PV panels was conducted. The results are shown in Figure 6-9 which records the electrical output from the individual panel groups, the recorded water temperature and the air temperature. These help understand the variation in output between each of the identical panel sets.

The first observation which can be noted from the data is that there is a shift between the peak electricity generation and the recorded air temperature. This indicates that it takes some time for the air to warm up. The temperature of the water body stays mostly constant and this is because it takes much more energy to heat up water than air for the same temperature difference, and is a consequence of their different specific heat capacities.

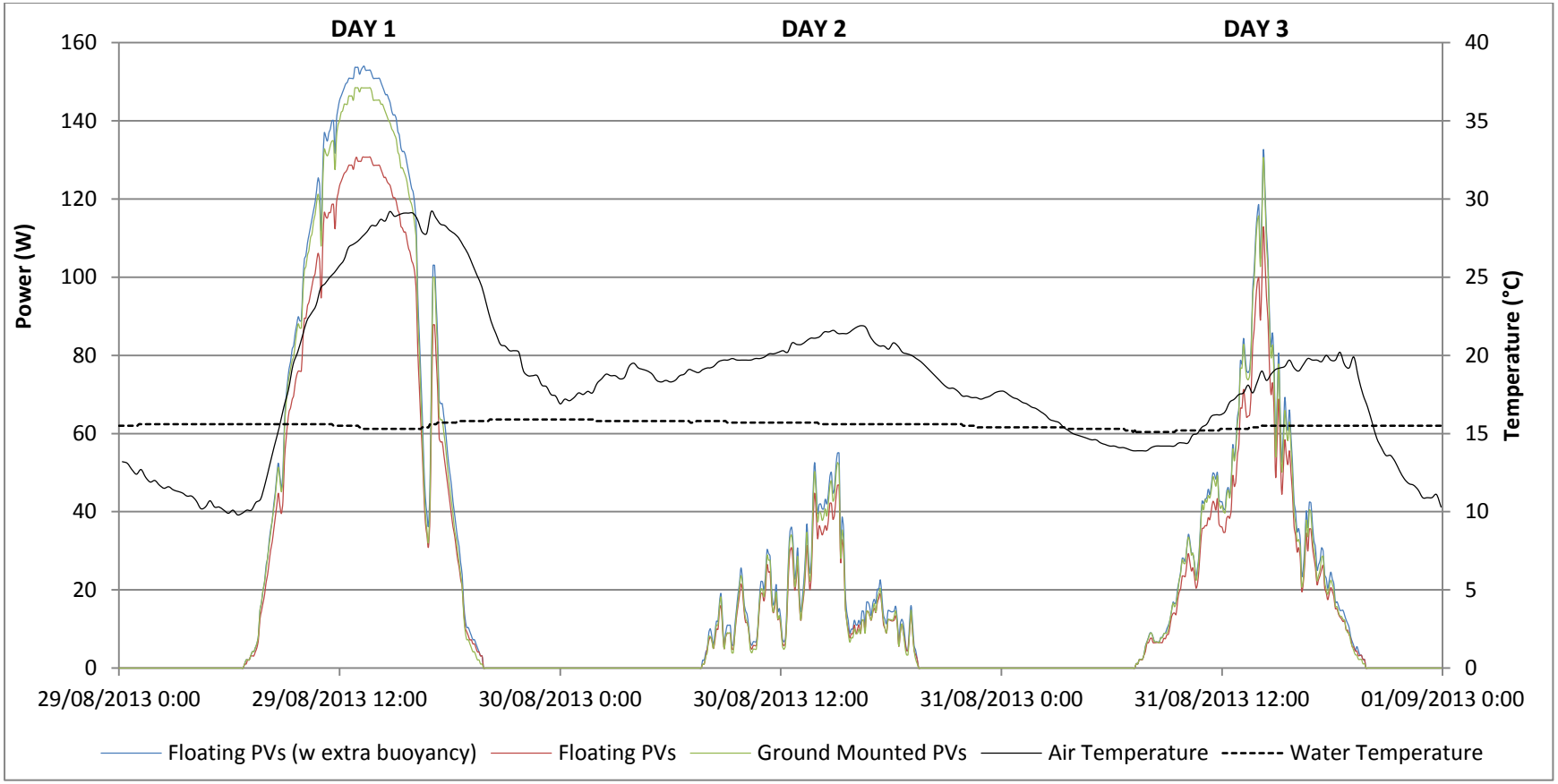

Figure 6-9: Electricity output from 3 sets of PV panels, each operating differently (1 set of 2 PV panels floating with extra buoyancy to allow them to be higher than the waterline, 1 set of 2 PV panels floating just at the waterline and 1 set of 2 PV panels installed on ground). Variation in electricity conversion resulting from i) sediment accumulation, ii) water absorption and iii) water cooling.

The major variations in electrical output can be seen from the data recorded on the first day, which had minimal cloud cover and relatively high solar intensity – so the temperature would be expected to have more effect on the conversion efficiency. The better performing group of panels were those from the floating array which had the added buoyancy to help ensure that no water remained on top of the panels. There was an average 15% variation in output between the two sets of floating PVs, which shows how detrimental a ~10mm layer of water can be to the electrical output [11].

The output from the ground mounted installation is relatively close graphically to the outputs recorded from the floating panels with the extra buoyancy. The slight difference is an indication of the variation in temperatures of the two array sets – on the first day illustrated at around the peak output the temperature of the ground mounted panels was almost 40°C whereas the temperature of the floating panels (with extra buoyancy) was close to 25°C. The recorded data shows a maximum improvement of 8% from onshore to offshore, and an average improvement of 5% in electrical output over the 3 days. This improvement can be attributed to the cooling effect the water underneath the panels. The simplicity in manufacturing and deploying the floating PV array, combined with the added cooling benefit could be key in feasibly moving such arrays from ground mounted to offshore environments (provided there are favourable economics).

6.2.6 Costs of the prototype

The primary concern for any project prior to development is how much it will cost. For the current concept, at large scale a cost model was developed. The results of these models are given

in the papers [60] and [61], which consider the economic potential of floating PV arrays (CAPEX of \$2,350/kW_p CAN) compared to other offshore renewable energy technology and when integrating them with an islanded grid system, respectively. The historical costs for the development of the prototype array are given in Table 6-1. The total cost came to \$6,498.32 CAN, which implies that the installed cost is \$11.40/W_p.

Table 6-1: Component cost of the floating PV array prototype (purchase date 2013)

Item	Quantity	Cost per Unit	Total
Thin film PV panels (570Wp)	6	\$ 702.23	\$ 4,213.38
Neoprene	1	\$ 214.70	\$ 214.70
PU 4 core cable	1	\$ 333.89	\$ 333.89
Single core PVC wire	1	\$ 58.51	\$ 58.51
Cable joints	2	\$ 19.60	\$ 39.20
Logger box	1	\$ 29.05	\$ 29.05
Logger	1	\$ 269.00	\$ 269.00
Charge controller	1	\$ 129.98	\$ 129.98
Dump load (300W)	2	\$ 65.98	\$ 131.96
Fans	2	\$ 7.98	\$ 15.96
Battery	1	\$ 84.74	\$ 84.74
Electronics	1	\$ 110.49	\$ 110.49
Misc.	1	\$ 267.46	\$ 267.46
Labour	12hrs	\$ 50 .00	\$ 600.00
		Total	**\$ 6,498.32**

The installed cost of \$11.40/W_p is high, even considering that this is a prototype installation and that economies of scale are not applicable. In Table 6-1, it can be noticed that the cost of the PV panels make up the majority of the final cost (~65%). Branker *et al.* [62] provides a figure of \$7.30 (2011) for the installed cost of a small scale residential thin film installation (including the balance of system). Reichelstein and Yorston [63] based on historical trends and technological

progress have models for the reduction in installed costs of PV, including thin film PV in North America. These suggest that technologically the cost of production and procurement should be lower than the purchase price of \$7.39/W_p paid for the PV panels in the development of this project (which excludes the balance of system). A proportion of the higher cost of the PV panels can be associated with the customisation costs (which would not be reflected in procurement for larger installation), but is mostly relative to the low market penetration of laminated thin film producers in North America which keeps their price at a premium.

7 Techno-Economic Analysis 1: Comparison with other Renewable Energy Technologies

Despite installed capacities of renewable energy technologies having increased from 742GW in 2000 to 1235GW in 2009 [64], the generating capacity from offshore technologies remains a small proportion of the global renewable electricity generation capacity, and comprises mainly offshore wind. As well as offshore wind, tidal barrages, tidal current turbines and wave energy technologies are considered in this chapter in a comparative techno-economic assessment that draws upon prior experience in formulating benchmark methodology [65]. Together with these developed offshore renewable energy technologies, the assessment is extended to include a novel concept for offshore photovoltaic (PV) technology, put forward as an alternative prospective marketable technology. Although tidal barrages strictly may not be considered an 'offshore' technology they are included within this techno-economic analysis, as a marine renewable energy technology and an alternative to tidal current turbines.

Much of the research on wave energy conversion devices was instigated following the 1970s oil crisis [66] and more recently following the Kyoto protocol agreement [67]. These are usefully summarised and compared by Millar [68]. Despite initial enthusiasms regarding the Pelamis wave energy device and its deployment (3 x 750kW in Agouçadura off the coast of Portugal) currently there are no operational commercial wave energy converters (WECs), however numerous wave energy testing and demonstrator projects have been deployed in the recent years (e.g. Oyster, Scotland; Dexa Wave, Malta etc...).

Until recently only two tidal energy projects with installed capacities greater than 10MW have been installed: at La Rance, France in 1966 and Annapolis Royal, Canada in 1984. The installation at Lake Sihwa (37°18′47″N 126°36′46″E), Korea of 254MW was commissioned in August 2011 [69], making it the world's largest tidal installation. Although large-scale performance assessment results for one TCT deployed in Strangford Lough, Northern Ireland in 2008 are promising, TCTs, like wave energy technologies, are still in a developmental phase. In contrast, offshore wind energy is currently being commercially deployed at GW scale; the clearest example of this is development in UK waters. Over three planning rounds, 47GW of offshore wind projects are planned in the UK, currently with 1.8GW operational, 2.4GW under construction, 1.2GW approved, 3.6GW submitted for planning permission and 38GW awarded but not yet submitted for planning. Any energy technology alternative for the offshore environment, whatever its stage of development, will thus have to compete commercially with offshore wind energy.

Reliable information regarding offshore energy technologies is difficult to obtain due to the commercial/propriety nature of the developments. This can make equitable assessment of the yield and economic performance of the options, including proposals for offshore floating PV, challenging but nevertheless was the objective of the work reported herein. Somewhat similar techno-economic reviews have been made for the individual offshore technologies [70-72].

Table 7-1: Wave and Tidal Commercial and Pilot Plants in Operation End 2009

Project Name	Type		Location	Installed Capacity	Year of Operation
Annapolis Royal Tidal Power Plant	Tidal	Commercial	Canada	20.00MW	1984
Baishan Tidal Power Plant	Tidal	Commercial	China	0.64MW	1978
Bay of Fundy	Tidal	Pilot Project	Canada	1.00MW	2009
Billia Croo Test Site	Wave	Pilot Project	UK	0.20MW	2003
Daishan Tidal Power Station	Tidal	Commercial	China	0.04MW	2005
Fall of Warness	Tidal	Pilot Project	UK	0.25MW	2008
Haishan Tidal Power Station	Tidal	Commercial	China	0.15MW	1975
Humber Estuary Tidal Power Project	Tidal	Pilot Project	UK	0.10MW	2009
Islay Project	Wave	Pilot Project	UK	0.50MW	2000
Jiangxia Tidal Power Generation Plant	Tidal	Commercial	China	3.20MW	1980
Jindo Uldolmok Tidal Plant	Tidal	Commercial	South Korea	1.00MW	2009
Kislaya Guba Tidal Power Station	Tidal	Commercial	Russia	1.70MW	1968
La Rance Tidal Power Plant	Tidal	Commercial	France	240.00MW	1966
North Sea Wave Dragon	Wave	Pilot Project	Denmark	0.02MW	2003
Port Kembla Wave Energy Project	Wave	Pilot Project	Australia	0.50MW	2006
Race Rocks Tidal Power Demonstrator	Tidal	Pilot Project	Canada	0.07MW	2006
Xingfuyang Tidal Power Plant	Tidal	Commercial	China	1.30MW	1980

Sources: US DoE, O'Rorke *et al.* [73], Zhang [74]

7.1 Offshore PV technology

Floating PV technology is a relatively new concept, with only a number of demonstrator projects having been deployed worldwide Figure 2-2. The techno-economic analysis conducted includes pontoon mounted floating PV and flexible floating thin film PV, as well as that of the 'conventional' offshore technologies.

Current PV technologies can be split in five groups [75]: silicon, cadmium telluride (CdTe) and cadmium sulphide (CdS), organic and polymer cells, hybrid photovoltaic cells, and thin film technology. Silicon photovoltaics are the most popular and commercially available [76], with three main product streams: mono-crystalline PV, poly-crystalline PV and amorphous (uncrystallised) silicon PV. Amorphous silicon (a-Si) is the most popular format adopted for thin

film technology, and exists in single-, double- and triple-junctions. With triple-junction being most efficient, ranging from 8-10% [75]. The crystallized silicon PV, due to their physical manufacturing is available in a rigid format only. Efficiency for crystalline PV wafers is significantly higher, at 18-21% for mono-crystalline and 13-14% for poly-crystalline [76].

Poly-crystalline silicon is considered for the pontoon based installations while amorphous silicon will be considered for the flexible system, due to their availability and being relatively cheap types of PV.

7.2 Motivation for Flexible Floating Thin Film PV

The main incentives for moving PV installations offshore are space availability, high specific yield and installed capacities compared to the conventional offshore renewable energy technologies, and potentially higher efficiencies (from the cooling effect) arising from the PV modules being in contact with the water. The offshore (marine and lacustrine) environment within which this new technology application is targeted, offers additional forces arising from waves, wind and tides which would not need to be considered in PV ground-mounted applications. Issues related to the system reliability and the accessibility for maintenance that in turn affects the O&M (operations and maintenance) costs are significant for all offshore energy technologies including PV installation. In ensuring survivability of marine structures, two approaches to design may be adopted. The majority of approaches involve ‘heavy’ engineering designed to resist the extreme environmental forces. An alternative approach where compliant structures are designed, leads to lower material intensity and hence offers prospects of lower

capital cost. By decreasing the loads that are experienced by compliant structures, the load imposed on station keeping, anchoring or foundation configurations may decrease accordingly.

In contrast to wave or tidal energy converters, offshore PV generating technology does not need to absorb energy from wave motion. For the former, power-take-off is achieved by ensuring relative motion between the structure and the water. For PV systems that absorb incident solar energy, the dynamics of the PV structure are not essential to energy conversion, but the PV structure must be supported by (float on) the water. Here, a flexible sheet of thin film amorphous silicon PV material is considered, that is encapsulated in a buoyant, marinized laminate and is in direct contact with the water. This represents a significant deviation from the design principles evident in Figure 2-2, which are all floating pontoon based. Such a material is manufactured using a roll to roll format that is scalable. By having panels in direct contact with the water surface (as shown in Figure 2-6), at the waterline (offering a self-cleaning and, for marine applications only, an accumulated salt clearing benefit) the panels can be cooled by the supporting water body, which thus would also act as a heat sink. In operation, PV panel temperatures would assume that of the water body and maintain higher efficiency operation than their land based counterparts mounted in air (with typically higher temperature, for the same climatic conditions).

Reliability of an installation is dependent upon the individual reliabilities of the components within that installation. By minimising the number of components which are included in an installation, the reliability of the entire installation would improve simply because there are fewer components to fail. PV electricity generation relies on a solid state technology to deliver

electricity, whereas conventional offshore renewable energy technologies rely on relative mechanical motion for power take off. The latter technologies thus have components that experience loads associated with power take off, that can be appreciable and hence tend to reduce reliability. The main loads that need to be considered for floating PV are associated with station keeping. For large scale floating PV installations (which are envisaged to include continuous strips of PV buoyant laminate, available in kilometre long lengths) the number of components for 10-100MW scales installed capacity would be significantly less than for competing offshore technologies, and due to the compliance and resilience of the materials, reliability is expected to be higher. Reliability is a primary concern for offshore renewable technologies because access to plant for maintenance is limited, specialised and expensive. Utilisation of a fundamentally reliable, solid state technology has the potential to resolve these access issues with consequent reductions in costs of operations and maintenance.

7.2.1 Advantages

The risk of collision is an important factor to consider in the development of an offshore infrastructure. For offshore wind and wave farms, navigation routes have to be altered and exclusion zones put in place to prevent potentially disastrous collision events of marine vessels with the offshore electricity generating devices. Although these collision mitigation techniques would still need to be put into place for offshore PV devices, the risk presented by the technology onto oncoming marine vessels would be appreciably less than for conventional offshore devices because the consequences of collision would be far less severe: due to the compliancy of the laminated floating thin film PV.

In addition to the cost of access for planned or unplanned maintenance another significant part of the operations and maintenance (O&M) cost for offshore technologies is the cost of insurance of the installation, which must cover the risk arising from collision of marine vessels with the installation. A reduction of the risk through reduction of the severity of consequences should imply a reduction in the insurance costs for the offshore PV technology compared with other conventional offshore renewable energy technologies.

Failure of the station keeping system through fatigue or extreme loading presents significant design challenge for all offshore renewable energy technologies and this includes the novel offshore floating PV concept as well as wave and tidal energy converters. Mooring failure in wave energy converters is primarily due to the huge loads that the device has to overcome in converting wave energy to mechanical power to rotate the on-board generators [29]. In an energy conversion system where the provision of the mechanical power is not required (as is the case with a solid state system such as the buoyant PV laminate described herein), the loads transmitted onto the mooring system may be appreciably reduced, and thus the risk of station keeping system failure may be reduced accordingly.

7.2.2 Disadvantages

The main fall back, of such a flexible device, compared to a pontoon based system is that it forfeits its ability to be oriented at optimal tilt to maximise the output in yield. In which eventuality the system would have to be reinforced, to avoid damage from additional forces arising from the wind shear and also in maintaining the system to face south. Yields from two

similar horizontal installations would also vary due to the decreased solar conversion efficiency of thin film relative to either poly or mono crystalline PV.

Additionally the threat of damage to renewable energy assets due to acts of vandalism is significant where proposals for marine renewable energy technology installation may be perceived as a threat to livelihoods or customary activities. This is no different for offshore PV installations than any other renewable energy technology, but highlights a need for engagement and development participation with communities and stakeholders with interests in the deployment area.

7.3 Case studies

Using a series of actual installation case studies for the various offshore technologies and the conceptual proposals for the novel PV technology, a comparative techno-economic analysis was undertaken where all appraisals shared the following:

- A common year of comparison (inflationary indices)
- A common evaluation methodology
- A common currency
- A common discount rate

7.3.1 Collection and appraisal of data for 'conventional' offshore renewables technologies

Details for offshore wind farm projects were well documented (e.g. from the European Wind Energy Association). Tidal and wave energy projects are largely still in their developmental stage of the technologies and scarcity of published information on economic or yield factors, footprint area etc. presented a challenge. Where possible these were estimated through reported data. Where this data was not available, the assumptions that were made to permit estimation are clearly stated and the methodology explained.

A common measure of generating capacity for renewable energy technologies is the capacity factor, which is the ratio of the actual electricity produced from an installation to the maximum electricity produced if it was generating at a rated capacity continuously. From reported observations (see the case studies listed in Table 7-3, further explained in consequent sub-sections) there was frequently significant disparity between predicted capacity factors in concept design stages relative to actual capacity factors reported following operations. In these cases the capacity factor prior was higher, indicating capacity factors which favour the manufacturer.

The footprint area for these projects is the total area which the energy project would occupy, to the potential exclusion of other offshore users. The area includes the area occupied by the technology itself and the area between the devices required to limit the wake effects or mooring/foundation interfaces. The offshore development footprint area is recognised as an important sea surface resource consumption metric and hence illustrated in Figure 7-1 for clarity.

It permits an assessment of the relative efficiency of occupancy of offshore areas by technologies of different types to be made.

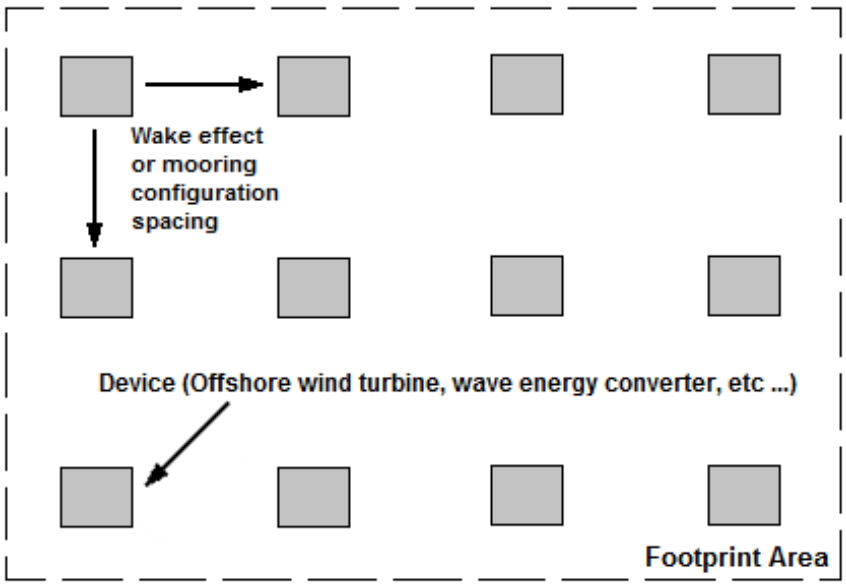

Figure 7-1: Footprint area of an offshore installation

For the O&M costs listed in Table 7-3, most of the values were deducted by interpolating data from Table 7-2. In the case of the tidal barrages this cost was taken to include the replacement costs of the turbines during the lifetime of the project. The data from Table 7-2 was compiled by SQW Energy in 2010, which is a United Kingdom based company, on behalf of the Sustainable Energy Authority of Ireland and Invest Northern Ireland using multiple sources. Other key sources used in compiling Table 7-3 include Future Marine Energy – Carbon Trust Report 2006 [77], Marine Energy Challenge Cost Estimation Methodology – Entec Carbon Trust Report 2006 [78], EPRI Assessment Offshore Wave Energy Conversion Devices 2004 [79] and Impacts of Banding the Renewable Obligations – Cost of Electricity Production – DTI 2007 [80].

Table 7-2: Wave and tidal costs, in 2010 CAN $ modified from [81]

	Cost of Electricity *($/kWh)*			Capital Cost *($/kW)*			O&M Costs *($ cents/kWh)*			O&M as a % of Capital Costs		
Energy Source	**Min**	**Max**	**Avg**	**Min**	**Max**	**Avg**	**Min**	**Max**	**Avg**	**Min**	**Max**	**Avg**
Wave	0.07	0.66	0.33	1,733	15,071	5,234	2.86	6.30	4.84	3.0%	5.9%	4.5%
Tidal	0.14	0.36	0.18	1,439	12,057	3,968	2.95	4.18	3.11	2.5%	5.1%	3.8%

7.3.2 Defining parameters for offshore renewable energy developments

Table 7-3: Case studies base data

Project Name	**Type**	**Technology**	**Installation**	**Design Life**	**Footprint**	**Installed Capacity**	**Capacity Factor**	**CAPEX**	**CAPEX[4] Currency**	**O&M Costs**	**O&M[2] Currency**	**O&M Year**
North Hoyle	Wind	Turbine	2003	20 Yrs	10.000 km²	60.00 MW	34.3% [82]	81.00 M	GBP	3,438.00 k/yr [83]	EUR	2006
Horns Rev I	Wind	Turbine	2002	20 Yrs	20.000 km²	160.00 MW	39.0% [84]	272.00 M [85]	EUR	10,295.00 k/yr [83]	EUR	2006
Thanet	Wind	Turbine	2010	20 Yrs	35.000 km²	300.00 MW	36.0% [86]	880.00 M [87]	GBP	18,921.60 k/yr	GBP	2010
Kentish Flats	Wind	Turbine	2005	20 Yrs	10.000 km²	90.00 MW	27.7% [88]	105.00 M [88]	GBP	5,037.00 k/yr [83]	EUR	2006
La Rance	Tidal	Barrage	1967	120 Yrs [89]	22.000 km² [90]	240.00 MW	25.7% [90]	617.00 M [91]	FRF	9,725.70 k/yr [92]	EUR	2007
Lake Sihwa	Tidal	Barrage	2010	120 Yrs [89]	42.441 km² [69]	254.00 MW	24.8% [69]	355.00 M [69]	USD	9,932.57 k/yr [81]	EUR	2007
Strangford Lough	Tidal	TCTs	2008	20 Yrs [93]	0.011 km²	1.20 MW	22.8%	8.54 M	GBP	57.85 k/yr [94]	GBP	2003
RITE[5] Project	Tidal	TCTs	2005	20 Yrs	0.053 km²	5.00 MW	24.0%	12.00 M [95]	USD	840.96 k/yr	USD	2009
Aguçadoura	Wave	Pelamis	2008	15 Yrs	0.220 km²	2.25 MW	32.5%	8.20 M	EUR	402.53 k/yr [96]	EUR	2010
Wave Hub	Wave	Various	2010	15 Yrs	8.000 km²	20.00 MW	32.5%	74.66 M	GBP	1,743.40 k/yr [81]	EUR	2010
Location	**Latitude**	**Type**	**PV Type**	**η**	**Installation**	**Life**	**Footprint**	**Inst. Cap.**	**C.F.**	**CAPEX**	**Currency**	**O&M Costs**	**Currency**	**Year**
Pole	90°	Solar	Crystalline	14%	2010	20 Yrs	1.000 km²	70.00 MW	8.6%	234.70 M	CAN	189.00 k/yr	USD	2010
Equator	0°	Solar	Crystalline	14%	2010	20 Yrs	1.000 km²	70.00 MW	20.5%	234.70 M	CAN	189.00 k/yr	USD	2010
Pole	90°	Solar	Thin Film	10%	2010	20 Yrs	1.000 km²	40.00 MW	10.7%	92.44 M	CAN	72.00 k/yr	USD	2010
Equator	0°	Solar	Thin Film	10%	2010	20 Yrs	1.000 km²	40.00 MW	25.6%	92.44 M	CAN	72.00 k/yr	USD	2010

Numbered references listed in reference list. Sources which are not referenced are explained in the consequent sections or widely available in the public media.

[4] Currencies to be converted to 2010 Canadian Dollars
[5] Roosevelt Island Tidal Energy (RITE) project

7.3.2.1 Wind Projects

North Hoyle, Kentish Flats and Horns Revs I wind farms have been operational since 2003, 2005 and 2002 respectively, and documented data is available for the power output. Using actual values for the power output from each of the wind farms, excluding abnormalities in the wind farms' operation – e.g. extensive maintenance on a number of wind turbines, the capacity factors were calculated according to the references given in Table 7-3.

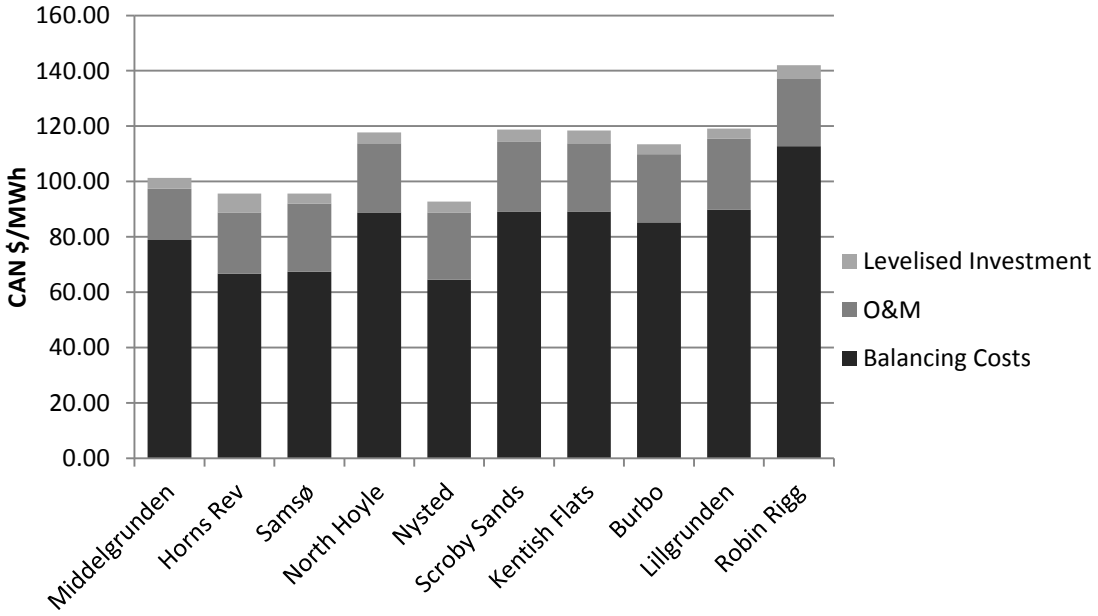

Figure 7-2: Calculated production costs for selected offshore wind farms, in 2010 CAN $ prices – inflated and indexed accordingly from EWEA [83]

Thanet, being a relatively new wind farm (installed in 2010) has not been in production long enough to establish a power production trend sufficient to estimate the capacity factor. Typical estimates of capacity factors for onshore wind in the UK have been at 35%, although from actual

statistics it has been shown that the capacity factor is more in the region of 26% for the onshore wind [97]. For offshore wind farms the actual capacity factors may be expected to be higher than onshore equivalents. As Thanet wind farm adopted modern wind turbine technology a 36% capacity factor was assumed [86]. The European Wind Energy Association [83] provides the values for the O&M costs for the wind farms reported in Table 7-3, presented graphically in Figure 7-2. For Thanet an estimated value relative to the other wind projects was used, pro-rated on the installed capacity.

7.3.2.2 Tidal Projects

Tidal barrage projects can be designed and built with design lives as long as 120 years (as in the case of La Rance, France). This same design life time was assumed for the Lake Sihwa tidal dam, considering replacement of the power generation units, including the turbines, generator etc., over the life span of both the Lake Sihwa and the La Rance projects. This cost is included in the annual O&M costs, which were taken to be EUR 1.8c per kWh for La Rance in 2010 according to Wyre Tidal Energy, WTE [92].

For the Lake Sihwa and Strangford Lough project, details about their operational costs are uncertain so Table 7-2 was used to determine the O&M costs of both projects. The Roosevelt Island Tidal Energy (RITE) project is a research based project, whose aim is to commercialise the deployment of tidal stream arrays. Verdant Power (the developer of the RITE project) gives prices of US $ 0.07 – 0.09 per kWh for the operational cost of the array. An average cost of US $0.08 per kWh was taken for the O&M costs of the RITE project, with a capacity factor of 24% resulting from the average of the other (La Rance, Strangford Lough and Lake Sihwa) tidal

projects' capacity factors. The capacity factors for La Rance and Strangford Lough projects were calculated from reported yields. For Lake Sihwa an estimated based on its declared operating mode [69] was used since this project has not been operational long enough to report annual outputs.

For the Strangford Lough 1.2MW SeaGen tidal unit operated by Marine Current Turbines Ltd. a capacity factor of 48% was stated by Douglas *et al.* [98]. This appeared to be high, considering the periods throughout the day during which electricity generation is low due to minimal or close to no current flow (according to the nature of tidal cycles). A press release by the company to inaugurate its 2GWh milestone, stated that at normal operation it took five months for the machine to produce 1GWh. By scaling up this trend to an entire year, the actual capacity factor is implied to be 23% rather than 48%. This rate is comparable with those reported for other tidal technologies.

The footprint occupied by the tidal barrage projects was determined according to the tidal basin area, while for the tidal stream projects it considered the turbine's array wake effect. For the Seagen marine current turbine (MCT) installed at Strangford Lough, a 10 times rotor diameter downstream spacing and 0.5 times rotor diameter lateral spacing is required to minimise effects of turbulent wakes downstream of the turbine [99]. The footprint area can thus be directly calculated using the rotor specification of the tidal turbine (of 20m). The RITE array has already been designed and installed, thus the array development configuration area is known from the project's case study report.

7.3.2.3 Wave Projects

The Pelamis machines in Aguçadoura - were deployed in 2008, only to be recovered some months later due to reliability issues with the hydraulic rams and very high potential costs related to unplanned maintenance. Consistent performance data are not available to establish the yield and hence the capacity factor for the wave farm, due to the limited time testing. A range from 25 – 40% is given for the capacity factor of the Pelamis machines [100]. This range was averaged at 32.5%, since measured power yields were not available to deduct a reliable figure and was assumed for both the Aguçadoura and Wave Hub wave farms.

The footprint area for the Wave Hub project was taken to be its exclusion zone, while an estimate of the footprint for Agucadoura was calculated using an aerial schematic. The Wave Hub project does not account for the cost of the actual wave devices since it only consists of the infrastructure required to connect up to 20MW of wave energy converters to the grid. The total capital cost and the O&M costs of the wave farm were estimated using Table 7-2, for a 20MW installation. The O&M costs for the Agucadoura project were interpolated from Deane *et al.* [96].

7.3.2.4 Yield and Capacity Factor of Offshore Photovoltaics

Photovoltaic technology harnesses the solar energy resource and converts this to electricity. Variations in the solar insolation influence the capacity factor of a PV device and the output yield in return. For the PV systems the capacity factor is:

$$CF = \frac{Actual \quad P_{out}}{Maximum \quad P_{out}} = \frac{G_T . p.A.\eta.L_m}{R.8760} \qquad [7\text{-}1]$$

where R is the panel's rating (W), G_T is the solar radiation falling on the panels (W/m^2), p is the packing ratio, A is the surface area of the panel's face, η is the panel's efficiency and L_m are the miscellaneous losses of the system. For these cases considered, the packing ratio, p was taken to be 50% with the total footprint of the project being 1 km^2. The efficiencies of the panels were assumed to be 14% and 10% for crystalline and thin film panels respectively. Miscellaneous losses, L_m were taken to be 15%, with inverter losses accounting for 6% and transmission for 5%.

The yield or the actual power output for offshore PVs is dependent upon the location's solar resource, the PV type, the orientation of the panels and the PV surface area which is exposed to solar radiation. The central concept of this work concerns thin film PV only, however, the cases considered here allowed for two types of offshore PV technology: crystalline and thin film, with identical installation sizes (in MW), for comparative purposes. The main varying factor for the electricity generated at one location to another was due to the reduction/increase in solar radiation at that location. The radiation values for the specified locations were taken for a specific latitude rather than longitude. This is due to the low variation in solar insolation across the different longitudes for each latitude. Hence the capacity factors given in Table 7-3, were estimated using insolation data [101] for the specified latitudes – these solar insolation data accounted for shading from cloud scattering and ground reflection.

The typical rating for crystalline panels is 0.14kWp/m^2 while for thin film panels it is 0.08kWp/m^2, based on the installed capacity of the panels per m^2. So for a certain footprint area, an established packing density and PV rating, the installed capacity for horizontal offshore PV installation can be calculated accordingly:

$$R = p.\dot{R}.A \qquad [7\text{-}2]$$

where R is the installed capacity of the offshore PV development (kWp), p is the packing density (%), $\dot{R}$ is the specific peak power of the panel (kWp/m^2) and A is the footprint of the instllation (m^2).

Table 7-4: Potential cost breakdown of offshore PVs

	Pontoon-Based *(Poly-crystalline Si)*	**Flexible System** *(Amorphous Silicon)*
Panels	$ 1,860 /kWp	$ 1,030 /kWp
Pontoon	$ 210 /kWp	-
Moorings	$ 275 /kWp	$ 275 /kWp
Installation	$ 715 /kWp	$ 715 /kWp
Grid Connection	$ 220/kWp	$ 220/kWp
Project Management	$ 110 /kWp	$ 110 /kWp
Total CAPEX	**$ 3,390 /kWp**	**$ 2,350 /kWp**

The capital costs (CAPEX) of such an offshore PV development are broadly dependent upon the installed capacity and the PV technology type. The CAPEX costs for an offshore PV installation would include the cost of the PV panels, infrastructural, deployment and grid connection costs. The CAPEX allocation for the last three items would be the same as that for a wave farm, with the PV arrays installed instead of the wave energy converters. The costs for the Agouçadoura commercial wave farm are reported to be $3.05M [102], with the 2.25MW wave park costing $12.38M (costs inflated to 2010 rates). Moorings, installation, grid connection and project management account for a total of 24% of the total investment [103] in a wave farm. Hence the

infrastructural and installation costs can be taken to be approximately $1320/kWp. The cost per Wp for crystalline PV is approximately $2.07 (additional 10% included for pontoon costs) and $1.03 for the thin film PV [104]. Thus the CAPEX was estimated to be $3390/kWp and $2350/kWp for crystalline PV and thin film PV respectively. For the operating and maintenance costs of the project, US $2700/MW and US $1800/MW were taken for the crystalline and the thin film technologies respectively as indicated in research comparing large scale application of PV technologies [21].

7.4 Economic analysis

The economic analysis was conducted for all of the case studies through inflation and annuitization of the capital cost. A common discount rate of 7.5% was taken for all the projects. The inflation indices applied were taken from the Chemical Engineering Plant Cost Index (CEPCI).

$$Inflated \quad Cost, \quad K(y_f) = K.\frac{x(y_f)}{x(y_c)} \qquad [7\text{-}3]$$

where K is the cost which requires indexing, $x(y_f)$ is the cost index at the inflated year and $x(y_c)$ is the cost index at the project installation year.

$$Annuitized \quad Cost, \quad K = K_o\left(\frac{i}{1-(1+i)^{-n}}\right) \qquad [7\text{-}4]$$

where K_o is the capital cost of the project, n is the project's lifetime and i is the discount rate of the project. The annuitized CAPEX and the O&M costs were then indexed to current prices.

By annuitizing all the capital costs and adding the O&M costs for a base year (2010), and converting currency to CAN $, the discounted cost of electricity produced from each technology could be estimated. Through the comparison of these costs, the economic competitiveness of each of the developments was assessed. The annual yield (power generated) from the cases considered is the product of the capacity factor, the rated capacity of the power plant and the annual hours per year (8760 hours – assuming 100% availability of each technology option).

The economic feasibility of an offshore technology not only relies upon its economic competitiveness in comparison to the other offshore technologies, but also to alternate forms of electricity generation. From Table 7-5 the average cost of electricity production in Ontario, Canada (Ontario borders four of the freshwater Great Lakes and the marine waters of Hudson Bay), is $9.45c per kWh ±20% for conventional technologies (according to 2010 index rates). This indicates that projects which generate electricity at costs higher than these values would not be economically competitive in the market (in Ontario) unless they are subsidised in some other way.

Table 7-5: Cost of electricity generation in CAN $ for alternate energy sources in Ontario, Canada modified from Ayres *et al.* [105] to 2010 index rates

		Cost per MWh		
	Inflation Index	**Coal**	**Natural Gas**	**Nuclear**
2003	401.7	53.75	73.94	77.03
2010	556.4	74.45	102.42	106.70

Production of renewable energy is frequently financially incentivised by national and regional administrations [106]; a feed-in-tariff (FIT) mechanism or contribution obligation mechanism, taxation incentives or capital subsidies could be offered. It is important to note that in this discounted cost of electricity produced metric adopted, no distortions of comparatives are introduced by modelling such incentives.

Table 7-6: Normalized costs for case studies (with indication of maturity level of each technology/installation)

Project Name	**Installed Capacity*** *(MW)*	**Normalized CAPEX** *(CAN $/MW)*	**Normalized O&M** *(CAN $/MW)*	**Maturity**
North Hoyle	60.00	4.27M	90.87k	Commercial stage
Horns Rev I	160.00	3.54M	102.04k	
Thanet	300.00	4.68M	100.58k	
Kentish Flats	90.00	3.06M	88.76k	
La Rance	240.00	2.85M	62.90k	First of its kind globally
Lake Sihwa	254.00	1.44M	60.70k	Commercial stage
Strangford Lough	1.20	13.53M	91.63k	Pre-commercial prototype in non-array configuration
RITE Project	5.00	3.45M	204.02k	Pre-commercial prototype in array configuration
Aguçadoura	2.25	5.50M	245.11 k	Pre-commercial prototype
Wave Hub	20.00	5.95M	119.43k	R&D stage
Crystalline: Polar	70.00	3.39M	2.79k	Fundamental technology mature, but application area is novel and unproven
Crystalline: Equatorial	70.00	3.39M	2.79k	
Thin Film: Polar	40.00	2.35M	1.86k	
Thin Film: Equatorial	40.00	2.35M	1.86k	

* Ideally projects of comparable scale in terms of installed capacity would be considered, but at this stage the maturity levels of each technology do not permit this.

The parameters for each case outlined in Table 7-3, were used to calculate the discounted cost of electricity, comprising the annuitized capital costs per kWh and O&M costs per kWh produced. These costs were estimated by first effecting currency conversions (with exchange rates corresponding to the date of installation), and then the capital costs for each case were annuitized

according to Equation 7-3 (with a discount rate of 7.5%) and then inflated to 2010 index rates using Equation 7-4. The results obtained from this analysis are illustrated in Figure 7-3 with the intermediate results tabulated in Table 7-6.

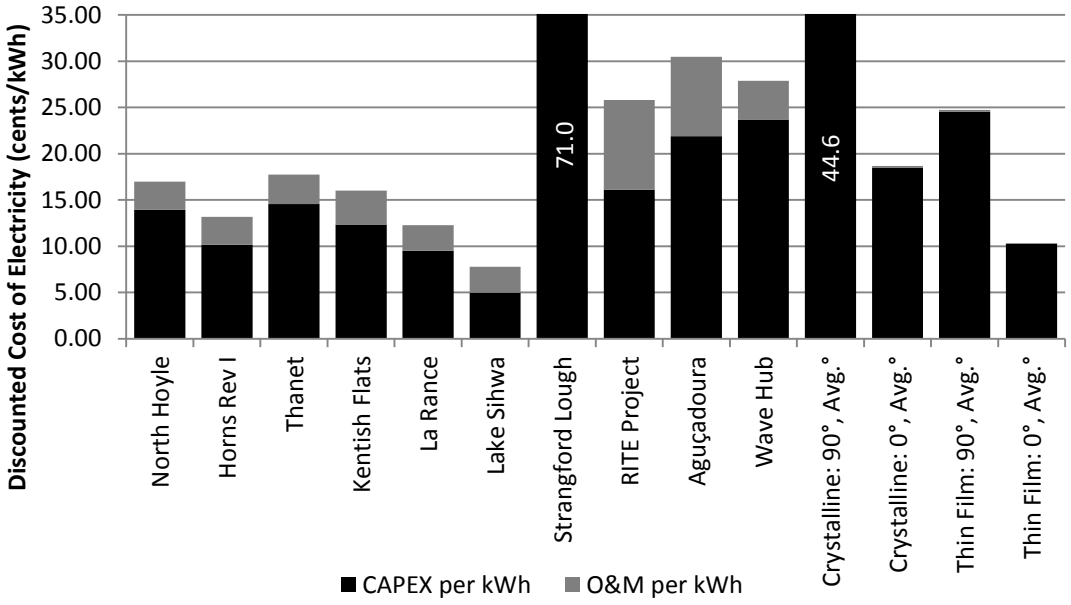

Figure 7-3: Electricity generation price (in 2010 CAN $ rates) for the different renewable energy technologies at a discount rate of 7.5% - PV technologies are reported for polar (90°) and equatorial (0°) regions

The lowest cost for offshore generation development within the cases considered was for Lake Sihwa (a tidal barrage system). Ignoring the PV developments momentarily, the next lowest was La Rance. This suggests that tidal barrage technologies may be the most competitive and should be encouraged. However the barriers to widespread adaptation of this technology are the very high capital intensity (with large maximum cash exposure) and the development construction

times, which could be as much as a decade for large projects. The environmental changes arising from tidal barrage systems are also significant [107].

Comparing the different ‘conventional’ offshore technologies (Table 7-7) it is apparent that tidal barrages are the most economical, followed by wind farms, tidal current turbines and finally wave farms. Offshore thin film PV technologies, at central latitudes compete with the large tidal barrage developments. In all but the most extreme northerly and southerly latitudes, offshore PV technology outperforms offshore wind. Offshore crystalline cases are within the range of offshore wave technologies, although the costs of pontoons or protection of the brittle PV structures are not accounted for, so it is likely that the discounted cost of this specific PV technology would be higher.

It is important to note that some of the cases observed, such as the Aguçadoura and Strangford Lough developments were demonstrator projects and so could be expected to return significantly higher discounted costs of electricity produced than commercial developments. While the floating PV assessments are based on proven PV technology, which is continually being improved to achieve higher efficiencies, these do represent novel application areas and hence present significant business risk. On comparison of Table 7-7 to Table 7-5, it is apparent that current offshore renewable energy technologies, on average, have a higher generation cost than conventional fossil fuel and nuclear plants, though electricity generation from tidal barrages and offshore thin film PV (at equatorial latitudes) is comparable with generation from a natural gas power plant.

Table 7-7: Average cost of electricity generation for each conventional offshore technology

Technology	Avg. Generation Cost*
Wind	$148.62/MWh
Tidal (Dams)	$100.54/MWh
Tidal (Streams)	$460.50/MWh
Wave	$482.01/MWh

* According to 2010 base year

7.5 Technology specific yield

The yield, or the electricity generating contribution of the technology, varies according to the energy specific resource intensity. A high energy density resource exploiting technology requires a smaller spatial footprint to contribute the same energy as a development exploiting a low density resource. In offshore environments, a large spatial footprint implies a large exclusion zone and hence more restrictions on marine traffic, fishing and other offshore users. By minimising the footprint area of the various technologies, the social impacts related to it can be reduced accordingly.

The yield is a measure of the power generated by the technology over a year which is the product of the installed rated capacity and the capacity factor over the 8760 hours in a year. Specific yield was obtained by normalizing the offshore energy development yield by the overall development spatial footprint as given in Table 7-3. The results for the specific yields by technology are illustrated in Table 7-8.

The kWh/kW indicates the electrical energy produced for each case relative to its installed, rated capacity. This indicates that wind technologies have the highest energy production potential,

compared to their installed capacity. The installed capacity per footprint area occupied (MW/km^2) presents the alternative perspective that offshore PV installations and tidal current stream turbines are the most power dense technologies compared to the other technologies when looked at in terms of the development scale rather than the individual turbine/generating unit scale. These same technologies consequently give the highest yields per footprint area occupied. This implies either that i) these particular technologies would be able to generate the same amount of energy as the alternate technologies (wind, wave and tidal barrages) in a smaller excluded area, or ii) in the same excluded area they would produce more energy (Figure 7-3 shows that this would also occur at lower cost).

Table 7-8: Annual Yield and installed capacity per km^2 of footprint for the offshore technologies

Project Name	Installed Capacity	Footprint	C.F.	Yield (MWh)	kWh/kW	MW/km²	GWh/km²
North Hoyle	60.0 MW	10.00 km²	34.3%	180,281	3005	6.00	18.0
Horns Rev I	160.0 MW	20.00 km²	39.0%	546,624	3416	8.00	27.3
Thanet	300.0 MW	35.00 km²	36.0%	946,080	3154	8.57	27.0
Kentish Flats	90.0 MW	10.00 km²	33.5%	264,114	2935	9.00	26.4
La Rance	240.0 MW	22.00 km²	25.7%	540,317	2251	10.91	24.6
Lake Sihwa	254.0 MW	42.44 km²	24.8%	551,810	2173	5.98	13.0
Strangford Lough	1.2 MW	0.01 km²	22.8%	2,397	1997	107.14	214.0
RITE Project	5.0 MW	0.05 km²	24.0%	10,512	2102	95.24	200.2
Aguçadoura	2.25 MW	0.22 km²	32.5%	6,406	2847	10.23	29.1
Wave Hub	20.0 MW	8.00 km²	32.5%	56,940	2847	2.50	7.1
Crystalline: Polar	70.0 MW	1.00 km²	8.6%	52,635	752	70.00	52.6
Crystalline: Equatorial	70.00 MW	1.00 km²	20.5%	125,794	1797	70.00	125.8
Thin Film: Polar	40.00 MW	1.00 km²	10.7%	37,596	940	40.00	37.6
Thin Film: Equatorial	40.00 MW	1.00 km²	25.6%	89,852	2246	40.00	89.9

The specific yields of PV developments are such that this may be the preferred technology option when deployable offshore area is limited. The electricity generating potential per unit area is more than double that for wind, implying that less than half the area could be required for the

same electricity generated. The most power dense technology was that involving tidal stream current turbines, which require approximately less than an eighth of the area required by a wind farm. This energy density of the resource leads to requirements of high resistance in foundation systems and supporting structures - that returns high cost. TCT units have many rotating parts and thus require routine maintenance. The access issue characteristic in high current areas where the resource is best mean that reducing these operating costs will always be a challenge.

8 Techno-Economic Analysis 2: Case for a Hypothetical Mine in the Ring of Fire

Clearly there are many technical aspects requiring investigation and discussion associated with floating thin film PV arrays, however, the principal issue explored in this analysis is the techno-economic balance between the competing floating PV concepts, taking the above factors, and others, into account, and as measured by a life-cycle (discounted) cost of electricity produced basis, with units of $/kWh.

Rather than considering a purely hypothetical situation which would only illustrate the relative merits of each concept, we deal with the urgent and real circumstances of the provision of power for proposed mining operations at McFaulds' Lake in Northern Ontario, Canada (in the Ring of Fire region). The reported outcomes of the analysis will have enhanced significance, relevance and usefulness for remote industrial scale consumers of electrical power, exemplified by the mining operations considered herein.

8.1 McFaulds' Lake

The McFaulds Lake area (52°46′03″N 86°03′29″W), in Northern Ontario, is situated in a region known as the Ring of Fire which is currently subject to mine exploration and appraisal activities. Access to the site is currently unavailable other than through a snow road, as mentioned previously, which can be maintained for short periods of time throughout the winter season. The McFaulds Lake area is situated approximately 250 km west of the community of Attawapiskat on James Bay and 575 km northwest of the town of Timmins (Figure 8-1). Regional access to

the McFaulds Lake project area is currently from Nakina, 300 km to the south, which is serviced by an all-weather road, railroad and a paved 1.2km airstrip [108]. The First Nations communities of Webequie and Ogoki Post / Marten Falls are located 90 km west and 130 km south southeast of McFaulds Lake, respectively. Both communities are currently served by regularly scheduled air service, primarily from Thunder Bay.

Figure 8-1: McFaulds Lake Location and Dimensions (Google Maps, 2011)

One of the challenges for the extraction of ore from such a site is the availability of energy to power machinery and to maintain the mine dry and within reasonable working temperature ranges. For mine development in Canada, energy demands of all forms (electricity, heat, and

motive) may total 200kWh per tonne of ore rock excavated and processed. Annual production rates of 1,000,000 tonnes of ore are not unusual. The implied average power requirements are around 23MW which are typically met through the provision of diesel to the site. Diesel is transported to remote mine site in tankers that use snow or ice roads, that may only be useable for short periods of winter. Sufficient diesel must be transported to sustain mine production throughout the year. These factors mean that for these case study circumstances the cost of fuel is significantly more expensive than the price for mainstream consumers. Furthermore, if the mine runs short of fuel, the two options facing the mining operation are to temporarily suspend production or to import diesel fuel by aircraft which can prove to be even more expensive. Thus one motivation for the consideration of photovoltaic arrays for this new mining development is reduced cost through the displacement of diesel generated electricity with electricity from photovoltaics.

There are other more practical reasons too. The so-called Hudson's Bay Lowland in which the proposed development exists comprises a vast peat land with high boreal to sub-arctic climate, and zones of discontinuous permafrost with thousands of lakes. Engineering any type of foundation on such land is technically challenging. The option of installing PV so that it floats on the surface of one of the many lakes, rather than being ground mounted, may thus be a rather practical solution.

8.2 Analysis parameters and scenarios

8.2.1 Solar generating capacity at McFaulds Lake

The average daily solar insolation data presented in Figure 8-2 reflect the average satellite monitored meteorological conditions for the site. The solar potential, *Y*, (kWh/annum) from an a-Si thin film or crystalline floating PV array on the McFauld's Lake, was calculated and represented in Table 8-1 using the following equation:

$$Y = G_{\beta} p.A.\eta.L_m \qquad [8\text{-}1]$$

where G_{β} (kWh/m^2) is the site's solar insolation; p is the packing density ratio[6]; A (m^2) is the project footprint; η (%) is the module efficiency; and L_m (%) are the miscellaneous losses, such as the array and transmission losses, mainly from the inverters.

[6] The ratio of surface area of PV panels to total area of the offshore site footprint of the PV farm, averaged from existing designs of the Loto (horizontal inclination design) and Floatovoltaics (optimal inclination design) floating PV projects designed by DAEIT and SPG Solar and located in Solarolo, Italy and Far Niente, California respectively. Further details are given by Trapani et al. (2013).

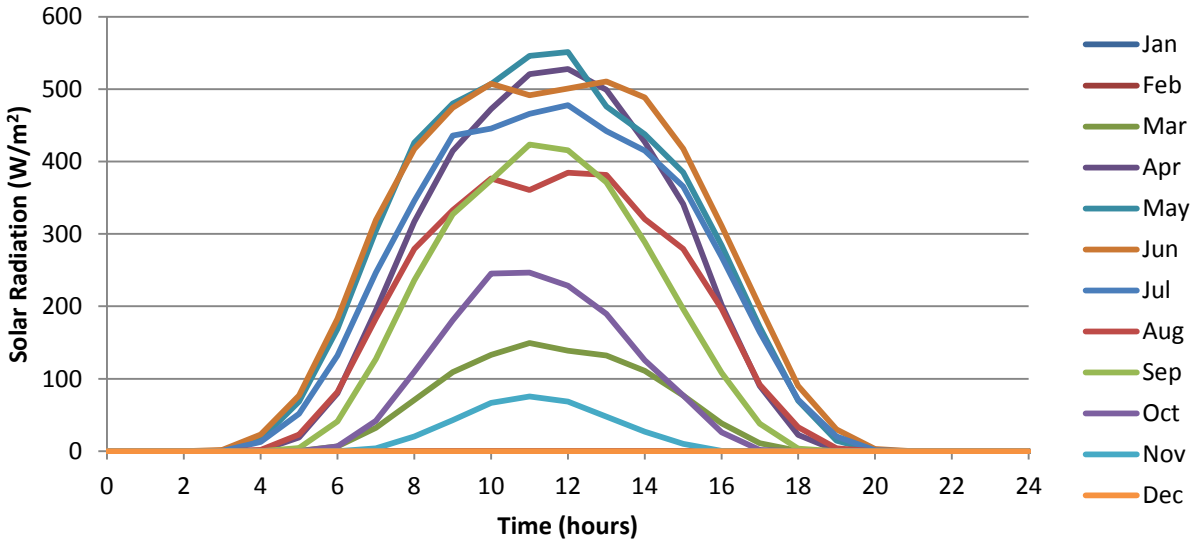

Figure 8-2: Monthly averaged horizontal solar radiation (HelioClim3 Satellite Data – 2003) for McFaulds Lake taking solar radiation to be zero from mid-November to mid-March

Table 8-1: McFaulds Lake total solar resource for a thin film and crystalline PV array (solar data accounting for climatic conditions) [101]

Month	**Solar radiation - horizontal** *kWh/m²/d*	**Yield Thin Film PV Panels (η = 7%)** *GWh*	**Yield Crystalline PV Panels (η = 14%)** *GWh*
Jan	1.11	0.00	0.00
Feb	2.18	0.00	0.00
Mar	3.53	16.37	32.75
Apr	4.85	43.54	87.08
May	5.52	51.21	102.42
Jun	5.74	51.53	103.06
Jul	5.50	51.02	102.04
Aug	4.48	41.56	83.12
Sept	2.98	26.75	53.51
Oct	1.84	17.07	34.14
Nov	1.19	5.34	10.68
Dec	0.82	0.00	0.00
Annual	**3.34 (Avg.)**	**434.2 (Total)**	**607.9 (Total)**

The results assume that the offshore PV installation lies horizontally on the water's surface (i.e. panels are not tilted) and that the PV panels do not generate electricity between mid-November and mid-March due to snow and ice accumulation upon the panels. The calculations estimating yield take the entire area of the lake to be 9.5km^2, with a packing density ratio of 0.5 and miscellaneous losses as described for Equation 8-1 as 10%.

8.2.2 Mine electrical consumption

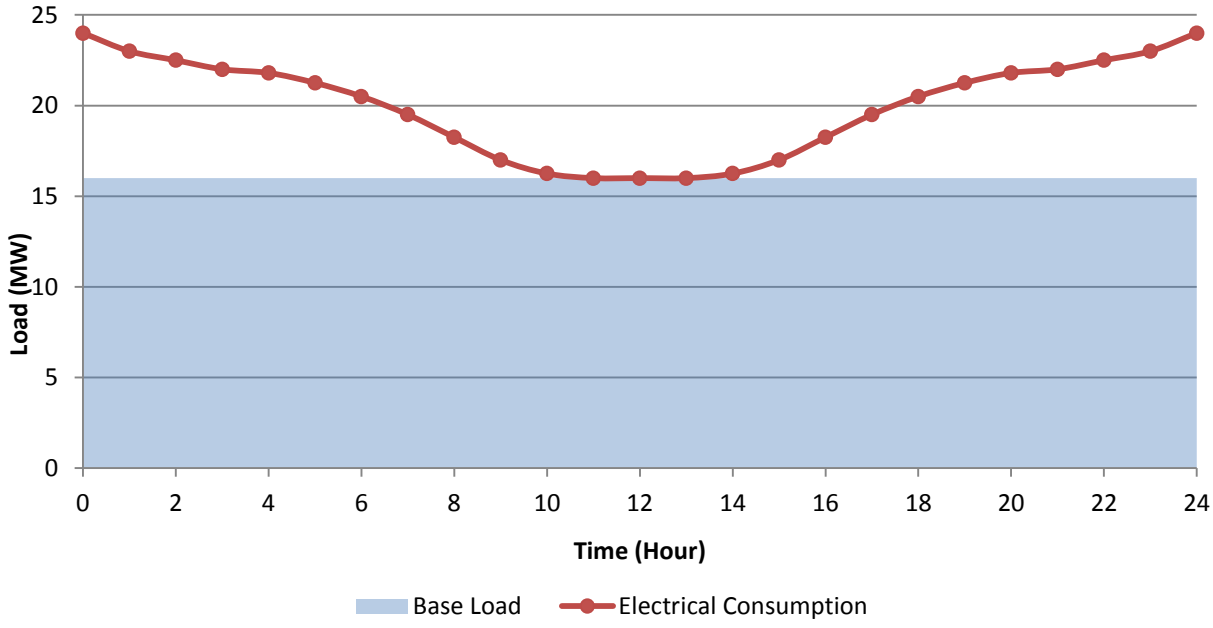

Figure 8-3: Electrical load scenario (24MW Peak, 16MW Base Load and 20MW Average Load)

Mines are typically round-the-clock operations with consistently high demand for electric power. Consideration of the variability and intermittency of electricity generated from solar PV dictates that a PV system will never replace a diesel generating set outright. Instead, the PV system will

have to operate in parallel with diesel engine prime movers and potentially other plant that can store electrical energy. The techno-economic assessment then must consider the efficiency of electrical energy production from, for example a diesel prime mover, when the combined system is operated so that PV produced electricity meets site demand first. Such a policy may push the diesel engine into part load condition where electricity that balances off demand in the islanded system is produced less efficiently.

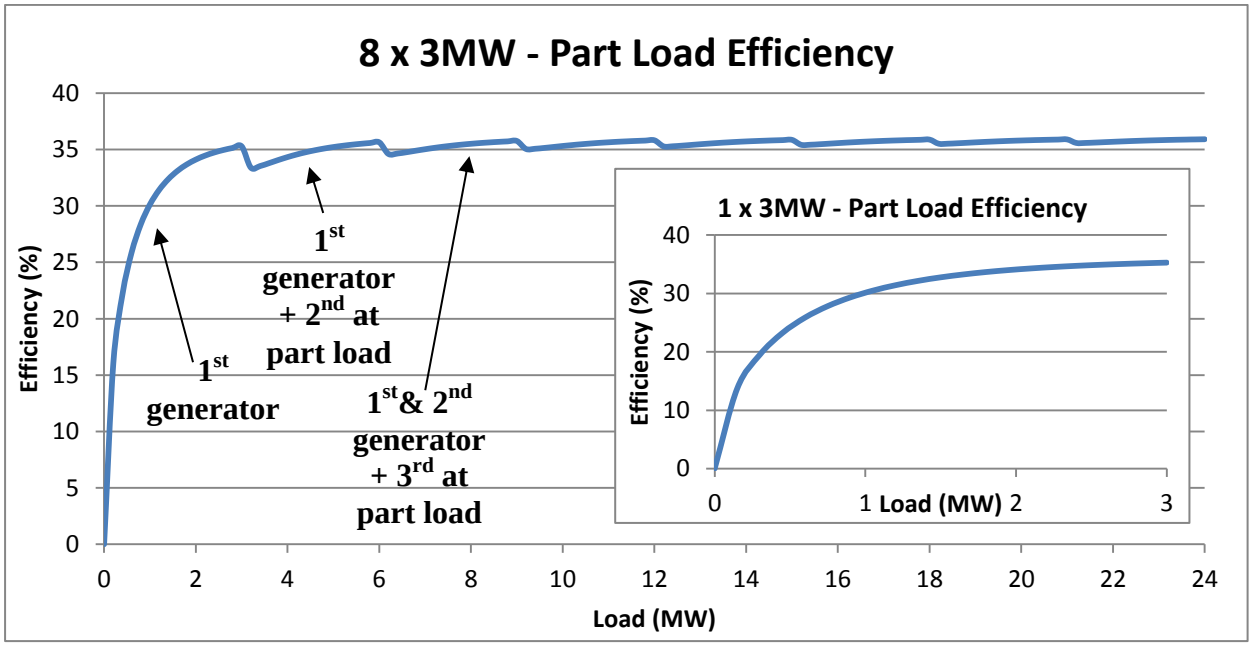

Figure 8-4: Efficiency curve for diesel generators combined in series and single generator [109]

In order to allow modelling of the integrated system a modulating hypothetical load scenario for the mine was created. Figure 8-3 illustrates the hypothetical, but reasonable, electrical load profile for a mine operated such that the 'swing' electrical loads due to dewatering pumps and ore hoist motors loads arise at night. For appraisal of either PV option, the base case electricity

supply solution comprised 8 x 3MW diesel generators and 4 x 4MW stand-by diesel generators, facing an average load of 20MW, peaks of 24MW and 16MW base load. The electrical load consumption profile assumed is not particularly favourable to PV integration, due to the mine's operation peaking when the exploitable solar resource is nil.

For a generating system comprising an array of diesel engine generating sets, the overall efficiency is the aggregate efficiency of each individual generator as described in the equation below:

$$\eta_{aggregate} = \frac{Load_1 + Load_2 + Load_3 + \ldots}{\frac{Load_1}{\eta_1} + \frac{Load_2}{\eta_2} + \frac{Load_3}{\eta_3} + \ldots} \quad [8\text{-}2]$$

The aggregate efficiency for the 8 x 3MW diesel generators is indicated in Figure 8-4, modelled from Saark et al. [109]. When electricity is delivered to the mine solely from diesel generators, the variation in the generators' efficiency is determined by the load offered by the mine. In contrast, when the generators are integrated with solar PV (which would displace diesel fuelled electricity production), the daily variation in solar radiation would also affect the fuel efficiency performance of the diesel generators.

8.2.3 PV – diesel integration scenarios

For the techno-economic analysis, 40MW of installed capacity of diesel generators (including the 16MW back up capacity) were considered. They were integrated with PV, considered across four scenarios of PV array installed capacity, as follows:

- 10MW array (maximum installation to benefit from an available feed-in tariff, FIT)
- 16MW array (PV installed, capacity matches mine base load)
- 20MW array (PV installed, capacity matches average rated power consumption)
- 24MW array (PV installed, capacity matches peak power consumption)

The scenarios taken into consideration for this study assume no solar generation from mid-November to mid-March. The project life, specific capital costs, operating and maintenance costs (including insurances) and fuel costs (where appropriate) adopted in this study are as presented in Table 8-2. These parameters are assumed inputs to the calculation of the discounted cost of electricity; the total annual costs (including annuitized capital expenditure) divided by the total electrical energy produced. For the annuities, a discounted rate of 10% was adopted which reflects a moderate risk investment. A diesel fuel price of $ 1.21/litre was taken to apply throughout the calculations (applicable for 2010) and all costs are in 2010 CAN $[7]. (Annuitized costs and inflated costs are calculated according to equations 7-3 and 7-4 in Section 7.4).

Table 8-2 shows that the discounted cost of electricity produced using the floating a-Si thin film PV technology are lower than those of the diesel generated electricity at a discount rate of 10%. By integrating the technologies, the expectation should be that the overall cost of electricity produced will be somewhat higher than ¢32.98/kWh (discounted cost of electricity of thin film PV only) and lower than ¢39.36/kWh.

[7] Conversion rate of 1 CAN$ = 0.969 USD$

Table 8-2: Costs of the different technologies used in the study (taking a discount rate of 10%), based on work in [60] for costs of the PV[8] and diesel generation costs based on a mine in Northern Ontario

Technology	**Project Life**	**CAPEX**	**O&M (excl. fuel)**	**Fuel**	**Discounted Cost of Electricity[1]**
	years	*CAN $/kW*	*CAN $/yr/MW*	*CAN $ cents/lt*	*CAN $ cents/kWh*
Diesel Generator	25	1,655	53,435	120.63	36.6
Thin Film PV	20	2,350	1,800	/	32.98
Crystalline PV	20	3,390	2,700	/	39.36

[1]Calculated at full load (with 24MW generating capacity used for the diesel generators)

8.3 PV and diesel integrated generation

Table 8-3: Electrical energy generation mix for the different scenarios

Scenario	**PV Installed Capacity**	**DG**	**PV**	**Total**
	MW	*GWh*	*GWh*	*GWh*
No PVs	0	173.78	0.00	173.78
FIT Array	10	165.35	8.43	173.78
Base Load	16	160.30	13.48	173.78
Avg. Load	20	156.93	16.85	173.78
Peak Load	24	153.56	20.22	173.78

[8] Breakdown of the costs are given in the referenced source, which account for the technology being offshore rather than onshore.

The integration method used in this analysis entailed the combination of the part load efficiency curve for the 8x3MW units, described in Figure 8-4, with the resulting generation requirement from the diesel generator after consideration of the electricity generation from the PV arrays. The electricity generation from the two sources, at the different levels of PV integration described by each of the scenarios is given in Table 8-3. In the instances where the PV panels are able to generate more electricity than required to meet the mine load, the PV potential contribution is wasted. Load shifting or energy storage could minimize the wasted potential. The variation in monthly fuel consumption, dependent upon the level of PV integration for either the a-Si thin film or crystalline PV arrays, is given in Table 8-4. Assuming that the electrical generation delivered from the a-Si thin film or crystalline PV panels is equal when the installed capacity is the same (with only the area required for the installation varying). These values reflect i) reduction in fuel consumption due to the electricity generated from solar energy, and ii) the diesel engines operating at part load efficiency according to the assumed mine demand curve.

Table 8-4: Fuel consumed by diesel generator with varying levels of PV integration (Tonnes)

		Jan	Feb	Mar	Apr	May	Jun	Jul	Aug	Sep	Oct	Nov	Dec	Total
PV Installed Capacity	**No PVs**	3624	3273	3624	3507	3624	3507	3624	3624	3507	3624	3507	3624	42666
	FIT Array (10MW)	3624	3273	3543	3204	3252	3136	3292	3376	3290	3509	3482	3624	40605
	Base Load (16MW)	3624	3273	3499	3023	3031	2914	3095	3222	3160	3445	3463	3624	39373
	Avg. Load (20MW)	3624	3273	3469	2902	2884	2768	2966	3119	3073	3399	3451	3624	38551
	Peak Load (24MW)	3624	3273	3441	2783	2732	2623	2831	3019	2991	3356	3440	3624	37735

8.4 Economic analysis of scenarios

In this section, for one scenario, we present the details of how the various cost and price figures have been used in order to arrive at the principal metrics used to discriminate the options considered. The complete set of results are then presented.

8.4.1 Sample calculation

McFaulds Lake lies within the Province of Ontario, Canada and so is also modelled as benefitting from the renewable energy incentives available within that province[9]. The Ontario Power Authority (OPA) has different tariff rates for solar energy technologies depending on installation size and the type of installation, i.e. roof top or ground mounted installations. The installation size ranges from 0 – 10MW [110]. Assuming the ground mounted installation tariff applies to offshore PV installations, the feed-in tariff for a 10MW installation is 44.3c/kWh. A sample calculation for the 10MW PV array scenario, benefiting from additional revenue arising from the FIT tariff as applicable in Ontario, is demonstrated in Table 8-5.

For the calculation in Table 8-5 the annuitized CAPEX and O&M costs, for both the diesel generators and floating PV array, are calculated using values from Table 8-2. The fuel costs for the diesel generator are estimated from the consumption of diesel (Table 8-4), assuming a fixed price of $1.21/litre, as specified earlier. The total annual cost for the PV + diesel integration is the sum of all annuitized capital expenditures, operation and maintenance and fuel costs for the

[9] Although currently off-grid systems are ineligible for FIT revenues in Ontario, this case was presented to highlight the economics with additional revenues from an external source for renewable electricity generation.

entire system. The net annual cost is the difference between the total annual cost and the total FIT benefit. The FIT benefit can be estimated from the amount of electricity generated from the floating PV in Table 8-3 in conjunction with the fixed price of the FIT benefit per kWh of electricity generated. Thus the discounted cost of electricity for the diesel PV hybrid can be established by dividing the total cost of electricity generation (net annual cost) by the total units of electricity consumed on site.

Table 8-5: Discounted cost of electricity calculation for the 10MW FIT scenario

Diesel generators (40MW$_e$)			
Annuitized CAPEX (i=10%, 25yrs)	$	7.293M	+
Annual O&M	$	2.137M	+
Annual fuel costs	$	51.56M	+
Thin film PV array (10MW$_p$)			
Annuitized CAPEX (i=10%, 20yrs)	$	2.760M	+
Annual O&M	$	0.018M	+
Annual fuel costs	$	/	
Total annual cost	$	63.77M	-
Total FIT benefit	$	3.732M	
Net annual cost	$	60.04 M	
Discounted cost of electricity produced incl. FIT		**34.548 c/kWh**	

The discounted cost of electricity of the diesel generators for the required demand, with no PV integration, was found to be 36.60c/kWh. For the 10MW scenario, not taking into consideration any revenue from the FIT tariff, the discounted cost of electricity was 36.70c/kWh for an a-Si thin film array integration and 37.40c/kWh for crystalline array integration. The higher costs without the FIT imply that the at the assumed rate of diesel a PV-diesel integration would not be feasible to finance unless an additional revenue was available such as the FIT.

8.4.2 Economics for all scenarios

Table 8-6: Discounted cost of electricity for each of the scenarios (not considering FIT)

	PV Installed Capacity	**Electricity Generation** *(MWh)*		**Fuel Consumption** *(Tonnes)*	**Annuitized CAPEX** *(Million $)*		**Annual O&M** *(Million $)*		**Fuel Cost**	**Discounted Cost**	**Electricity Offset**
	MW	*PV*	*DG*	*DG*	*PV*	*DG*	*PV*	*DG*	*Million $*	*$ cents/kWh*	*%*
Thin Film Integration	0	0	173777	42666	0.00	7.29	0.00	2.14	54.18	36.60	0.00
	10	8425	165352	40605	2.76	7.29	0.02	2.14	51.56	36.70	4.85
	16	13480	160297	39373	4.42	7.29	0.03	2.14	49.99	36.75	7.76
	20	16850	156927	38551	5.52	7.29	0.04	2.14	48.95	36.79	9.70
	24	20220	153557	37735	6.62	7.29	0.04	2.14	47.92	36.84	11.64
Crystalline Integration	0	0	173777	42666	0.00	7.29	0.00	2.14	54.18	36.60	0.00
	10	8425	165352	40605	3.98	7.29	0.03	2.14	51.56	37.40	4.85
	16	13480	160297	39373	6.37	7.29	0.04	2.14	49.99	37.87	7.76
	20	16850	156927	38551	7.96	7.29	0.05	2.14	48.95	38.21	9.70
	24	20220	153557	37735	9.56	7.29	0.06	2.14	47.92	38.54	11.64

The discounted cost of electricity for the remaining scenarios was calculated in a manner similar to that described by the sample calculation in Section 8.4.1, with the FIT ignored (the projects are greater than the 10MW eligible threshold). The results for the integrated plants are given in Table 8-6. They imply the mine's electrical consumption profile is as shown in Figure 8-3, and does not involve load shifting or similar demand side management.

Table 8-6 shows that for whatever level of integration for either a-Si PV or crystalline PV the economics are not favourable since the discounted cost of electricity with the PV array is higher than that of the diesel generation itself. If load shifting, e.g. water pumping during peak solar time rather than other times was considered, more savings could be realised by allowing the system to run at higher full load efficiencies and also allow larger PV installations to be integrated into the system.

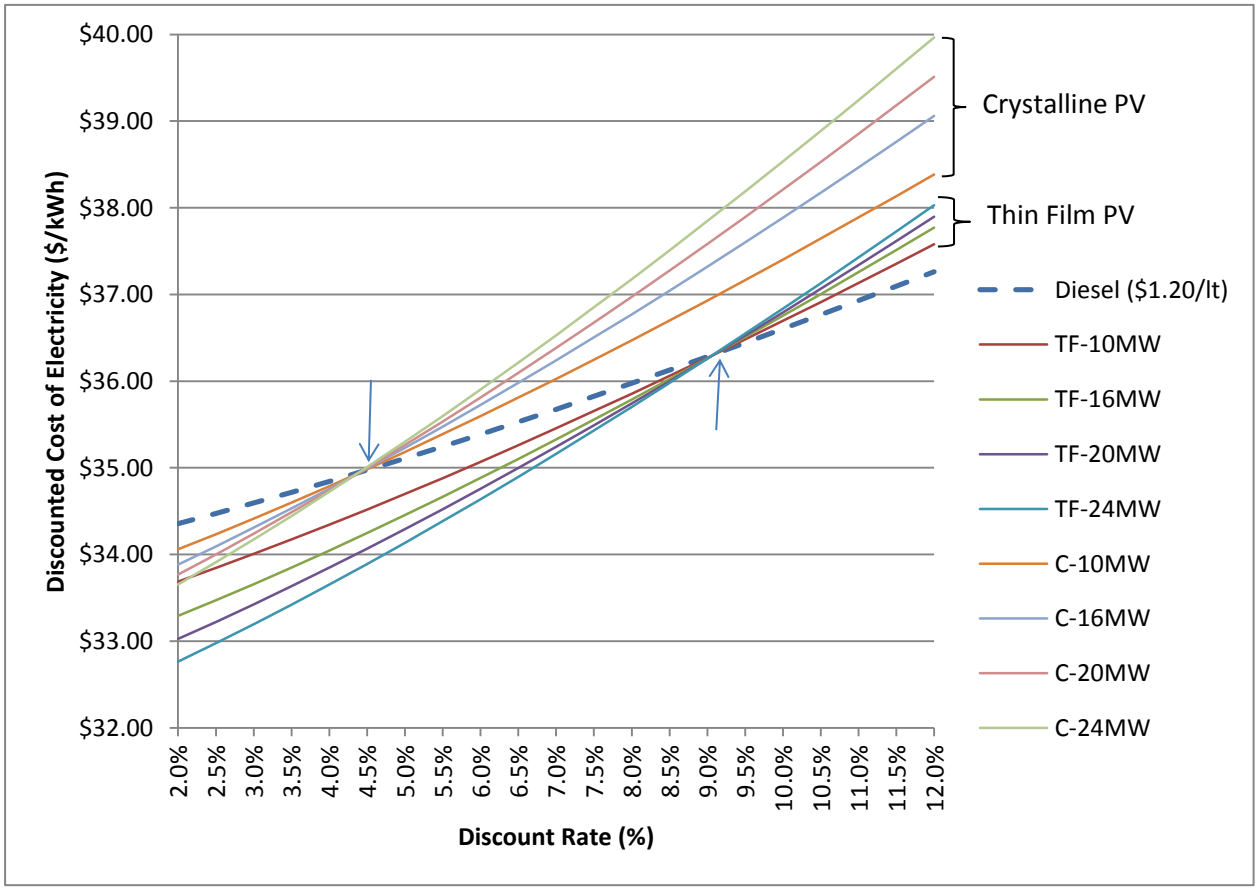

Figure 8-5: Varying discounted costs of electricity for the levels of PV integration scoped within the techno-economic analysis for (TF) thin film and (C) crystalline systems at different discount rates.

Also if the project discount rate was taken to be ~ 9.2% or less for thin film PV integration, the generation of electricity from PV would be at breakeven point (point at which individual discounted cost of electricity from PV equals that from diesel generation) – this is illustrated in Figure 8-5. For crystalline, the breakeven point is lower at 4.3% and this is due to the higher CAPEX costs. So mining companies assessing the feasibility of floating PV integration with their existing diesel electricity generating system, will need to consider both the discount rate applicable to the project as well as the current and projected cost of diesel fuel.

8.4.3 Economic Considerations

The discounted costs of electricity presented in Table 8-2 assume that all electricity that can be produced by the system can be usefully used to meet system use. The four scenarios considered are essentially distinguished by their installed capacity relative to the key points on the mine's daily load profile illustrated in Figure 8-3. The feed-in-tariff (FIT), 10MW project scenario, would be able to usefully offset diesel generation at any time, as would the 16MW PV array that is scaled to meet base load. Systems any larger than this capacity may not face sufficient load from the mine to consume all of the potential output from the PV when the solar resource is the highest. For installed capacities matching average and peak loads, the discounted cost of electricity are thus higher than they could have been if the load profile was changed so that the peak load occurred around noon, when the solar resource is highest. The particular operations of a mine could permit more flexible load shifting to suit the source of electricity generation. We have been conservative in the analysis by using an adverse mine load profile, presenting a mine load profile which peaks around mid-day, at the point in which the solar resource is the highest,

would make maximal use of the electricity generated from PV and allow greater capacities of installed PV capacity.

Table 8-7: Discounted cost of electricity for each of the scenarios with fuel cost at $1.29/litre

	PV Installed Capacity	Electricity Generation (MWh)		Fuel Consumption (Tonnes)	Annuitized CAPEX (Million $)		Annual O&M (Million $)		Fuel Cost	Discounted Cost	Electricity Offset
	MW	*PV*	*DG*	*DG*	*PV*	*DG*	*PV*	*DG*	*Million $*	*$ cents/kWh*	*%*
Thin Film Integration	0	0	173777	42666	0.00	7.29	0.00	2.14	57.94	38.77	0.00
	10	8425	165352	40605	2.76	7.29	0.02	2.14	55.14	38.75	4.85
	16	13480	160297	39373	4.42	7.29	0.03	2.14	53.46	38.75	7.76
	20	16850	156927	38551	5.52	7.29	0.04	2.14	52.35	38.75	9.70
	24	20220	153557	37735	6.62	7.29	0.04	2.14	51.24	36.75	11.64
Crystalline Integration	0	0	173777	42666	0.00	7.29	0.00	2.14	57.94	38.77	0.00
	10	8425	165352	40605	3.98	7.29	0.03	2.14	55.14	39.46	4.85
	16	13480	160297	39373	6.37	7.29	0.04	2.14	53.46	39.88	7.76
	20	16850	156927	38551	7.96	7.29	0.05	2.14	52.35	40.17	9.70
	24	20220	153557	37735	9.56	7.29	0.06	2.14	51.24	40.45	11.64

In the economic analysis undertaken although floating a-Si PV arrays offered a discounted cost of electricity generation cheaper than for floating crystalline PV arrays this was still not enough to cover the costs associated with integration. The cost of fuel would have to be $1.29/litre before any financial benefit can be derived the integration with the PV. Table 8-7 shows how the economics would look with the higher cost of fuel. So current economics would not be able of offering a feasible alternative to remote mine sites with fuel lower than $1.29/litre unless they benefit from a carbon credit or a renewable energy incentive. Since the discounted cost of floating a-Si PV arrays is lower than that of diesel, with maximal utilisation of the PV potential, at large enough scales it would bring costs slightly down.

In the study the discounted cost for fuel generation reflects a fuel price of $1.21/litre that is typical for a bulk consumer of diesel, such as a mine, delivered to a remote location in Canada.

The capital and operation and maintenance costs also reflect installation and operation in a remote location. Diesel generators located closer to transportation networks would be expected to have lower discounted cost of electricity produced, but would be unlikely to compete with the grid electricity that would be available in those locations.

The balance-of-plant items represented in the capital costs for the photovoltaic systems are based on published research data of marine renewable energy, such as wave farms. They are taken to be the same for both competing PV technologies; suitable adjustments were made for the different areas they occupy. Aside from the differences in the fundamental procurement cost of the panels, of either type (crystalline silicon panels approximately doubling in price), a major distinction between capital costs arises from the uses of a floating structure or not. The panel's procurement cost are prevailing market prices, they do not consider the relative tightness of supply of the a-Si thin film PV market; the quoted price for a-Si thin film PV panels is higher than market price. The use of a prevailing market price is motivated by the scale of procurement considered for any of the cases – which is large.

Even though the case study presents a specific example of a mine in the far north of Ontario, the findings of this case study economic analysis will be of relevance to any large scale industrial consumer of electricity. We have included in the economic analysis, the availability of a FIT which exists in Ontario, for completeness in the examination of a McFaulds Lake development. Despite this site specific finding, it illustrates the effect of similar incentives in different administrations. At the scale of installation considered herein, the effect of such an incentive is

diminished as there are thresholds of the installed capacity on which incentives can be claimed (or the electricity produced by that installed capacity).

8.5 CO_2 emission analysis

Table 8-8: Embedded carbon in crystalline [111] and thin film PV [112]

Process	Thin Film PV $kgCO_2/m^2$	Crystalline PV $kgCO_2/m^2$
Manufacturing Process	21.3	51.1
Panels	20.1	20.1
Inverter	2.3	2.3
Support	19.9	19.9
Balance of System (BOS)	2.3	2.3
Capital Inputs	18.4	18.4
Transportation	0.13	0.53
Total	84.4	114.6

Table 8-8 presents the list of processes which emit CO_2 during the manufacturing and installation of the PV arrays. The pontoon is taken to be made from PVC cubes (8 such cubes in a $12m^2$ area with dimensions of 0.5m x 0.5m x 0.4m and a cube thickness of 1mm[10]) which have an embedded carbon of $640kgCO_2$/tonne [113] and a density of $1.4g/cm^3$. The transportation component included the distance where the PV arrays would be installed, at McFaulds Lake, using a factor of $0.03kgCO_2$/tonne.km travelled by a road freight (60 tonne articulated truck) [114]. Crystalline PV compared to a-Si thin film has a higher efficiency so for the same installed capacity a larger area needs to be occupied by the thin film array.

[10] Following the design of the FLOTOVOLTAICO® which was installed in Bubano, Italy.

The data from Table 8-8 was combined with the project areas as indicated in Table 8 (which reflect spacing or packing ratio of 0.50) to calculate the total embedded carbon for each scenario and technology, as shown in Table 8-9. Taking a fixed emission rate of 2.74 kgCO_2/kg of diesel [115] the carbon savings were also estimated by accounting for the reduction in litres of diesel (Table 8-4) through the installation of the PV arrays. The carbon savings exclude any potential emissions arising from the decommissioning of the PV system after the design life of the project.

Table 8-9: Embedded carbon and carbon savings according to PV array type and size

	Project Area		**Project Embedded Carbon Installed**		**Lifetime Carbon Offset**	
	Thin Film PV	**Crystalline PV**	**Thin Film PV**	**Crystalline PV**	**Thin Film PV**	**Crystalline PV**
	m^2	*m^2*	*tonnes CO_2*	*tonnes CO_2*	*tonnes CO_2*	*tonnes CO_2*
FIT Array (10MW)	285,714	142,857	12,057	8,186	100,782	104,653
Base Load (16MW)	457,143	228,571	19,291	13,097	160,986	167,180
Avg. Load (20MW)	571,429	285,714	24,114	16,371	201,123	208,866
Peak Load (24MW)	685,714	342,857	28,937	19,646	240,978	250,269

The case study does not consider economies of scale for either the diesel or the PV installations, and thus has to be considered when looking at the trends in Table 8-9 (none of which consider the FIT). The embedded carbon in the a-Si thin film PV and crystalline PV is small relative to the carbon embedded in the diesel generation. This is why for equal capacities of PV there is similar offset of CO_2 lifetime savings. The footprint area for the technologies will be lower for crystalline PV due to its higher efficiency, but the different areas have been taken into account in the economic analysis. The data presented in Table 8-8 offer a comparison in technologies for embedded CO_2 emissions considering land mounted applications, for which data is available,

augmented by the challenges in transportation to a remote location. For crystalline PV the material type and quantity required for a pontoon mount is assumed comparable with the quantity and material for a land mount. However the added requirement of a pontoon for buoyancy was included in the embedded CO_2 estimate.

Another crucial consideration for either type of offshore PV systems is the land use change factor. This factor is considered "capital" or embedded carbon in renewable energy developments that are significant but not reflected in Table 8-8 prepared by Myrans [111] and Pacca et al. [112]. In remote areas which are forested, the carbon emissions recognised by the IPPC include land use and land-use, change forestry (LULUCF). If grassland or woodland is cleared to make way for a PV development, there will be an impact on the LULUCF emissions. Taking a boreal forestation for the site, the annual CO_2 absorbed by photosynthesis is 963g of CO_2/m^2 [116]. So over the biggest land expansion considered in Table 8, if 685,714m^2 of forest land was to be replaced by a solar farm the carbon balance would be -12,049 tonnes of CO_2 (annuitized) rather than -660 tonnes of CO_2 absorbed by the natural ecosystem over one year. This implies that the LULUCF would be very positive (-11,389 tonnes of CO_2), since the carbon offset is in terms of diesel emission savings which are a lot higher than what could be naturally absorbed by a forest occupying the same area as the solar farm. In a water environment the CO_2 absorption would be ~ 10.7g of CO_2/m^2 annually (taking an equal O_2 to CO_2 dilution) [117] and should not be impacted significantly by the floating panels since the CO_2 dilution is based on water concentration. Hence the LULUCF would be slightly better when considering the offshore environment since there are no big changes to the ecosystem to consider in the analysis.

9 Techno-Economic Analysis 3: Case for Islanded Grid Community of Malta

The islands of Malta are located in the Mediterranean basin enjoying an average daily insolation of 5.29kWh/m^2, at latitude of 35° 50 N, with minimal land space availability due to its 316km^2 small size. Electricity generation for the island is solely dependent upon fossil fuels which are high in CO_2 emissions. According to the EU Directive [118] of the European Parliament and of the Council, on the promotion of the use of energy from renewable energy sources, it requires member states to achieve a share of energy of the gross final consumption from renewable energy. As per Annex I of this directive, Malta is required to produce 10% of its energy from renewable energy sources by 2020. Malta must find alternative feasible solutions for production of electricity, which is challenging because the amount of land that can be allocated to energy production is low due to the high population density.

A comparison for the countries within the European Union [119] indicates a high potential for electricity generation from solar energy in Malta. A figure of 3.55% is given for the PV area coverage (not accounting for the shading factor) for the production of the country's demand in 2005 – considering panels with a specific installed capacity of 0.105kW_p/m^2. At a shading factor of 50%, this would entail approximately 1180MW_p of installed PV capacity over an area equivalent to circa 7% (or 22.08km^2) of the country's area. This chapter will present a techno-economic analysis study, considering the integration of offshore photovoltaics (due to ground mounted restrictions) together with the existing oil-fired power stations on the islands. Similar

techno-economic analyses have been conducted for islanded communities or remote regions [120-123].

Malta is made up of three islands (Malta, Gozo and Comino), totalling 316km^2 in area. This archipelago is situated in the middle of the Mediterranean Sea, just beneath Sicily, with a population 410,567 according to the latest census of 2007; with the majority of the people living on the biggest of the islands, Malta. The main economy of the country is tourism and Malta depends almost entirely on importation for the supply of natural resources and consumer goods. There are no pipeline or cable connections yet available with any neighbouring countries (e.g. Italy, Libya). Plans are in place for a cable interconnection (electrical) to Sicily commencing in 2013, installation is planned to be completed by the end of 2014.

9.1 Geographic Motivation and Constraints of Malta

Table 9-1: Land use in Malta, according to the 2006 CORINE Land Cover Change data.

Land Use	*km^2*	*%*
Agricultural Area	137.20	43.49
Urban/Commercial Area	86.54	27.43
Protected Land	49.61	15.72
Complex Vegetation	38.20	12.11
Mineral Extraction Sites	3.54	1.12
Dump Sites	0.41	0.13

Majority of land use in Malta (Table 9-1) is for agricultural purposes with 114.53km^2 of land registered as being utilised for this purpose according to the 2010 census. In the same census [124], 12,529 holdings are recorded for the registered land (both utilised and unutilised). This would indicate that for a parcel of land / holding the specific area averages at 0.009km^2 (see

Figure 9-1 inset for a visual representation of typical landholding size and shape). C*irca* 200 holdings are larger than 5ha [124]. As 98% of holdings have sole owners, a multi-MW installation would almost inevitably involve multiple holding owners, increasing the contractual and legal complexity of any proposed development. Agricultural land which is leased to the holding owners by the government is constrained to *Chapter 199 of the Agricultural Leases (Reletting) Act* which allows a lessor's application (to obtain lease) if they prove that "the field was allowed to lie fallow[11] for at least twelve consecutive calendar months". Considering that 2/3rd of the agricultural land is state owned [125] and hence be subject to the *Chapter 199 of the Agricultural Leases (Reletting) Act,* this would further diminish possibility for ground-mounted installations on currently agricultural land. The scarcity and constraints of land on the Maltese islands require alternative sites for large scale PV to be explored, such as moving them offshore. An offshore installation would also avoid displacement of agricultural activity, currently attributable to *circa* 2% of the country's GDP.

The ratio of area of territorial waters to area of land mass for Malta is approximately 10, implying that the resource potential from solar electricity generation is significantly larger offshore than it is onshore. Malta has territorial waters spanning over 3,000 km^2 and control over approximately 61,000 km^2 of the Mediterranean Sea [126] (Figure 9-2). The waters surrounding the island are almost landlocked by the countries surrounding the Mediterranean Sea, with ocean access through the Suez Canal and the Strait of Gibraltar. Water level variation due to the tidal

[11] Literally speaking means to exist unplanted for a period of time, while figuratively speaking means to remain unused and neglected, this leaves the act open to legal interpretation.

effects is negligible around the Maltese coastline and tidal currents are slight. Also the characteristic waves within the Mediterranean basin tend to be of lower period and significant wave height nature compared to ocean waves, due to the shorter fetches over which the wind acts.

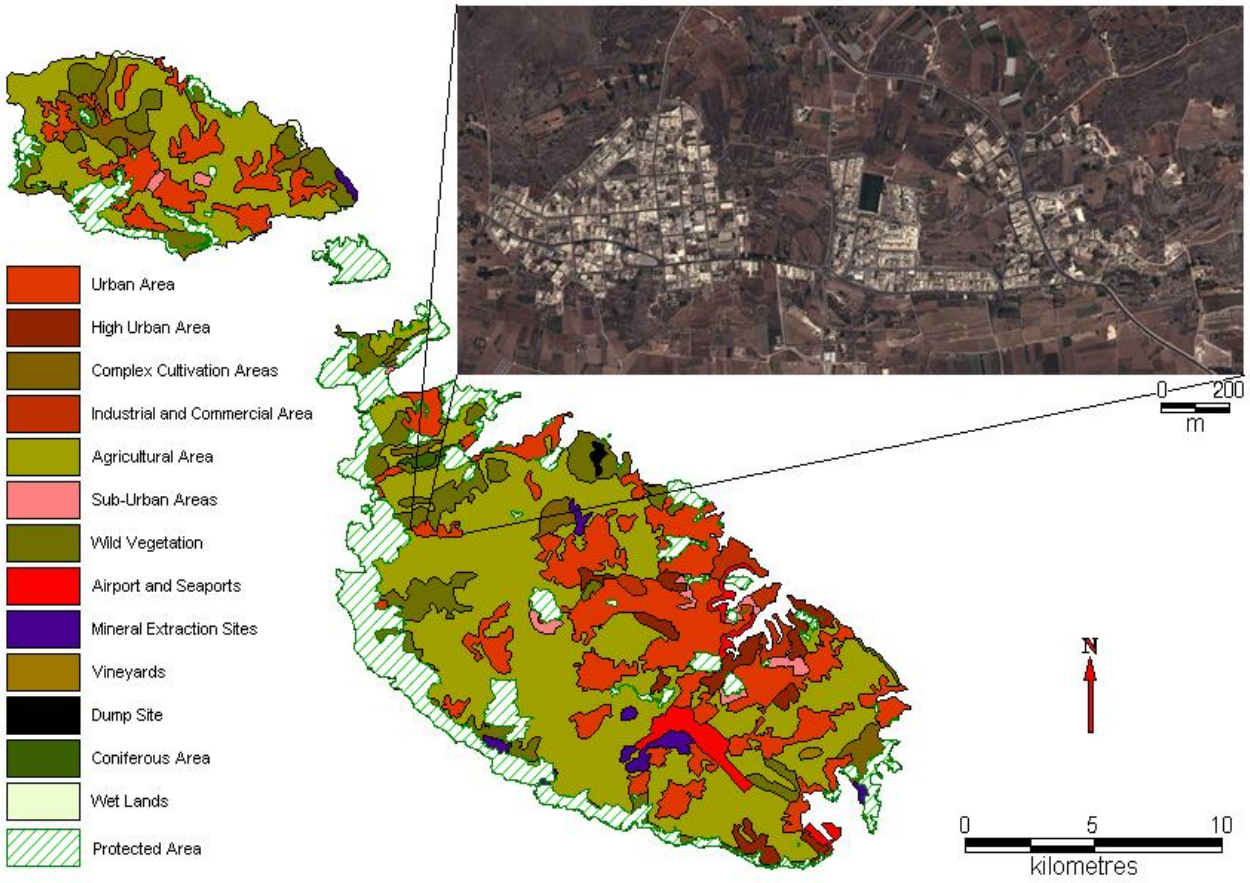

Figure 9-1: Map of the Maltese Islands showing land use according to CORINE Land Cover Change (CLC) data (2006), with a satellite image showing a section of the urban and agricultural area (land holdings).

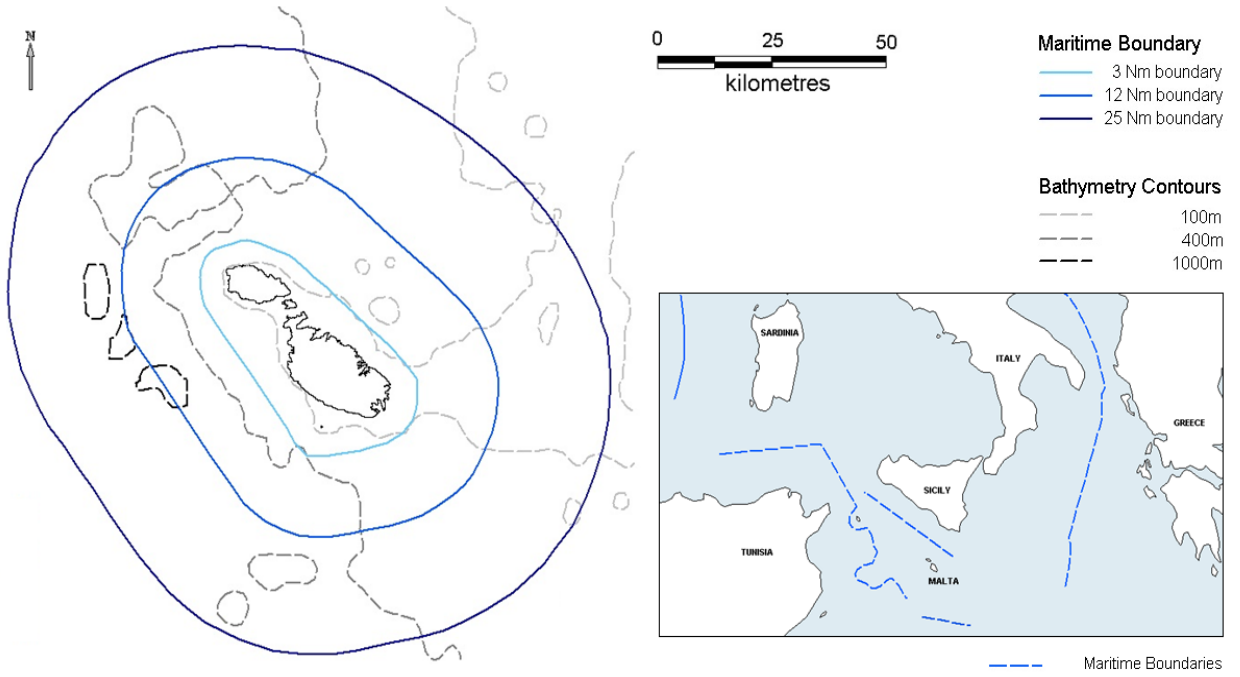

Figure 9-2: Map of the Maltese Islands showing Territorial Waters (12Nm boundary) and Fishing Zone (25Nm boundary), and the southern and western maritime boundaries of Malta, modified from Blake (1997) [126].

9.2 Resource, Infrastructure and Demand

9.2.1 Solar Resources

The total annual solar radiation on the horizontal surface in the waters offshore of the Maltese islands (at a latitude of 35.9° and Longitude of 14.6°) is 1932.9kWh/m^2 (5.29kWh.m^2/d x 365d) according to the data given in Table 9-2. The calculations undertaken in preparation of Table 9-2 assume that the panels lie perfectly horizontal on the surface of the lake and that the PV panels generate electricity all year round. Yield estimates in Table 9-2 assumed miscellaneous losses of

10% from total electricity generation and depict an efficiency of 7% for thin film arrays and 14% for crystalline arrays; packing density is not accounted for when calculating the specific yield from either technology.

Table 9-2: Malta solar and technical PV (for horizontal oriented panels) resource averages including climatic conditions [101].

Month	**Solar radiation - horizontal** *kWh/m²/d*	**Yield a-Si PV (η = 7%)** *kWh/m²*	**Yield Polycrystalline PV (η = 14%)** *kWh/m²*
Jan	2.67	5.79	11.59
Feb	3.70	7.25	14.50
Mar	5.00	10.85	21.70
Apr	6.36	13.35	26.71
May	7.29	15.82	31.64
Jun	8.02	16.84	33.68
Jul	8.11	17.60	35.20
Aug	7.21	15.65	31.29
Sept	5.76	12.09	24.19
Oct	4.18	9.07	18.14
Nov	2.84	5.97	11.93
Dec	2.31	5.01	10.03
Annual	5.29 (Avg.)	135.16 (Total)	270.60 (Total)

9.2.2 Existing Electricity Generation Infrastructure

Enemalta is the public entity which is responsible for the electricity generation and distribution to consumers in Malta. It operates two power stations, including five generating stations (Table 9-3): two of which produce steam for electricity generation through the combustion of heavy fuel oil (HFO) with 0.7% S and the other three combust gas oil with 0.1% S. The power stations are on two sites, one at Marsa and the other at Delimara. The open cycle gas turbines (OCGT) are mainly utilised as peaking plants, with the base load being supplied by the steam turbines from the HFO plants. The combined installed generating capacity for Malta is 562.5MW.

Table 9-3: Electricity generating power stations Malta [127].

GTs Gas Turbines 3 Units	Installed Capacity (MW)	37.5	37.5	37.5				
	Minimum Load (MW)	4	4	4				
	Efficiency at Full Load	32%	32%	32%				
CCGT[12] Combined Cycle GT 1 Unit	Installed Capacity (MW)	110						
	Minimum Load (MW)	20						
	Efficiency at Full Load	40%						
MPS Marsa Steam Turbines 7 Units	Installed Capacity (MW)	60	30	30	30	30	30	10
	Minimum Load (MW)	35	15	15	15	15	15	4
	Efficiency at Full Load	29%	25%	25%	25%	25%	25%	25%
DPS Delimara Steam Turbines 2 Units	Installed Capacity (MW)	60	60					
	Minimum Load (MW)	26	26					
	Efficiency at Full Load	32%	32%					

As of 2005, Enemalta also committed itself to purchase all renewable energy generated on the islands. A 100km inter-connector power line with Sicily is planned for and is expected to be operational by the end of 2014, which will increase the available capacity by 200MW and provide opportunity for electricity export (although it is primarily designed for electricity importation). This would allow the retirement of the Marsa Station which currently breeches the emission limit set by the EU concerning integrated pollution prevention and control (IPPC) directive and is due for closure by 2015. Hence the electricity mix for 2020 is expected to include 200MW of capacity from the interconnector, an expansion of capacity of 144MW [14] at Delimara power station (bringing the total installed capacity to 264MW) and 100MW installed capacity from renewable energy installations with assumed capacity factor at 25% (at similar levels of demand).

[12] Split between 2 x 37MW gas turbines and 1 x 36MW steam turbine

9.2.3 Load Demand

From recorded load data supplied by Enemalta [127] (Table 9-4), the base load condition for the Maltese power system can be seen to be in the early morning hours, between 1 – 5am. The main trend for the demand profile in winter is an increase in electricity consumption until 8am (at which time a plateau is achieved), an increase to peak conditions in the evening (~ 6pm) and then a decrease back to the base load. In summer, the peak is shifted to morning hours, reflecting usage of air conditioning systems. The base load is higher in summer (c. 225MW), when the greatest influx of tourists is measured on the islands, than it is in winter (c. 170MW). For the weekends, the base load is generally lower, with two peaks occurring, the first just before noon and the second in the evening.

Table 9-4: Base and peak loads for monthly weekday (WD) and weekend (WE) demand profiles based on Enemalta monthly demand profiles for 2010 [127].

		Jan	**Feb**	**Mar**	**Apr**	**May**	**Jun**	**Jul**	**Aug**	**Sep**	**Oct**	**Nov**	**Dec**
WD	Base Load (MW)	162	163	161	158	165	181	235	230	216	189	164	168
	Peak Load (MW)	293	294	302	271	268	293	352	350	335	316	286	323
WE	Base Load (MW)	156	165	148	162	167	184	226	203	208	194	165	165
	Peak Load (MW)	259	290	272	242	238	271	305	291	282	286	276	308

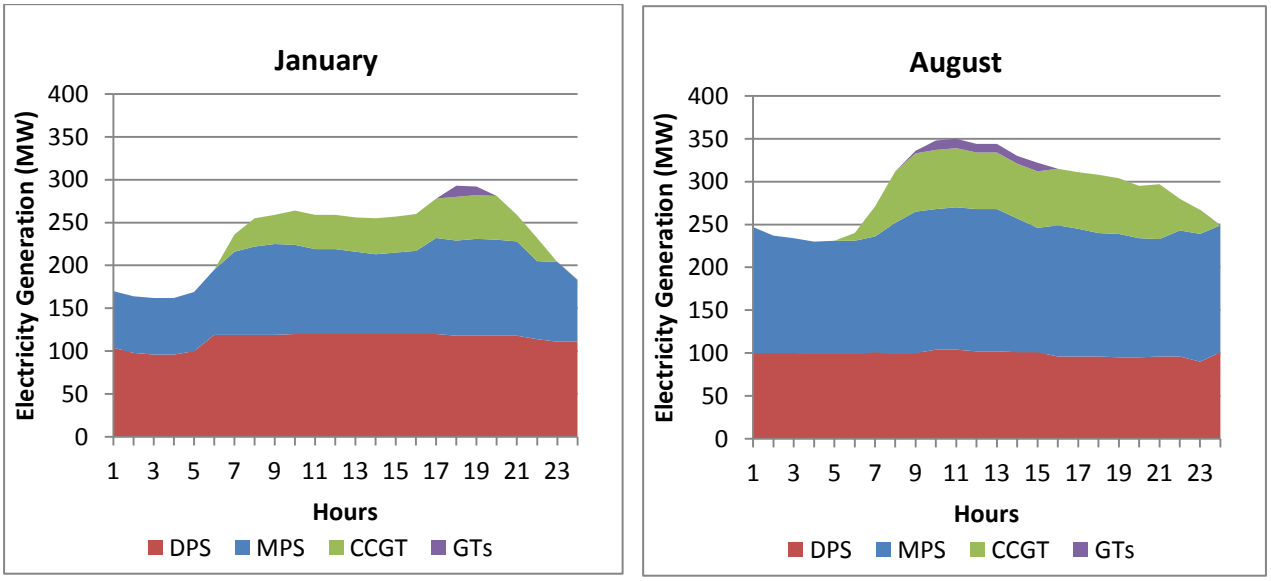

Figure 9-3: Weekday (2010) demand profiles – January and August, for Malta [13]

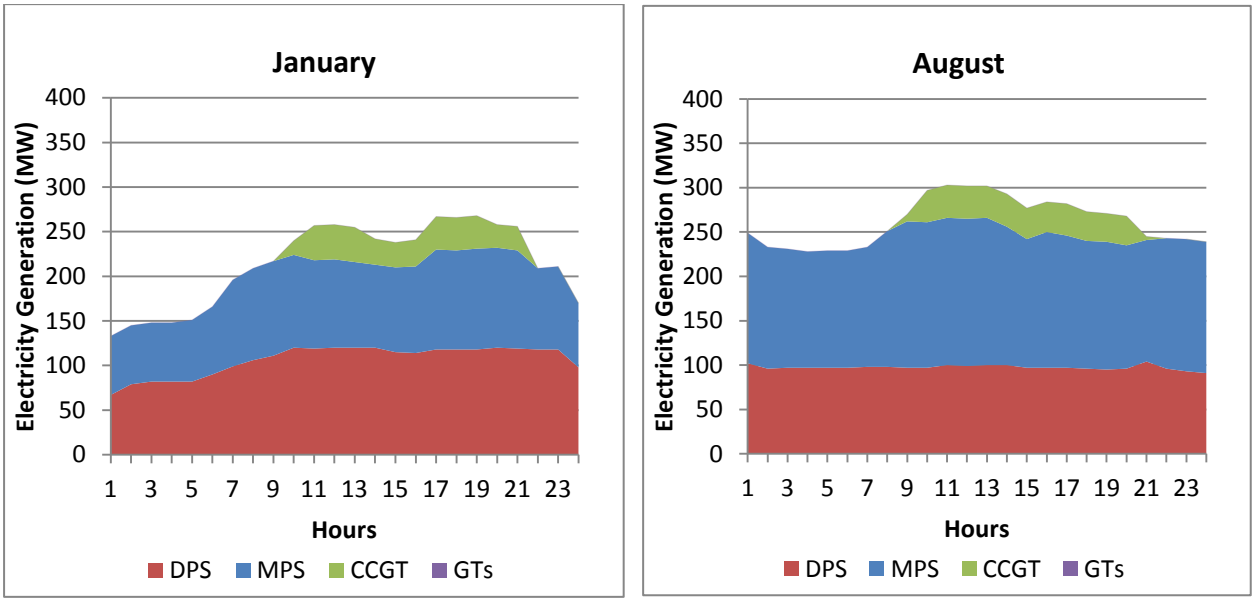

Figure 9-4: Weekend (2010) demand profiles – January and August, for Malta [127].

For the analysis of integration of PV, the demand profiles are based on typical weekday (Figure 9-3) and weekend (Figure 9-4) profiles for each month. Collectively these represent an annual

electrical consumption for the Maltese Islands of 2,188,767 MWh (Table 9-5), implying an aggregate load factor for the islands' power stations of 44.4%, where this is considered the ratio of the actual electricity generated to the maximum possible electricity that could be produced.

$$\text{Load Factor, } C_p = \frac{\text{Actual } P_{out}}{\text{Max } P_{out}} = \frac{2{,}188{,}767\text{MWh/year}}{562.5\text{MW} \times 8760\text{hrs/year}} = 44\% \quad [9\text{-}1]$$

Table 9-5: Representative monthly electricity consumption data according to demand profiles for 2010 [127].

	Days		MWh/Day		Total
Month	**WEs**	**WDs**	**WEs**	**WDs**	*(MWh)*
Jan	10	21	5,804	5,604	168,524
Feb	8	20	5,369	5,656	156,072
Mar	8	23	5,028	5,647	170,105
Apr	8	22	5,060	5,415	159,610
May	10	21	5,131	5,593	168,763
Jun	8	22	5,942	6,019	179,950
Jul	9	22	6,715	7,193	218,681
Aug	9	22	7,139	7,432	227,751
Sep	8	22	5,991	6,700	195,328
Oct	10	21	5,787	6,389	192,039
Nov	8	22	5,802	5,510	167,636
Dec	8	23	5,685	6,036	184,308
			Total (MWh)		2,188,767

9.3 Solar and Fossil Fuel Electricity Generation

9.3.1 Part Load Efficiency of Turbines

The power stations employed in Malta use three different technologies to produce electricity: i) steam turbine, ii) gas turbine (GT), and iii) a combined cycle gas turbine (CCGT). All turbine generating units, within the Marsa and Delimara power stations, permit variable speed

adjustments to modulate the specific production of electricity. This modulation of output comes with the consequence of reduced efficiency at part load.

In the following, the procedure assumed for the calculation of the combined part load efficiency is explained, using the gas turbine units only, for illustration. For three of these units running in a coordinated fashion, with maximum output of 112.5MW, the part load efficiency calculation was split into three stages:

- At loads 0 – 37.5MW : 1 unit working
- At loads 37.5 – 76MW : 2 units working, 1 at full load (η = 32%)
- At loads >76MW : 3 units working, 2 at full load (η = 32%)

The combined efficiency curve for the gas turbines is given in Figure 9-5, and the part load efficiency of the individual turbines was modelled with the following expression:

$$\eta=\eta_{\infty}\left\{1-exp\left(-\left[\frac{\alpha}{\beta}\right][100\cdot\alpha\cdot L]^{\alpha}\right)\right\} \quad [9\text{-}2]$$

where η is the efficiency ratio at any load, L, η_{∞} is the efficiency ratio of the generating unit at full load, and α and β are the shape factors of the part-load efficiency curve. The aggregate efficiency was computed by Equation 8-2 in the previous chapter.

Similarly the combined curve of efficiency for the steam turbines at both Marsa and Delimara can be compiled (Figure 9-6), taking into account the different full load efficiencies of each generating unit as given in Table 9-3. (60MW units at Delimara having a full load efficiency of 32%, while the 60MW unit at Marsa has a full load efficiency of 29% and the rest of the generating units at Marsa have an efficiency of 25% at full load) [127].

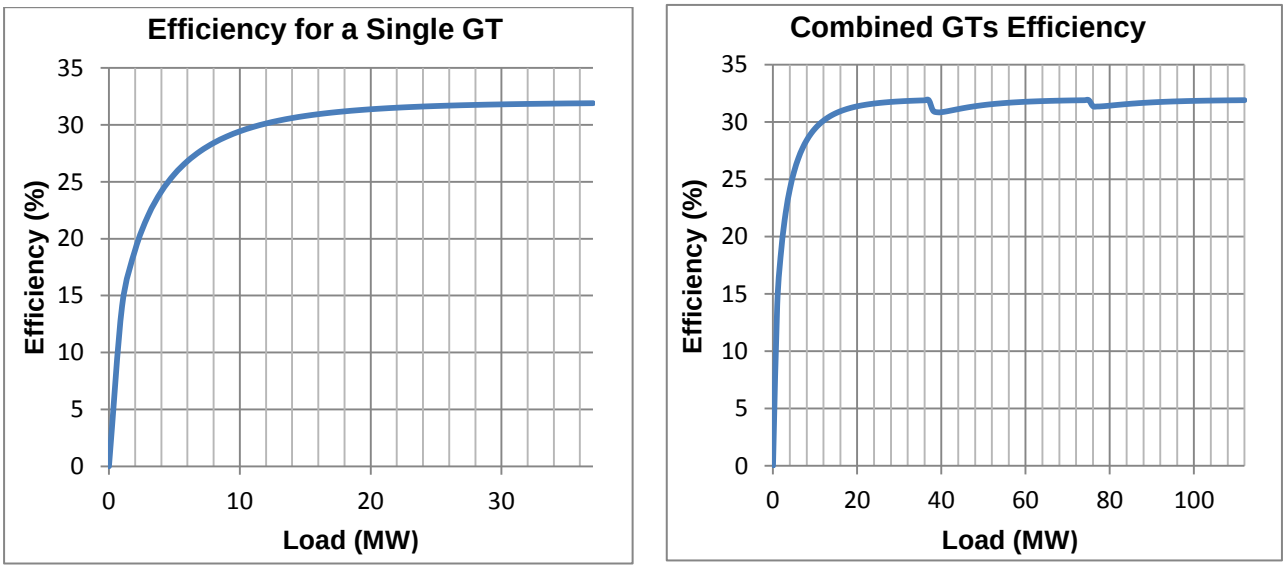

Figure 9-5: Efficiency curve for a single unit 37.5MW gas turbine (left); aggregate efficiency curve for 3 such 37.5MW gas turbines units (right)

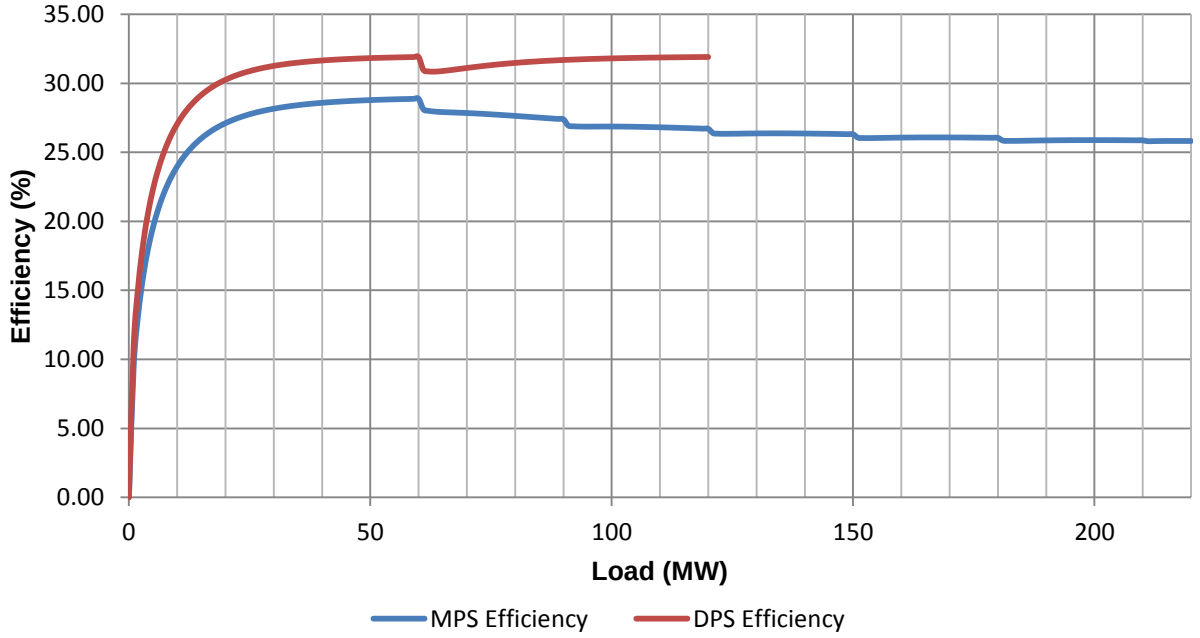

Figure 9-6: Combined efficiencies curve for the steam turbines at Marsa and Delimara

9.3.2 PV and Oil-Fired Power Station Integration

Although more efficient, the CCGT and the GTs are used only as peaking plants and this is due to the higher fuel cost associated with these plants which run on gasoil rather than heavy fuel oil. When considering integration of PV generated electricity, the most expensively produced electricity from the conventional plants was displaced first. This corresponded to a top to bottom order in Table 9-3. As PV electricity was admitted on the system, conventional units were modulated down in a right to left order in Table 9-3.

The model produced the integrated PV scenarios starting from a system which abided to the minimum load conditions without any generation from PV being considered in the electricity mix. The calorific values for the two types of fuel consumed (Table 9-6) were determined according to the fuel rates published in Enemalta's annual report [128] for the year of consideration, from the CCGT and Delimara steam turbine units since they are mostly run at full load.

Table 9-6: Calculated calorific values according to averaged fuel rates for 2010 [127].

Calorific Value (kWh/kg)		**Fuel Rates (kg/kWh)**	
Heavy fuel oil 0.7%S	11.573	Steam Units Delimara	0.270
Gasoil 0.1% S	12.002	CCGT	0.209

The change in part load efficiency was computed after the conventional plants were integrated with PV and the minimum load condition was applied. Using the determined calorific values (Table 9-6) the increase/decrease in fuel consumption for each of the turbines was calculated. An example of a 10MW integrated PV system is highlighted in Table 9-7 (multi-MW arrays are

used in the analysis to allow economies of scale to apply). The table shows the effect of the PV integration over a year, showing the overall dispatched conventional fossil fuel electricity according to the available electricity from the 10MW rated floating PV array.

Table 9-7: Example of a 10MW PV installation

		No PV	**PV Integration**		
PV	Electricity Generation	-	18053		MWh
GTs	Electricity Generation	29690	23857	-5833	MWh
	Fuel Consumption	7796	6252	-1543	Tonnes
CCGT	Electricity Generation	404893	393036	-11857	MWh
	Fuel Consumption	84625	82172	-2453	Tonnes
MPS	Electricity Generation	968456	968264	-192	MWh
	Fuel Consumption	310194	310125	-70	Tonnes
DPS	Electricity Generation	766926	766754	-172	MWh
	Fuel Consumption	207117	207071	-46	Tonnes

The negative values in Table 9-7 indicated a reduction in fuel consumed / electricity generated. For the example illustrated, the steam turbines at the Marsa plant are required to generate more electricity when integrated with the PV array than they had to before integration. This is due to some generation being shifted from the GTs and CCGT, to abide by the minimum load conditions of these turbines, and in order to optimise electricity generation by the system. Note that the actual generated amounts reported by Enemalta do not reflect the minimum load thresholds adopted here and imply that occasionally some conventional units operated appreciably below full load.

9.3.3 Economic Analysis of Scenarios

The generating cost of electricity can be estimated for each scenario by accounting for the total annual costs (including the annuitized capital costs, O&M and the fuel costs) of electricity generated throughout that year. The capital and annual O&M costs for each type of the technologies at the Enemalta power stations is published in a report [129] with figures for 2005 per MW of installed capacity (Table 9-8). Taking into consideration the diversity and size of each plant, the annuitized CAPEX (after applying inflation rates [130]) was estimated for the plant in 2010 costs. A discount rate, *i* of 8% was taken throughout the economic analysis, equivalent to the rate applied at Enemalta. Gas oil and HFO fuel prices are taken to be €570/tonne and €366/tonne respectively, according to trading data for the central Mediterranean region [131] in 2010.

Table 9-8: Capital expenditures and O&M costs (excluding fuel costs) for the power station in 2010 costs

	Heavy Duty Gas Turbine	Combined Cycle Plant	Steam Plant	
Capital Cost	495	936	1349	Euro/kW
O&M Cost	3.52	6.94	1.85	Euro/MWh
Life Expectancy	20	20	30	Years
Fuel Use	Gasoil	Gasoil	HFO	
Fuel Cost	570	570	366	Euro/Tonne

The cost for the poly-crystalline PV panels and a-Si PV panels was taken to be €1.401 and €0.776 per W_p respectively. With regards to the actual offshore PV installation, if an offshore PV system was to replace a wave energy converter in a wave farm, the infrastructure required would be the same for both. The costs for the Aguçadoura commercial wave farm are €9.32M for a 2.25MW installation (inflated to 2010 costs). Moorings, installation, grid connection and project management account for a total of 24% of the total investment [103] in a wave farm. Hence the infrastructural and installation costs can be taken to be approximately 994€/kW_p for a marine floating PV array of the same rating. This cost can be taken to be common for either thin film or crystalline installation, since it does not include the actual cost of the panels and support structure as is indicated by Table 9-9. Also due to the thin film mooring experiencing less force, since it is not designed to withstand the impacts of the waves, it is expected that the mooring costs would be less than for a pontoon based system.

Table 9-9: Capital expenditures and O&M costs for the floating PV arrays [60].

	Pontoon-Based (Poly-crystalline Si) *Million €/MW*	**Flexible System (a-Si)** *Million €/MW*
Panels	1.4012	0.7759
Pontoon	0.1582	-
Moorings	0.2072	0.2072
Installation	0.5386	0.5386
Grid Connection	0.1657	0.1657
Project Management	0.0828	0.0828
Total CAPEX	2.5537	1.7702
Annuitized CAPEX	0.2601	0.1803
Annual O&M	0.0020	0.0014

These capital costs for the thin film and crystalline PV were taken together with those for conventional power generating capacity to estimate the average annuitized cost per unit of electricity for a system operating in an integrated fashion. The resulting discounted cost of electricity per unit produced for a range of array sizes is given in Table 9-10, calculated according to data given in Table 9-8 and Table 9-9.

The key result evident in Table 9-10 is that the discounted cost of electricity produced when integrated with a-Si PV is lower than when it is not integrated. Moreover as the installed capacity of a-Si PV increases, so the system cost of electricity reduces further. This trend continues until 320MW a-Si PV installed capacity (for 2010, equivalent to approximately 25% of annual demand), when further increases in installed capacity increase the aggregate generation cost due to the lowered efficiency of conventional plant and hence higher fuel costs. As the discounted cost of pontoon mounted crystalline PV is higher than the system generation cost of conventional plant alone, the generation cost of any scale of integration with this technology is higher. This rules crystalline PV out as an economically deployable technology.

At *circa* 250MW of installed PV, at peak solar production, not all of the electricity potential from the PV array is required to displace the electricity generation from fossil fuels. With a storage system the whole electricity potential from the PV array can be exploited, allowing increased penetration levels from the PV. Due to the restriction on the uptake of electricity generation from PV, the discounted cost of electricity reaches a minimum value of 13.525 € cent/kWh (for thin film) at around 315MW of installed capacity. After this point the discounted

cost of electricity rapidly goes up, since the PV integration is offsetting less and less of the current electricity generation.

Table 9-10: Electricity, fuel and cost of electricity for an integrated oil-fired and varying level of PV integration.

PV Installed Capacity	**Electricity Generation** *MWh*					**Fuel Consumption** *Tonnes*				**Discounted Cost of Electricity with PV** *€ cent/kWh*	
MW	**PV**	**GT**	**CCGT**	**MPS**	**DPS**	**GT**	**CCGT**	**MPS**	**DPS**	**Thin Film**	**Crystalline**
0	0	29690	404893	968456	766926	7796	84625	310194	207117	14.040	14.040
0.5	903	28955	404802	968544	766761	7589	84606	310225	207073	14.038	14.040
1	1805	28684	404184	968528	766763	7520	84478	310219	207073	14.037	14.041
5	9027	26226	399305	968652	766756	6872	83467	310264	207071	14.026	14.044
10	18053	23857	393036	968264	766754	6252	82172	310125	207071	14.013	14.050
15	27080	21912	385783	968335	766855	5742	80669	310151	207098	14.000	14.056
20	36106	20206	378141	968662	766849	5300	79085	310262	207097	13.988	14.063
25	45132	18629	370976	968182	767045	4897	77606	310097	207149	13.977	14.069
40	72212	14406	346678	970246	766423	3794	72573	310810	206982	13.943	14.091
60	108318	12052	308364	975076	766155	3170	64615	312478	206909	13.900	14.123
80	144424	11460	267784	980596	765700	3013	56137	314382	206786	13.859	14.156
100	180530	11217	238343	974972	764902	2951	49971	312458	206571	13.818	14.189
150	270795	10607	203936	922853	761773	2792	42736	294913	205728	13.717	14.274
200	361060	10374	190905	850349	757277	2729	39985	271199	204516	13.632	14.373
250	451325	10241	184580	792282	731536	2694	38662	252136	197565	13.567	14.494
300	539612	10107	180123	743511	696611	2660	37731	236391	188135	13.527	14.640
320	572367	10054	178691	725652	683202	2647	37432	230725	184514	13.527	14.714
340	603386	10000	175166	713166	668247	2634	36678	226814	180475	13.537	14.798
360	631566	9884	174181	698242	656096	2601	36470	222144	177195	13.561	14.896

The effect of the part load efficiency can be noted through variation of the minimum load conditions for each of the units. When the limit was set at 10MW for the GTs, rather than 4MW, the discounted count of electricity with no PV was 14.036 € cent/kWh compared to 14.040 € cent/kWh as indicated in Table 9-10. Having no minimum load condition set, the cost of

electricity increases to 14.082 € cent/kWh, showing that running turbines on lower part-loads has higher fuel consumption associated with it.

With an (Malta to Sicily) inter-connector in place by the end 2014, the increased flexibility available in system operation may lead to effective use of larger amounts of PV installed capacity and operation of all conventional units in the system more efficiently at full load. The carbon savings through the adoption of offshore PVs are considerable and equivalent to a 25% reduction annually (accounting for the embedded carbon) when considering a 250MW installation.

The directives of the European Union require Malta to produce 10% of its total energy consumption from green energy sources. A 120MW installation of thin film floating PV is capable of attaining the quota for electricity, while also lowering electricity costs.

9.3.4 CO_2 Balance

The net gain/loss of CO_2 from the installation of renewable energy technology depends on the quality of fossil fuel which is offsetted and how much CO_2 was emitted in manufacture, installation and delivery of the PV array to site. The specific rated power for the offshore PV, taking into consideration the footprint area (spacing between the panels), is $0.04kW_p/m^2$ for a-Si thin film and $0.07kW_p/m^2$ for the poly-crystalline PV.

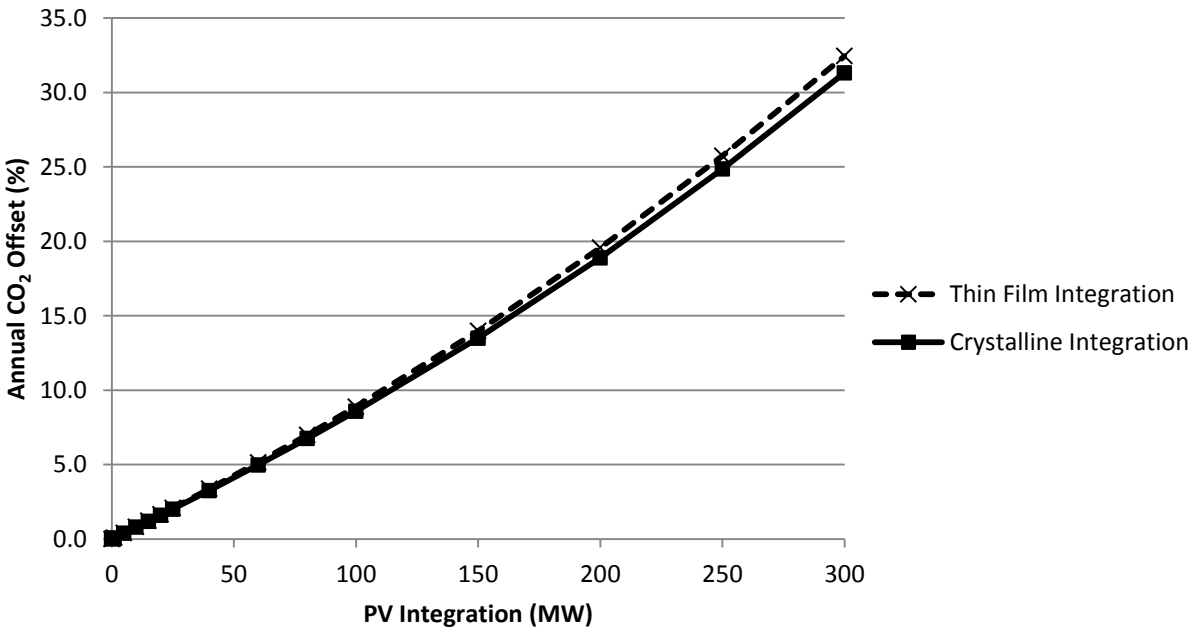

Figure 9-7: Annualised CO_2 savings at different levels of penetration by the offshore PV arrays

Table 8-8 presents the list of processes which emit CO_2 during the manufacturing, installation and transportation of the PV arrays. According to the International Energy Agency [19] the CO_2 emissions from the generation of electricity in Malta was at 850g CO_2/kWh for 2009. Considering the specific fuel rates for different levels of PV integration, the resulting CO_2 emissions from the oil-fired plant could be estimated. The savings were calculated over the lifetime of the offshore PV arrays, set at 20 years, and accounted for the embedded carbon required for the installation of the PV arrays. Figure 9-7 shows the annual carbon savings percentage (considering data from Table 8-8 and CO_2 emissions with no PV estimated at 1,844 x 10^3Tonnes) which could be expected from the addition of the floating PV renewable energy technology to the current fossil fuel based electricity mix.

10 General Discussion

Renewable energy technologies (for electricity generation) have been gaining traction over the past years mainly due to initiatives by policy makers focussed on reducing the dependence on fossil fuels and reducing CO_2 emissions associated with electricity generation. Multi-MW operations require large land footprints, which may lead to disruption of the local ecosystem and land change impacts. Abassi & Abassi [132] discuss such issues for biomass operations, while Tsoutsos *et al.* [133] relates the same land use issues to solar installations. It is evident that land use issues are of concern, not only due to changes which cannot sustain the ecosystem, but also due to pressure for land for use in agriculture purposes [1]. To illustrate, an in-depth GIS based analysis of land use was presented for the islands of Malta in Chapter 9. This island which is under very high land use pressure, as a country of the EU, has no choice but to consider offshore technologies to meet its renewable energy obligations [118]. As a solid state, reliable technology, PV provides motivation for moving solar farms offshore, because the Maltese solar resource is plentiful.

One of the major challenges with deployment offshore is reliability of the system, since equipment is exposed to a harsh environment which to date has only been mitigated through consideration of installation on heavily engineered platform structures. Reliability has been identified by Wolfram [134] as a barrier to market penetration of marine energy converters of all types in the renewable energy sector. Similar issues could be forecast with deployment of solar PV on large pontoon arrays, to resist in their sea-keeping design concept. In contrast, the design

concept at the heart of this research is one where the structure is conceived not to resist, but to yield, with consequent significant reductions in material costs for mooring and sea-keeping.

10.1 Floating Thin Film PV Concept

The concept as has been described throughout the previous chapters is focussed on a design which allows the thin film PV structure/array to deform with water wave motion and so to minimize load transfer from the waves to the system, which would otherwise be a major source of reliability issues. The calculation undertaken in Section 3.1 within this document highlights the low impact of such a thin film structure on the wave environment. This is so small that no change could be predicted in the hydrodynamic motion relative to that of the sea waves.

There are various array layouts which could be customised to particular location, voltage requirements or mooring systems. The main aims of the design are to minimise cable runs to avoid voltage losses, allow easy deployment and decommissioning, and electrical controllability (allowing disconnection of a single panel without disruption to the whole system). The design in Figure 6-1 addresses the key design aims by having a singular central bus running through the centre of the array, micro-inverters to optimise the electrical output from the panels and to allow controllability, and a rectangular array design which permits deployment and decommissioning from a circular drum at one of the ends, in a similar fashion to the way modern fishing vessels deploy nets.

10.1.1 Results

The testing (experimental or numerical) undertaken was motivated by the gap in knowledge between what would be expected for a conventional thin film PV laminate in dry conditions, in comparison to those of thin film flexible PV panels experiencing motion on a water body. Deployment in this unusual environment immediately raised questions relating to how the electrical yield would vary due to the wave motion compared to an array which was maintained perfectly horizontal.

The electronics within a PV panel are all interconnected and so variation in the solar intensity on the surface affects the net electrical output. The variation in solar intensity due to the panels' motion partially results from over cast shadowing by the panels themselves and due to the different inclinations of each individual panel relative to the direction of incident solar radiation. A methodology for modelling such a dynamic system is given in Chapter 4. Results show that for higher latitudes the impact of the deformation of the array of panels is greater because the sun has a lower solar altitude. Table 4-2 and Table 4-3 show that at central latitudes the expected yield considering the panel's motion would be higher than if the same panel was flat.

Additionally the temperature of the water could be modelled concurrently in order to better estimate the electrical yield, taking into consideration the variation in efficiency of the panels as they are cooled down by the underlying water (reducing over heating of the panels; Figure 10-1). The methodology could equally be applied to real waveforms rather than just regular waves.

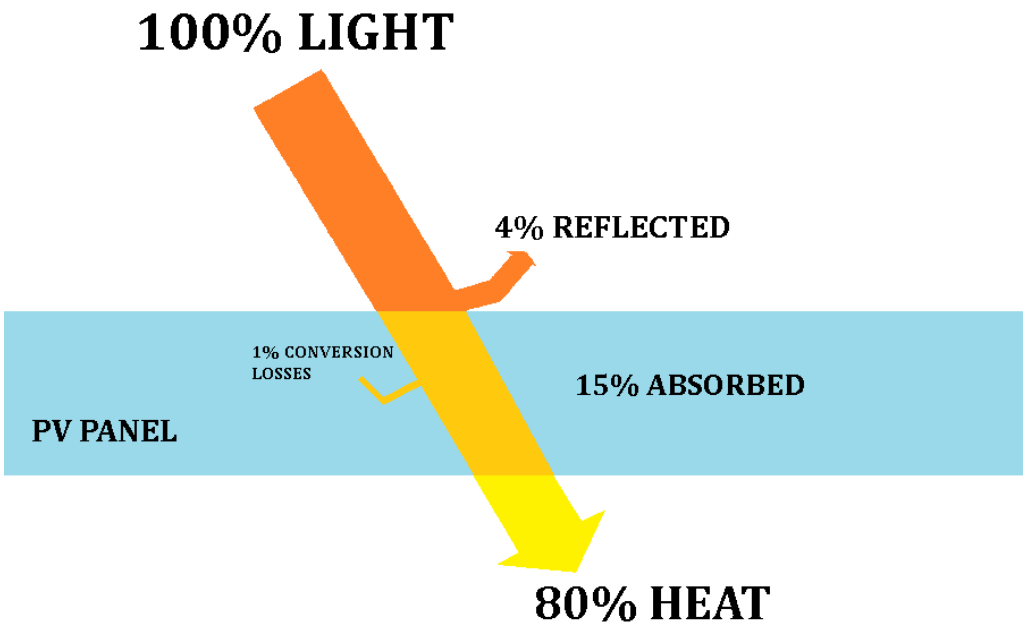

Figure 10-1: Bypass heat in PV electrical conversion

Cooling of the thin film floating PV prototype accounted for a 5% improvement in electrical yield, during the test days – where the panels were fully water saturated. What made the major difference in the electrical output was the surface cleanliness of the panels. Although solar output is not completely diminished by shallow depths (e.g. 1cm) on top of the panel [13] and the water actually helps with the thermal cooling, a concern is that the water layer does not allow self-cleaning to occur (especially in low wave motion environments). This can be appreciated from Figure 10-2, where the 4 panels on the right were operated under are *circa* centimetre of water[13].

[13] Note that the panels were flooded post to the results being recorded in Chapter 6 although some sedimentation was still present during the testing, it was not as severe as in Figure 10-2.

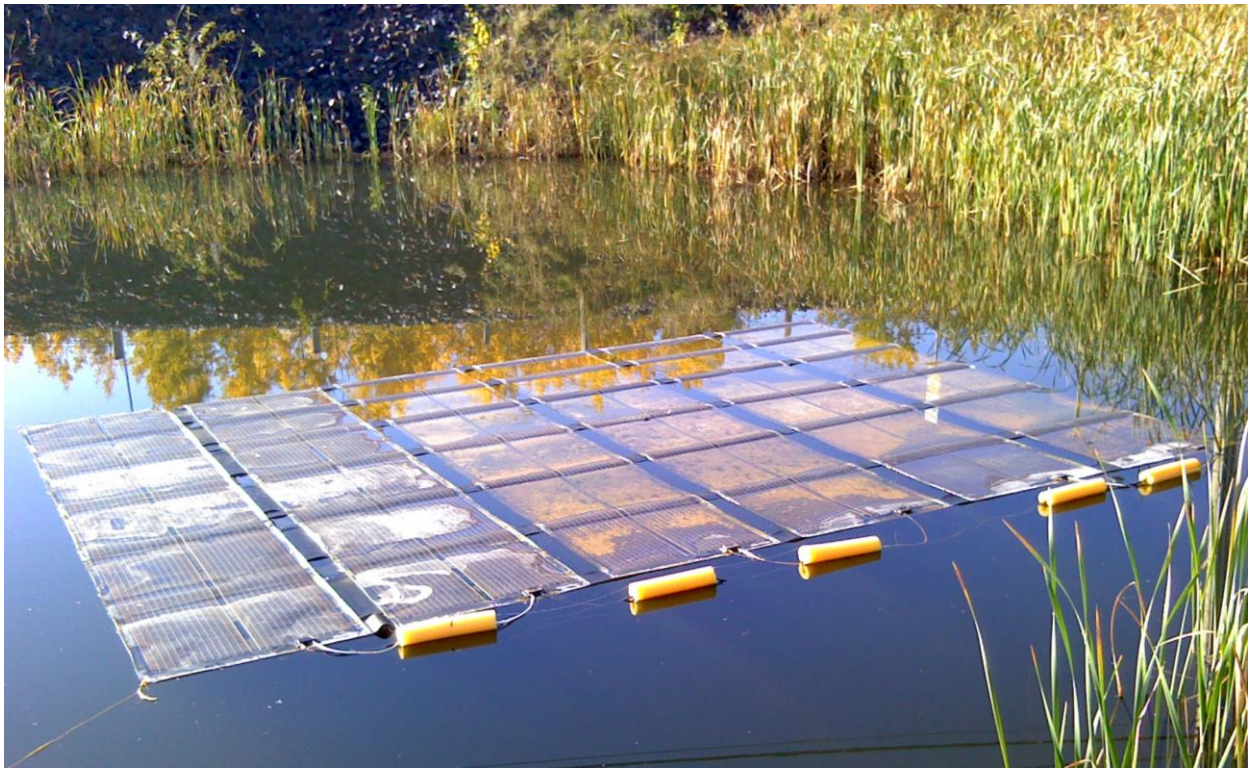

Figure 10-2: Floating PV array with 4 panels on right operating under a cm of water after a 4 month deployment

Cleaning and testing of a pair of panels showed a 1% improvement in efficiency (from 3% to 4%), indicating that significant yield loss could be expected if the design did not prevent accumulation of sediment. The white contours on the panels on the left, in Figure 10-2, are consistent with the research outlined in Chapter 5 which notes calcium diffusion and 'whitening' of the panels when left submerged in water. Also this indicates that the panels are water saturated, since the 'whiteness' was observed to not be apparent when the samples tested were dried.

The notion that the arrays would be water saturated lead to mechanical testing under these conditions to determine what effect it would have on the mechanical characteristics. The ‘deformation’ modulus was determined to assess the stiffness of the material by applying tensile loads to dry samples, and samples cut from the floating PV prototype (which had a mass that indicated that they had experienced 1.4% water absorption).

One of the main concerns raised by many at the start of the project was the risks associated with operating electrical equipment in wet conditions. This was not so much concern relating to the electrical connections, because suitable waterproof components can be procured, but more in terms of water leakage into the panel along paths arising from laminate de-bonding, which would create shorting. During lab and field tests, there was no water leakage apparent in the panels which were deployed on the lake for four months, nor in samples that were kept submerged for almost a year. Water leakage was only noted after the composite was cut and the ETFE border was removed. This only occurred on the top surface where laser etched grooves permitted the penetration of the water. The penetration of the water resulted in weakening of the EVA glue which kept the composite together and so de-bonding of the ETFE laminate from the top surface. After a week of submersion in such a condition (with samples cut without the ETFE border) rusting was apparent on the top surface. No sign of rusting was observed in any of the intact panels or samples which were exposed to the wet environment.

10.1.2 Challenges and Lessons

The main challenge initially was the sheer novelty of the concept which meant that basic ground work had to be covered first before proceeding with the more technical or large scale research.

This firstly consisted of the proof of the concept which was determined as soon as the prototype was deployed on the water surface and it remained operational for the four months of testing. The system was decommissioned at the conclusion of the field work portion of this research (upon which permission to deploy was granted).

A key challenge in the construction of the prototype was the procurement of the electronics and electrical equipment which in most cases had to be sourced internationally, due to lack of local suppliers. Sourcing of the laminated thin film PV in Canada provided to be very difficult, since all of Canadian manufacturing plants provide for glass encapsulation. A major producer of laminated thin film panels, *Uni-Solar*, was identified in Detroit, USA which unfortunately went out of business in the months soon after. The other supplier of the laminated thin film PV was *Power Film Inc.*[14] (also American), which was mainly contracted by the US Army for their remote power needs. This meant that their products had to be sourced from an American manufacturer; since it is the policy of products used by the US Army, and implied that costs of components were higher than on the open market. The advantage of working with *Power Film* was that due to their experiences with specific products contracted by the US Army, they could be flexible in their designs. So for the purposes of this research, *Power Film* was able to design a product according to the requirements of the project (stainless steel external materials, ETFE lamination, double width panels etc...). Procurement of the polyurethane, PU connectors and cablings (4 core) was also somewhat difficult and had to be imported from abroad.

---

[14] A-Si panels at US \$5.61/W_p at 4.5% efficiency (according to data acquired through the realisation of the prototype).

The limited suppliers of the components, especially for the laminated thin film PV, required for the assembly of the project extended the timeframes for the construction of the floating thin film PV array. For supply of larger quantities of thin film panels, alternative suppliers would have to be identified (because *Power Film* is limited in its production capacity, due to much of its production being contracted to the US Army). North American companies which manufacture thin film PVs, and would be able of supplying the necessary production, are *First Solar*[15] (USA) and *Everbrite Solar*[16] (Canadian), although they would have to upgrade their machinery to polymer encapsulation (rather than their current glass encapsulation process) so that a flexible system could be achieved.

Practically, in the demonstration project difficulties were encountered in assembling of the data logging system and the integrated electricity disposal units. Many of the issues were related to the different independent components which were being used, which had to be programmed and adapted to work together. In retrospect, a micro-inverter would have been as cost effective if connected to two panel groups, and would have solved the data logging and electricity disposal issues within a single unit which was already pre-programmed. The only component which would be required, other than the variable resistive load which is needed to dispose of the electricity either way, is a grid frequency simulator, otherwise the micro-inverter would not be able to function.

---

[15] CdTe panels at US \$0.68/W_p at 14.4% efficiency and embedded carbon of 18g CO_2 eq/kWh (assumed irradiance of 1700kWh/year).

[16] Information of the thin film product is limited due to the plant coming into operation in 2013 and fully operational in 2014.

The final challenge to be addressed is the sagging of the PV panels when deployed in the array on the water. Although the buoyancy was enough to keep the array afloat, the segmented installation of the buoyancy underneath the panels resulted in sagging of the section in between (can be noted from Figure 10-2). This led to a constant water layer being present, which allowed sediment deposition of top of the panels and some occlusion of the solar radiation effective on the panels (~0.5%). For the two panels on the left of Figure 10-2 additional buoyancy was added along the whole back and this avoided sagging happening and resulted in better yield, discussed in (Section 6.2.4).

10.2 Techno-economics

Economics are a major factor in the realisation of a commercial project and unless a positive return on investment is guaranteed, the project stands little chance of being undertaken. During the initial stages of this research techno-economic models were carried out to determine whether floating PV arrays would be an economically feasible alternative to existing renewable solutions, when augmenting electricity supply at a remote site and with grid integration.

The techno-economic analysis fundamentally depended on the estimated costs for the floating PV technology. At the time, these costs were adapted from a land based installation and taken to apply to an offshore deployment, considering the cost of the laminated thin film PV panels and the costs of being offshore (which were derived from economics expected from a wave farm,

since other than the electricity generating device it would be virtually the same[17]). The cost estimates for a large scale array are given in Table 7-4. These take a cost of $1.03/$W_p$ CAN for the laminated thin film PV based on the 2012 PV market. The final installed estimate per kW_p was $2,350 CAN.

Table 10-1: Updated large scale costs of floating thin film PV, considering *First Solar* CdTe PV and an inflation rate of 0.65% from 2012-2013

	a-Si Floating PV	**CdTe Floating PV**
	2012 Inflated to 2013 Costs	*2013 Costs*
Panels	$ 1,097 /kWp	$ 700 /kWp
Moorings	$ 293 /kWp	$ 293 /kWp
Installation	$ 762 /kWp	$ 370* /kWp
Grid Connection	$ 234/kWp	$ 234/kWp
Project Management	$ 117 /kWp	$ 117 /kWp
Total CAPEX	**$ 2,503 /kWp**	**$ 1,714 /kWp**

* Reduced cost is proportional to the increase in efficiency from a-Si (7%) to CdTe (14.4%)

The actual historical costs are those recorded for the procurement of the prototype, which, as expected, would be higher [49], even though they do not include installation costs. The installed costs proportioned to a kWp were $11,400 CAN as presented in Table 6-1. These costs are four times as much as those estimated in Table 7-4 for a commercial array, even though they do not

[17] The mooring costs were slightly reduced to reflect on the fact that the flexible floating thin film PV array would not subject the mooring lines to as much loading and so the material properties would not need to be able withstand the same amount of force.

include planning costs. Much of the higher cost is associated with the price paid for the PV panels in contrast to what the approximate market PV price ($7.39/$W_p$ rather than $1.03/$W_p$).

Financial reporting for the last quarter of 2012 for *First Solar* gives a manufacturing cost of $0.70/$W_p$ (converted from $0.68/$W_p$ USD) which correlates with the price taken in accordance with the PV market. Recomputing Table 7-4 with the higher end CdTe panels from *First Solar* with the latest costs and efficiency, results in the updated costs for large scale floating PV in Table 10-1.

If a higher efficiency is taken into account the techno-economic assessment would be more favourable; and floating thin film PV would become a practical solution to the modelled analysis undertaken for McFaulds Lake in Chapter 8 and for the Maltese grid integration study in Chapter 9. For example, reconsidering the same cost of thin film PV at an integration of 60MW for the Maltese islands, with an efficiency of 14.4% rather than 7%, the discounted cost of electricity is €13.24 cents/kWh rather than €13.90 cents/kWh originally computed. Also since both of the case studies heavily depend on the cost of fossil fuels, expected future increases in the unit cost of fuel would inevitably make renewable energy technologies such as the one proposed within this research even more attractive.

10.3 Environmental Scoping Overview

If the development of the floating thin film array is going to advance further with larger demonstrator projects at bigger installed capacities and with potential of even larger generating stations at commercial sizes, an environmental impact assessment would be essential. This would

analyse each of the aspects which would be expected to have an impact of the marine environment (positive or negative). In most parts the issues of environmental impacts would be similar to those for a wave farm and thus could draw from work in this field [135, 136]. The water surface coverage by the panels would also have to be investigated independently. Impacts of reduced gas exchange at the water surface and solar energy within the water column would have to be quantified.

Margheritini *et al.* [137] in a review on EIA scoping for wave energy converters lists the criteria against which the EU determines the likelihood of certain environmental impacts. These criteria are:

- (*D*) Distance from shore
- (*S*) Stability elements (moorings)
- (*z/d*) Obstruction to water column
- (*w/a*) Obstruction to the sea surface
- (*P*) Power take-off

and are the basis upon which the impact matrix[18] can be compiled, given in Table 10-2.

[18] Designed on the guidelines of the European Marine Equipment Council (EMEC)

Table 10-2: Impact matrix for a wave energy converter (WEC) which could be adapted to a floating thin film PV array with typical activities and stress receptors, from[137].

Receptor **Activity**	Geology and geomorphology	Sediment distribution and movement	Hydrography and hydrographic processes	Landscape and seascape	Atmosphere	Coastal species	Water column species	Seabed species	Seabirds	Commercial sea and harbour issues	Local economy	Recreation and communities	Archaeology
Installation													
Mooring/foundation system													
Electric transmission infrastructure													
Vessel presence													
Operation and maintenance													
Mooring/foundation system													
Electric transmission infrastructure													
WE device presence													
Heating and cooling system													
Chemical coating													
Noise emissions													
Vibrations													
Light													
Decommissioning													
Vessel presence													
Mooring/foundation removal													
Electric transmission removal													
Accidental events													
Oil spills													
Sinking													
Uncontrolled floating													
Collision													

The compilation of the impact matrix will take into consideration the expected impact of the project on each of the outlined receptors in Table 10-2 (details of the receptors and activities related to WECs are given in the three year EquiMar project study [138]). The impact of each of the activities on the receptors will depend not only on the technology type but also on the location of the planned installation which will factor the environment type. A compiled Table 10-2 may be presented in an EIA with input values varying from 5 to 0, with 5 being an area of major concern, 4 being of moderate concern, 3 being of minor concern, 2 being of negligible concern, 1 having no impact and 0 having positive effects. Any values 3 or higher may have to be discussed within the EIA and any prevention and mitigation possibilities included.

Table 10-3: Expected impacts based on the associated classification impacts for each criteria in [137]

FLOATING THIN FILM PV ARRAY

Classification	**Expected impacts**
D: Offshore	• Negligible impact on local communities • Minor impact on coastal processes and coastal species • Major impact on navigation and fishery
S: Simple mooring lines	• Minor impact on benthic habitats • Negligible impact on geology • Minor impact on archaeology • Minor impact in water column species
z/d: Little obstruction, for $0<\|z/d\|\leq 0.1$ *w/a*: Very obstructive, for $\|w/a\|>0.3$	• Moderate impact in water column species (from surface occlusion) • Moderate impact on benthic habitats (from surface occlusion) • Major impact on navigation and fishery • Major interference with marine animal movements • Negligible impact on coastal processes • Negligible impact on local communities
P: Solid state PV	• May generate electromagnetic fields

z – energy device draft; *d* – water depth; *w* – device area; *a* – footprint of solar floating farm

A preliminary environmental outline is given in the Table 10-3, based on the criteria given in [137] and their descriptions, taking into consideration the physical properties of the thin film floating PV array. The results show that the major impacted areas are i) fishing and navigation[19], since they would not be excluded from that zone, ii) the water column species, as the large surface area coverage would block light and oxygen diffusion having some potentially adverse effects if the area is large enough, and iii) the benthic habitat, as any effect in the water column would consequently affect the seabed habitat too. With regards to the type of power output the expected impacts are similar to those of a surface electrical cable line. The solid state type of electricity production eliminates the risks associated with mechanical machines, such as oil spillages, noise etc...

The EIA scoped on the receptors in Table 10-2 is an important step in the planning stage of large scale projects and will be one of the barriers to commercialisation. Proper impact determination and mitigation through consultation of the scientific community and the public will be essential. It is important that a project that is focussed on producing sustainable energy is also benign to the environment and as famously quoted in the Brundtland Report [139] have a "development that meets the needs of the present generation without compromising the ability of future generations to meet their own needs".

[19] Fishing and navigation is impacted significantly because of the area the thin film PVs would occupy. With regards to collision, the impact would be minor since the arrays are deformable and would not damage the vessel in any way. This would be advantageous over other marine structures, since it would not have to have as high a collision collateral insurance.

11 Conclusions and Recommendations for Future Research

11.1 Conclusion

The research undertaken saw the evolution of a new technological application for offshore large scale electricity generation; that of the floating flexible thin film PV. The need for this technology arises from limitations on land use for renewables and the growing need for electricity. Section 2.3 presented within shows how floating PV technology has evolved between 2007 and 2013, and apart from the concept herein was limited to PV panels mounted on floating pontoons. Floating PV pontoons may only be implemented economically in sheltered environments, because otherwise sea-keeping infrastructure may be prohibitively expensive. A basic overview of the resulting mooring loads, in section 3.2, has indicated that for floating thin film PVs the required mooring rating for the same installed capacity would be significantly less – so mooring costs are expected to be accordingly reduced.

Techno-economic assessments for both the pontoon based PV and flexible type floating PV were established in Chapters 7-9. The additional costs related to the requirement of a pontoon, the higher specs of the moorings and additional O&M costs indicate that floating thin film PV will be the better economical option. Efficiency for a-Si thin film PV is lower than that of crystalline PVs, although this dependent on the type of PV being considered and could be comparable to the crystalline yield. Higher yields can be achieved with CdTe and CIGS type PVs, with lower yields for a-Si PV (costs are comparable for all three because of the roll-to-roll thin film technique).

Results reported in Chapter 7 indicated that floating thin film PV are economically competitive, at ~$0.11/kWh in central latitudes at a discounted rate of 7.5%, even against the more mature renewable energy technologies such as offshore wind. As expected, economics are better for arrays installed in equatorial latitudes rather than polar latitudes, since the solar resource is greater. If a higher efficiency was taken than the one described, the yields would also be greater, resulting in a lower discounted cost of electricity produced. The suitability for integration with diesel generators at remote mine sites required the cost of diesel to be $1.29/litre or higher. The load the integration was modelled on had lower electricity consumption when the solar intensity was the highest during the day, so load shedding or storage would make floating thin film PV economically competitive.

For the techno-economic study in Chapter 9 the dynamics were more challenging due to consideration of a whole grid system. The model had to consider not only the variation in solar intensity and the electrical consumption profile, but also the operability of the power station. This had to consider i) the minimum running load, and ii) the part load efficiency of fossil fuelled plant. Due to the high cost of operation of the conventional power plant, cost savings could be made even when not all the solar potential was utilised. For larger solar penetration, electricity storage is essential unless exportation of electricity is a possibility, since then larger installed capacities of PV can be installed to match the morning and evening peak, while exporting the redundant production of electricity around noon.

When determining the yield for the techno-economic studies, the arrays were assumed to be lying perfectly horizontal and without being affected by the temperature difference from the

water. This is not the case in reality; the effect of wave driven motion on the electrical yield was studied in Chapter 4, while the effect of the water temperature was noted through experimental results in Chapter 6. Results from Chapter 4 show that the motion may have positive effect at central latitudes (by as much as ~ 16% for N/S propagations and ~ 3% for E/W propagations) due to the higher position of the sun, while this is negative in higher latitudes (by as much as ~ -27% for N/S propagations and ~ -32% for E/W propagations). The results which account for the cooling from the water in Chapter 6 show that during the experimental period a recorded average 5% increase in yield was measured.

Water absorption by PV panels was found to reach full saturation within the ETFE a-Si thin film PV composite at 1.4% at 23°C. Mechanical reliability was tested for a water saturated thin film PV sample (Chapter 5). Electrical reliability could be considered from the 45 day testing in Chapter 6. This showed a 1% drop in efficiency due to sediment accumulation, with a further 0.5% due to operating conditions. Chapter 6 also highlights the specifications for the prototype developed, which primarily acted as a proof of concept exercise. Electrical production data was recorded from the prototype floating PV array over a period of 2 months, with the panels recovered four months after deployment. Results and observations attained, motivated changes in design that ensured equal distribution of the buoyancy on individual panels (to minimise sag and water pooling within which the sediment could accumulate) and resulted in better yield.

Overall the research aimed to investigate the perceived main barriers for floating thin film's PV technology at the outset of the project, and hence the barriers for commercial exploitation of the concept. This has been limited to technical and economic issues, for which the significant

contributions of the work are highlighted in Section 11.2. Other issues relevant to the research and which could be addressed as part of future work are discussed in Section 11.3.

11.2 Original Contributions

This research aimed to scope and develop a novel idea for a renewable energy technology application. The main contribution of the thesis is in development and realisation of this concept. These, along with the supporting contributions to render the undertaking a holistic research, are listed as follows:

1. Comparison in wave energy impact from VLFSs and floating thin film PV systems
2. Synthesis of precedent practice in the development of floating photovoltaic technologies
3. Techno-economic model for integrated floating PV arrays (pontoon and flexible) and other mainstream offshore technologies
4. Development of a model to compute the predicted yield from a large scale floating thin film PV array in sea waves (methodology applicable to both regular and irregular waves)
5. Model for estimating electrical output from a PV cell at a specified solar intensity based on shape parameters within the IV curve and normal specifications given by the manufacturer
6. Water absorption characterisation in ETFE laminated thin film PVs at different temperatures
7. Tensile testing of water saturated thin film PV composites
8. Realisation of the world's first flexible floating PV prototype
9. Electrical performance testing of the floating thin film PV prototype

11.3 Recommendations for Future Work

The evolution of the floating thin film PV for large scale commercial development is very much dependent on the direction future work will take. The research undertaken within this thesis is only the basic backbone and there are other considerations which will need to be taken into account. A long term, larger demonstrator will provide required data to accurately establish electrical output, as well as other determining factors including mooring loads. Additional experimentation on water absorption and related short term electrical reliability should be considered for different types of thin film materials, e.g. CIGS, CdTe etc., from which the floating thin film PVs could be composed (a-Si PV was adopted investigated herein).

Dynamics of the demonstrator should also be evaluated and compared with that of the oncoming waves to verify the negligible change in hydrodynamics. The motion of the panels will inevitably result in fatigue failures, so it would be useful to determine reliability statistics for this mode of failure. Fatigue failure testing can be concluded through accelerated methods, as is common with the reliability testing of mooring lines. This repeatedly and frequently exposes the mooring system being tested to extreme loading events observed within a given year (excluding the mild environmental conditions, which would have a lesser impact) and hence allowing response to multiple years of extreme conditions to be characterised in a short time.

An environmental impact assessment (EIA) will be necessary in order to ensure that such an installation would not be hazardous to the environment in which it will be set. Most of the areas of concern have been addressed through EIA reports for wave farms. Additional aspects which are not considered for wave farms are i) electromagnetic fields possibly being present along the

surface of the water where the panels are present and ii) sunlight impacts to the water column and seabed arising from the reduced oxygen diffusion across the water-air interface and sunlight penetration into the water.

The path to commercialisation is very much dependent not only on the technical aspects of the project, but also social acceptance. Social aspects should thus not be overlooked; experience from many renewable energy projects have shown that this could be what makes or breaks the concept.

References

[1] J.A. Foley, R. DeFries, G.P. Asner, C. Barford, G. Bonan, S.R. Carpenter, F.S. Chapin, M.T. Coe, G.C. Daily, H.K. Gibbs, J.H. Helkowski, T. Holloway, E.A. Howard, C.J. Kucharik, C. Monfreda, J.A. Patz, I.C. Prentice, N. Ramankutty, P.K. Snyder, Global Consequences of Land Use, Science, 309 (2005) 570-574.

[2] J. Spanring, N. Depine, B. Erler, M. Feichtner, J. Gradwohl, W. Krumlacher, H. Muckenhuber, A. Reininger, F. Reisinger, A. Ruplitsch, E. Seitler, A. Skringer, A.K. Plessing, High performance barrier films for next generation photovoltaic module encapsulation, in: Photovoltaic Specialists Conference, 2008. PVSC '08. 33rd IEEE, 2008, pp. 1-4.

[3] B. Erler, S. Degiampietro, P. Pertl, A.K. Plessing, A. Skringer, F. Kessler, Multi layer materials for the encapsulation of thin film modules, in: Photovoltaic Energy Conversion, 2003. Proceedings of 3rd World Conference on, 2003, pp. 1896-1898 Vol.1892.

[4] L.W. McKeen, L.K. Massey, Film Properties of Plastics and Elastomers, Elsevier Science, 2004.

[5] J. Ahmad, K. Bazaka, L.J. Anderson, R.D. White, M.V. Jacob, Materials and methods for encapsulation of OPV: A review, Renewable and Sustainable Energy Reviews, 27 (2013) 104-117.

[6] L.D. Chambers, K.R. Stokes, F.C. Walsh, R.J.K. Wood, Modern approaches to marine antifouling coatings, Surface and Coatings Technology, 201 (2006) 3642-3652.

[7] I.P. Parkin, R.G. Palgrave, Self-cleaning coatings, Journal of Materials Chemistry, 15 (2005) 1689-1695.

[8] A. Nakajima, K. Hashimoto, T. Watanabe, K. Takai, G. Yamauchi, A. Fujishima, Transparent Superhydrophobic Thin Films with Self-Cleaning Properties, Langmuir, 16 (2000) 7044-7047.

[9] R.E. Payne, Albedo of the Sea Surface, Journal of the Atmospheric Sciences, 29 (1972) 959-970.

[10] M.J. Dvoracek, B. Hannabas, Prediction of albedo for use in evapotranspiration and irrigation scheduling, IN: Visions of the Future. ASAE Publication 04-90. American Society of Agricultural Engineers, St. Joseph, Michigan., (1990) 692-699.

[11] J. Kopec, B. Pawlak, Application of approximate formulae to analyse the spectral distribution of the light attenuation coefficient, Oceanologica Acta, 21 (1998) 623-630.

[12] M. Rosa-Clot, P. Rosa-Clot, G.M. Tina, P.F. Scandura, Submerged photovoltaic solar panel: SP2, Renewable Energy, 35 (2010) 1862-1865.

[13] G.M. Tina, M. Rosa-Clot, P. Rosa-Clot, P.F. Scandura, Optical and thermal behavior of submerged photovoltaic solar panel: SP2, Energy, 39 (2012) 17-26.

[14] R. Lanzafame, S. Nachtmann, M. Rosa-Clot, P. Rosa-Clot, P.F. Scandura, S. Taddei, G.M. Tina, Field Experience With Performances Evaluation of a Single-Crystalline Photovoltaic Panel in an Underwater Environment, Industrial Electronics, IEEE Transactions on, 57 (2010) 2492-2498.

[15] C. Ferrer-Gisbert, J.J. Ferrán-Gozálvez, M. Redón-Santafé, P. Ferrer-Gisbert, F.J. Sánchez-Romero, J.B. Torregrosa-Soler, A new photovoltaic floating cover system for water reservoirs, Renewable Energy, 60 (2013) 63-70.

[16] M. Z. B. Alam, S. Ohgaki, Evaluation of UV-radiation and its residual effect for algal growth control, in: M. Tomonori, H. Keisuke, T. Satoshi, K.H.S.T. Hiroyasu SatohA2 - Tomonori Matsuo, S. Hiroyasu (Eds.) Advances in Water and Wastewater Treatment Technology, Elsevier Science B.V., Amsterdam, 2001, pp. 109-117.

[17] H. Bahaidarah, A. Subhan, P. Gandhidasan, S. Rehman, Performance evaluation of a PV (photovoltaic) module by back surface water cooling for hot climatic conditions, Energy.

[18] TTi, Floatovoltaic, Retrieved from: http://www.civicsolar.com/sites/default/files/documents/ttibrochure1009-43953.pdf [Last accessed: 22/12/2013], (2007).

[19] M. Smyth, J. Russell, T. Milanowski, Solar Energy in the Winemaking Industry, Springer 2011.

[20] F. Helfer, C. Lemckert, H. Zhang, Impacts of climate change on temperature and evaporation from a large reservoir in Australia, Journal of Hydrology, 475 (2012) 365-378.

[21] Y.S. Ueda, Tsurugi; Tatebe, Shinya; Itoh, Akihiro; Kurokawa, Kosuke, Performance Analysis of PV Systems on the Water, in: 23rd European Photovoltaic Solar Energy Conference, Valencia, Spain, 2008.

[22] R. Hammond, D. Srinivasan, A. Harris, K. Whitfield, J. Wohlgemuth, Effects of soiling on PV module and radiometer performance, in: Photovoltaic Specialists Conference, 1997., Conference Record of the Twenty-Sixth IEEE, 1997, pp. 1121-1124.

[23] PiEmme, Floating system for photovoltaic panels to realize PV floating plants on water Retrieved from: http://www.pontili-galleggianti.com/floating_platforms_pv_plants_on_water.html [Last accessed: 22/12/2013], (2011).

[24] C. Ferrer Ferrer, C. Ferrer Gisbert, M. Redón Santafé, J. Ferrán Gozálvez, F. Sánchez Romero, J. Torregrosa Soler, E. Pons Puig, Technical performance of a photovoltaic floating cover system, in: International Conference on Agricultural Engineering-AgEng 2010: towards environmental technologies, Clermont-Ferrand, France, 6-8 September 2010., Cemagref, 2010.

[25] J. Bione, O.C. Vilela, N. Fraidenraich, Comparison of the performance of PV water pumping systems driven by fixed, tracking and V-trough generators, Solar Energy, 76 (2004) 703-711.

[26] J. Freilich, J.M. Gordon, Case study of a central-station grid-intertie photovoltaic system with V-trough concentration, Solar Energy, 46 (1991) 267-273.

[27] R. Cazzaniga, M. Rosa-Clot, P. Rosa-Clot, G.M. Tina, Floating tracking cooling concentrating (FTCC) systems, in: Photovoltaic Specialists Conference (PVSC), 2012 38th IEEE 2012, pp. 514-519.

[28] G.M. Tina, M. Rosa-Clot, P. Rosa-Clot, Electrical behaviour and optimization of panels and reflector of a photovoltaic floating plant, in: Proceedings of the 26th European Photovoltaic Solar Energy Conference and Exhibition (EU PVSEC'11), 2011, pp. 4371-4375.

[29] P.R. Thies, J. Flinn, G.H. Smith, Reliability assessment and criticality analysis for Wave Energy Converters, in: Proceedings of the 8th European Wave and Tidal Energy Conference, Uppsala, Sweden 2009.

[30] M. Rosa Clot, P. Rosa Clot, S. Carrara, Apparatus and method for generating electricity using photovoltaic panels, in, WO Patent 2,010,026,542, 2010.

[31] X.-j. Chen, Y.-s. Wu, W.-c. Cui, J.J. Jensen, Review of hydroelasticity theories for global response of marine structures, Ocean Engineering, 33 (2006) 439-457.

[32] S.R. Massel, Ocean Waves Breaking and Marine Aerosol Fluxes, Springer, 2007.

[33] I. Papaioannou, R. Gao, E. Rank, C.M. Wang, Stochastic hydroelastic analysis of pontoon-type very large floating structures considering directional wave spectrum, Probabilistic Engineering Mechanics, 33 (2013) 26-37.

[34] S. Das, S. Das, P. Sahoo, Determination of motion characteristics of a floating body with respect to the variations in degrees of freedom: An analytical study, Ships and Offshore Structures, 3 (2008) 255-262.

[35] J. Morison, J. Johnson, S. Schaaf, The force exerted by surface waves on piles, Journal of Petroleum Technology, 2 (1950) 149-154.

[36] SolidWorks, Solidworks Premium Fluid Flow: Commercial License, in, 2014.

[37] T.S. Garrison, Oceanography: An Invitation to Marine Science, Brooks/Cole, Cengage Learning, 2009.

[38] G. Boyle, O. University, Renewable energy: power for a sustainable future, Oxford University Press in association with the Open University, 1996.

[39] T.E. Conners, S. Banerjee, Surface Analysis of Paper, Taylor & Francis, 1995.

[40] D. Millar, R. Thurley, Experiences of wave buoy deployment, Retrieved from: http://www.primare.org/resources/files/DeanMiller-RichardThurley.pdf [Last accessed: 05/05/2014], (2007).

[41] V. Krivtsov, B. Linfoot, Basin Testing of Wave Energy Converters in Trondheim: Investigation of Mooring Loads and Implications for Wider Research, Journal of Marine Science and Engineering, 2 (2014) 326-335.

[42] R.P. Trask, R.A. Weller, Moorings, in: H.S. Editor-in-Chief: John (Ed.) Encyclopedia of Ocean Sciences, Academic Press, Oxford, 2001, pp. 1850-1860.

[43] R.E. Harris, L. Johanning, J. Wolfram, Mooring systems for wave energy converters: A review of design issues and choices, Marec2004, (2004).

[44] Sound and Sea Technologies, Advanced Anchoring and Mooring Study, in, Oregon Wave Energy Trust, Portland, OR, 2009.

[45] CCE, CCE2-01, Retrieved from: http://mooring.ucsd.edu/projects/cce/img/cce2_01_imp.png [Last accessed: 6/05/2014], (2010).

[46] J.G. Corripio, Vectorial algebra algorithms for calculating terrain parameters from DEMs and solar radiation modelling in mountainous terrain, International Journal of Geographical Information Science, 17 (2003) 1-23.

[47] B.Y.H. Liu, R.C. Jordan, The long-term average performance of flat-plate solar-energy collectors: With design data for the U.S., its outlying possessions and Canada, Solar Energy, 7 (1963) 53-74.

[48] SODA, Time Series of Solar Radiation Data, Solar Energy Services for Professionals, HelioClim3: http://www.soda-is.com/eng/services/services_radiation_free_eng.php [Last accessed 20.02.2013] (2005).

[49] M.J. Tucker, E.G. Pitt, Waves in ocean engineering, Elsevier, 2001.

[50] K. Nishioka, T. Hatayama, Y. Uraoka, T. Fuyuki, R. Hagihara, M. Watanabe, Field-test analysis of PV system output characteristics focusing on module temperature, Solar Energy Materials and Solar Cells, 75 (2003) 665-671.

[51] K. Trapani, M. Redón Santafé, A review of floating photovoltaic installations: 2007–2013, Progress in Photovoltaics: Research and Applications, (2014).

[52] C.M. Tan, B.K.E. Chen, K.P. Toh, Humidity study of a-Si PV cell, Microelectronics Reliability, 50 (2010) 1871-1874.

[53] ISO, ISO 62, in: Plastics - Determination of water absorption, 2008.

[54] ASTM International, D882 in: Standard Test Method for Tensile Properties of Thin Plastic Sheeting, West Conshohocken, PA, 2012.

[55] X. Chen, L. Zhai, S. Zhao, Moisture absorption and diffusion characterization of molding compound, Journal of Electronic Packaging, 127 (2005) 460-465.

[56] J.W. Chin, T. Nguyen, K. Aouadi, Sorption and diffusion of water, salt water, and concrete pore solution in composite matrices, Journal of Applied Polymer Science, 71 (1999) 483-492.

[57] A. Ellison, W. Zisman, Wettability studies on nylon, polyethylene terephthalate and polystyrene, The Journal of Physical Chemistry, 58 (1954) 503-506.

[58] A. Virtuani, D. Pavanello, G. Friesen, Overview of temperature coefficients of different thin film photovoltaic technologies, in: 25th European Photovoltaic Solar Energy Conference and Exhibition/5th World Conference on Photovoltaic Energy Conversion, 2010, pp. 6-10.

[59] Power Film Inc., http://www.powerfilmsolar.com/, in.

[60] K. Trapani, D.L. Millar, H.C.M. Smith, Novel offshore application of photovoltaics in comparison to conventional marine renewable energy technologies, Renewable Energy, 50 (2013) 879-888.

[61] K. Trapani, D.L. Millar, Proposing offshore photovoltaic (PV) technology to the energy mix of the Maltese islands, Energy Conversion and Management, 67 (2013) 18-26.

[62] K. Branker, M.J.M. Pathak, J.M. Pearce, A review of solar photovoltaic levelized cost of electricity, Renewable and Sustainable Energy Reviews, 15 (2011) 4470-4482.

[63] S. Reichelstein, M. Yorston, The prospects for cost competitive solar PV power, Energy Policy, 55 (2013) 117-127.

[64] 2009 Renewable Energy Data Book, in, Energy Efficiency & Renewable Energy, U.S. Department of Energy, 2010.

[65] Protocols for the Equitable Assessment of Marine Energy Converters, in: D. Ingram, G. Smith, C. Bittencourt-Ferreira, H. Smith (Eds.), The Institute for Energy Systems, The University of Edinburgh, Edinburgh, 2011.

[66] A. Clement, P. McCullen, A. Falcao, Fiorentino, A., , F. Gardner, K. Hammarlund, et al., Wave Energy in Europe: Current Status and Perspectives, Renewable and Sustainable Energy Reviews, (2002).

[67] J. Falnes, A Review of Wave-Energy Extraction, Journal of Marine Structures, 20 (2007) 185 - 201.

[68] D. Millar, Wave and Tidal Energy Technologies, in: F. Armstrong, K. Blundell (Eds.) Energy … Beyond Oil, Oxford University Press, 2007.

[69] Y.H. Bae, K.O. Kim, B.H. Choi, Lake Sihwa Tidal Power Plant Project, Journal of Ocean Engineering, 37 (2010) 2679 - 2688.

[70] A. Madariaga, I.M. de Alegría, J.L. Martín, P. Eguía, S. Ceballos, Current facts about offshore wind farms, Renewable and Sustainable Energy Reviews, 16 (2012) 3105-3116.

[71] C.M. Johnstone, D. Pratt, J.A. Clarke, A.D. Grant, A techno-economic analysis of tidal energy technology, Renewable Energy, (2012).

[72] O. Siddiqui, R. Bedard, Feasibility assessment of offshore wave and tidal current power production: a collaborative public/private partnership, in: Power Engineering Society General Meeting, 2005. IEEE, 2005, pp. 2004-2010 Vol. 2002.

[73] F. O'Rorke, F. Boyle, A. Reynolds, Tidal Energy Update 2009, in, Dublin Institute of Technology - School of Mechanical and Transport Engineering, Applied Energy, 2009.

[74] L. Zhang, Relevant Ocean Energy Activities in China, Canada and the World of Ocean Renewable Energy Symposium, (2006) 16 - 35.

[75] B. Parida, S. Iniyan, R. Goic, A review of solar photovoltaic technologies, Renewable and Sustainable Energy Reviews, 15 (2011) 1625-1636.

[76] D.M. Bagnall, M. Boreland, Photovoltaic technologies, Energy Policy, 36 (2008) 4390-4396.

[77] J. Callaghan, R. Boud, Future Marine Energy. Results of the Marine Energy Challenge: Cost competitiveness and growth of wave and tidal stream energy, Carbon Trust, (2006).

[78] ENTEC UK Ltd, Marine Energy Challenge Cost Estimation Methodology, Carbon Trust, (2006).

[79] M. Previsic, R. Bedard, G. Hagerman, E2I EPRI assessment: Offshore wave energy conversion devices, Online at http://oceanenergy.epri.com/attachments/wave/reports/004_WEC_Device_Assess_Report_Rev1_MP_6-16-04.pdf [accessed 1 March 2008], (2004).

[80] DTI, Impact of banding the renewables obligation - costs of electricity production, Department of Trade and Industry, London, Available from: http://webarchive.nationalarchives.gov.uk/+/http://www.berr.gov.uk/files/file39038.pdf [Last accessed: 29/04/2014] (2007).

[81] G. Connor, Economic Study for Ocean Energy Development in Ireland: A Report to Sustainable Energy Authority Ireland and Invest Northern Ireland, in, Invest Northen Ireland, 2010.

[82] T. Weaver, Financial appraisal of operational offshore wind energy projects, Renewable and Sustainable Energy Reviews, 16 (2012) 5110-5120.

[83] EWEA, The Economics of Wind Energy, in, The European Wind Energy Association, March 2009.

[84] Danish Energy Agency, Data on Operating and Decommissioned Wind Turbines (as at end Spetember 2010), in, http://www.ens.dk/da-DK/Info/TalOgKort/Statistik_og_noegletal/Oversigt_over_energisektoren/Stamdataregister_vindmoeller/Documents/AnlaegProdTilNettet.xls, 2010.

[85] X. Sun, D. Huang, G. Wu, The current state of offshore wind energy technology development, Energy, 41 (2012) 298-312.

[86] G. Boyle, Offshore Wind: The Potential to Contribute a Quarter of UK Electricity by 2024, Wind Engineering, 21 (2007) 65 - 74.

[87] Vattenfall inaugurates world's largest offshore wind farm, Renewable Energy Focus, 11 (2010) 4.

[88] Y. Feng, P.J. Tavner, H. Long, Early Experiences with UK Round 1 offshore wind farms, Proceedings of the Institution of Civil Engineers, 163 (2010) 167-181.

[89] C. Fry, All at sea [tidal power], Power Engineer, 19 (2005) 24-27.

[90] H. Andre, Ten Years of Experience at the "La Rance" Tidal Power Plant, Ocean Management, 4 (1978) 165 - 178.

[91] S. Sheth, M. Shahidehpour, Tidal energy in electric power systems, in: Power Engineering Society General Meeting, 2005. IEEE, 2005, pp. 630-635 Vol. 631.

[92] La Rance Barrage, in, Wyre Tidal Energy, http://www.wyretidalenergy.com/tidal-barrage/la-rance-barrage, 2010.

[93] C.A. Douglas, G.P. Harrison, J.P. Chick, Life cycle assessment of the Seagen marine current turbine, Proceedings of the Institution of Mechanical Engineers, Part M: Journal of Engineering for the Maritime Environment, 222 (2008) 1-12.

[94] T. Whittaker, P.L. Fraenkel, A. Bell, L. Lugg, The Potential for the Use of Marine Current Energy in Northern Ireland, in: The Exploitation of Marine Currents in Northern Ireland, Department of Trade and Industry; Department of Enterprise, Trade and Investment; Northern Ireland Electricity, [Online] http://www.detini.gov.uk/part_4_-_page38-50.pdf, 2003.

[95] E. Block, Tidal power: an update, Renewable Energy Focus, 9 (2008) 58-61.

[96] J.P. Deane, G. Dalton, B.P. Ó Gallachóir, Modelling the economic impacts of 500MW of wave power in Ireland, Energy Policy, 45 (2012) 614-627.

[97] N. Boccard, Capacity Factor of Wind Power Realized Values vs. Estimates, Energy Policy, 37 (2009).

[98] C.A. Douglas, G.P. Harrison, J.P. Chick, Life Cycle Assessment of the Seagen Marine Current Turbine, Proc. IMechE, 222 (2008).

[99] A.S. Bahaj, Generating electricity from the oceans, Renewable and Sustainable Energy Reviews, 15 (2011) 3399-3416.

[100] G.J. Dalton, R. Alcorn, T. Lewis, Case study feasibility analysis of the Pelamis wave energy convertor in Ireland, Portugal and North America, Renewable Energy, 35 (2010) 443-455.

[101] NASA, Surface meteorology and Solar Energy, in: RETScreen, Atmospheric Science Data Center, 2008.

[102] K. Burman, Ocean Energy Technology Overview, in, Energy Efficiency & Renewable Energy: US Department of Energy, 2009.

[103] J. Callaghan, Results of the Marine Energy Challenge: Cost competitiveness and the growth of wave and tidal stream energy, in, Carbon Trust, London, 2006.

[104] Solar Panel and Inverter Price Comparison, in, Sun Electronics, 2010.

[105] M. Ayres, M. MacRae, M. Stogran, Levelised Unit Electricity Cost Comparison of Alternative Technologies for Baseload Generation in Ontario, in, Canadian Energy Research Institute, 2004.

[106] D. Jager, C. Klessmann, E. Stricker, T. Winkel, E. Visser, M. Koper, et al., Financing Renewable Energy in the European Energy Market, in, European Commission, 2011.

[107] J. Wolf, Walkington, H. I. A., J., , R. Burrows, Environmental Impacts of Tidal Power Schemes, Proceedings of the Institution of Civil Engineers-Maritime Engineering, 162 (2009) 165 - 177.

[108] J.G. Bryant, Summary report for Plantinex Inc. McFaulds South project, Northwest Ontario, Canada, in, Bryant Groundwater Consulting, Penetanguishene, Ontario, 2008.

[109] W.v. Saark, E.H. Lysen, D. Cocard, P. Beutin, G.F. Merlo, B. Mohanty, J.v.d. Akker, A.R. Idris, A. Firag, A. Waheed, A. Shaheed, M. Latheef, A. Wajee, The first PV-diesel hybrid system in the Maldives installed at Mandhoo Island, in: 21st European Photovoltaic Solar Energy Conference and Exhibition, Dresden, Germany, 2006.

[110] OPA, Feed-in tariff for renewable energy projects in Ontario, in, Ontario Power Authority, 2010.

[111] K. Myrans, Comparative energy and green carbon assessment of three green technologies for a Toronto roof, in, University of Toronto, 2009.

[112] S. Pacca, D. Silvraman, G.A. Keolean, Life Cycle Assessment of the 33 kW Photovoltaic System on the Dana Building at the University of Michigan: Thin Film Laminates, Multi-Crystalline Modules, and a Balance of System Components, in, University of Michigan, 2006.

[113] J. Leadbitter, PVC and sustainability, Progress in Polymer Science, 27 (2002) 2197-2226.

[114] J. Burnet, Forestry Commission Scotland - Greenhouse Gas Emissions Comparison - Carbon benefits of timber in construction (ECCM Report 196), in, 2006.

[115] J.L. Bernarl-Agustin, R. Dupo-Lopez, D.M. Rivas-Ascaso, Design of isolated hybrid systems minimizing costs and pollutant emissions, Renewable Energy, 31 (2006) 2227-2244.

[116] Y. Malhi, D.D. Baldocchi, P.G. Jarvis, The carbon balance of tropical, temperate and boreal forests, Plant, Cell & Environment, 22 (1999) 715-740.

[117] C.S. Cockell, L. Kaltenegger, J.A. Raven, Cryptic photosynthesis—extrasolar planetary oxygen without a surface biological signature, Astrobiology, 9 (2009) 623-636.

[118] European Comission, Directive 2009/28/EC of the European Parliament and of the Council, Official Journal of the Eurpoean Union, (2009).

[119] M. Šúri, T.A. Huld, E.D. Dunlop, H.A. Ossenbrink, Potential of solar electricity generation in the European Union member states and candidate countries, Solar Energy, 81 (2007) 1295-1305.

[120] A. Khelif, A. Talha, M. Belhamel, A. Hadj Arab, Feasibility study of hybrid Diesel–PV power plants in the southern of Algeria: Case study on AFRA power plant, International Journal of Electrical Power & Energy Systems, 43 (2012) 546-553.

[121] S. Rehman, L.M. Al-Hadhrami, Study of a solar PV–diesel–battery hybrid power system for a remotely located population near Rafha, Saudi Arabia, Energy, 35 (2010) 4986-4995.

[122] M.S. Ngan, C.W. Tan, Assessment of economic viability for PV/wind/diesel hybrid energy system in southern Peninsular Malaysia, Renewable and Sustainable Energy Reviews, 16 (2012) 634-647.

[123] J. Dekker, M. Nthontho, S. Chowdhury, S.P. Chowdhury, Economic analysis of PV/diesel hybrid power systems in different climatic zones of South Africa, International Journal of Electrical Power & Energy Systems, 40 (2012) 104-112.

[124] National Statistics Office, Census of Agriculture, in: Unit B3: Agricultural and Fisheries Statistics, and Directorate B: Buisness Statistics: Agricultural and Fisheries Statistics (Ed.), European Statistical System, Malta, 2012.

[125] MRRA, Rural Development Programme for Malta 2007-2013, in: Rural Development Department (Ed.), Ministry for Resources and Rural Affairs, Malta, 2009.

[126] G.H. Blake, Coastal state sovereignty in the Mediterranean sea: the case of Malta, GeoJournal, 41 (1997) 173-180.

[127] Enemalta Corporation, Plant system load and operation data, in, Personal Communication 2011.

[128] Enemalta Corporation, Annual Report 2010 and Financial Statements 2009, in, http://www.enemalta.com.mt/enemaltastorage/images/files/annual%20reports/annual%20report%202010.pdf [Last accessed: 25/09/2012], Enemalta Website, 2011.

[129] Enemalta Corporation, Electricity generation plan: 2006 - 2015, in, Marsa, Malta, 2009.

[130] CEPCI, Chemical Engineering Plant Cost Index, in, 2011.

[131] Platts, European marketscan - January release, 43 (2011).

[132] T. Abbasi, S.A. Abbasi, Biomass energy and the environmental impacts associated with its production and utilization, Renewable and Sustainable Energy Reviews, 14 (2010) 919-937.

[133] N.S. Board, M.A. Commission on Physical Sciences, D.E.P. Sciences, O.N. Research, C.D. Naval Surface Warfare Center, N.R. Council, Twenty-Second Symposium on Naval Hydrodynamics, National Academies Press, 2000.

[134] J. Wolfram, On assessing the reliability and availability of marine energy converters: the problems of a new technology, Proceedings of the Institution of Mechanical Engineers, Part O: Journal of Risk and Reliability, 220 (2006) 55-68.

[135] H. Smith, C. Pearce, D.L. Millar, Further analysis of change in nearshore wave climate due to an offshore wave farm: An enhanced case study for the Wave Hub site, Renewable Energy, 40 (2012) 51-64.

[136] W.J. Grecian, R. Inger, M.J. Attrill, S. Bearhop, B.J. Godley, M.J. Witt, S.C. Votier, Potential impacts of wave-powered marine renewable energy installations on marine birds, Ibis, 152 (2010) 683-697.

[137] L. Margheritini, A.M. Hansen, P. Frigaard, A method for EIA scoping of wave energy converters—based on classification of the used technology, Environmental Impact Assessment Review, 32 (2012) 33-44.

[138] J.P. Kofoed, A. Pecher, L. Margheritini, B. Holmes, T. McCombes, C. Johnstone, C. Bittencourt, C. Retzler, L. Meyers, EquiMar: Equitable Testing and Evaluation of Marine Energy Extraction Devices in Terms of Performance, Cost and Environmental Impact: Deliverable D4. 2 Data Analysis & Presentation to Quantify Uncertainty, in, European Commission, 2010.

[139] G.H. Brundtland, Report of the World Commission on environment and development:" our common future.", United Nations, 1987.